

Supporting Information

Highly Fluorescent Aryl-Cyclopentadienyl Ligands and Their Tetra-Nuclear Mixed Metallic Potassium-Dysprosium Clusters

Selvakumar Arumugam,^{a,±} Pulikanti Guruprasad Reddy,^{b,±} Maria Francis,^b Aditya Kulkarni,^b Sudipta Roy^{b,*} and Kartik Chandra Mondal^{a,*}

^aDepartment of Chemistry, Indian Institute of Technology Madras, Chennai 600036, India. Email: csdkartik@iitm.ac.in

^bDepartment of Chemistry, Indian Institute of Science Education and Research (IISER), Tirupati 517507, India. Email: roy.sudipta@iisertirupati.ac.in

± SA and PGPR contributed equally to this work.

Contents:

S1. General methods and materials

S2. Syntheses and characterization of triaryl substituted Cp ligands **1-2**

S3. Synthesis and characterization of potassium cyclopentadienides **3-4** and complexes **5-6**

S4. Investigation of photophysical properties of ligands **1-2**

S5. Crystallographic details for ligands **1** and **2**

S6. Computational Details

S7. Crystallographic details for complexes **5** and **6**

S8. Spectral data

S9. Additional synthesis and spectral data

S10. References

S1. General methods and materials

Benzaldehyde, 4-methylbenzaldehyde, 4-methylacetophenone, acetic acid, potassium and anhydrous DyCl_3 were purchased from commercial sources and used as received. Nuclear magnetic resonance (NMR) spectra for newly synthesized compounds were recorded on the Bruker 400 MHz NMR spectrometer. Electron spray ionization mass (ESI-MS) spectra were recorded with an Agilent 6545A Q-TOF mass spectrometer. FT-IR spectra were recorded for the solid samples using KBr pellets on a Jasco FT/IR-4100 Spectrometer in 400–4000 cm^{-1} range. Absorption spectra were obtained on Jasco V-650 UV–Vis Spectrophotometer in the range of 200–800 nm. Fluorescence spectra were recorded on a JASCO FP-6300 spectrofluorometer. The syntheses of complexes **3–6** were carried out under argon atmosphere using standard Schlenk line technique or in an argon filled MBraun Eco Plus glove box, where O_2 and H_2O levels were kept below 0.1 ppm at all times. All solvents (THF and toluene) were dried by refluxing over Na/K alloy for 8–12 h under argon atmosphere followed by distillation. Further, the dried and oxygen free solvent was stirred for 12 h over 4 Å molecular sieves and distilled under vacuum and stored over molecular sieves (with oxygen and moisture content < 10 ppm). Deuterated solvents, e.g., C_6D_6 , CDCl_3 and DMSO-D_6 were purchased from Sigma-Aldrich and further purified by stirring over Na/K alloy for two days, followed by reflux for 4 h and distillation under vacuum.

X-Ray Crystallography

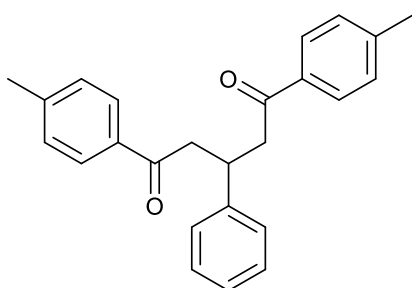
Crystals of **1**, **2**, **5** and **6** were selected and covered with perfluorinated oil on a glass slide. Suitable single crystal was selected using a polarized microscope and mounted on the tip of a MiTeGen[®]MicroMount, equipped with a goniometer head and crystal cooling device. Single crystal data were collected on a Bruker Axs Kappa Apex2 CCD diffractometer,¹ with graphite-monochromated Mo- $\text{K}\alpha$ ($\lambda = 0.71073$ Å) radiation at 200 K/296 K. The data was integrated using SAINT PLUS.² and absorption correction was done using multi-scan absorption correction method (SADABS).³ The structures were solved by direct method (SHELXS-97) and refined using SHELXL-2018/3 program and WinGX v1.70.01^{4,5,6} program packages. All non-hydrogen atoms were refined anisotropically. CCDC reference numbers: 2006636, 2006639, 2007965, 2006659 contains the supplementary crystallographic data for ligands **1**, **2** and complexes **5**, **6**, respectively. These data can be obtained free of

charge from the Cambridge Crystallographic Data Centre via www.ccdc.cam.ac.uk/data_request/cifdata.

S2. Syntheses and characterization of triaryl substituted Cp ligands 1 and 2

Synthesis of 4,4'-(4-phenylcyclopenta-1,3-diene-1,2-diyl)bis(methylbenzene) (1):

Step-1: Synthesis of 3-phenyl-1,5-di-*para*-tolylpentane-1,5-dione (1a):



This synthesis was carried out under ambient condition. A 1:2 molar mixture of benzaldehyde (7 g, 65.96 mmol), 4-methyl acetophenone (18.58 g, 138.51 mmol) and sodium hydroxide pellets (10.55 g, 263.84 mmol) were taken in a mortar and crushed together with a pestle until the liquid reactants turn into a red

solid (Note: It is an exothermic reaction, hence proper precautions should be taken). The resultant red solid mass was dissolved in ethyl acetate: water (1:2, v/v) mixture and transferred into a 500 mL separating funnel. The ethyl acetate layer was extracted and washed several times with the brine solution/water in order to remove un-reacted NaOH. The organic layer (ethyl acetate) was then separated and dried by passing through anhydrous sodium sulphate. After removing ethyl acetate using rotary evaporator under reduced pressure, the resultant crude solid was stirred for 30 min in the presence of excess *n*-hexane (200 mL) to remove the un-reacted starting materials (benzaldehyde and 4-methyl acetophenone), followed by filtering through Büchner funnel and subsequent washing with *n*-hexane. The resultant pure white solid of 3-phenyl-1,5-di-*para*-tolylpentane-1,5-dione (**1a**) was dried in a temperature controlled hot air oven at 65 °C for 24 h. The weight of the isolated compound was 19.42 g (83% Yield). ¹H NMR (400 MHz, CDCl₃, 298 K) δ ppm: 7.84 (d, 4H, *J* = 8.2 Hz, ArH), 7.27-7.26 (m, 4H, ArH), 7.24-7.14 (m, 5H, ArH), 4.08-4.01 (m, 1H, methine), 3.45 (dd, 2H, *J* = 8.0 Hz, 16 Hz, -CH₂, *cis* to carbonyl), 3.31 (dd, 2H, *J* = 8.0 Hz, 16 Hz, -CH₂, *trans* to carbonyl), 2.39 (s, 6H, ArCH₃); ¹³C NMR (101 MHz, CDCl₃, 298 K) δ ppm: 198.30, 143.98, 143.87, 134.46, 129.28, 128.60, 128.30,

127.49, 126.64, 44.87, 37.35, 21.66. **HRMS** (ESI-TOF) m/z calculated for $C_{25}H_{25}O_2$ $[M+H]^+$: 357.1849 found: 357.1866.

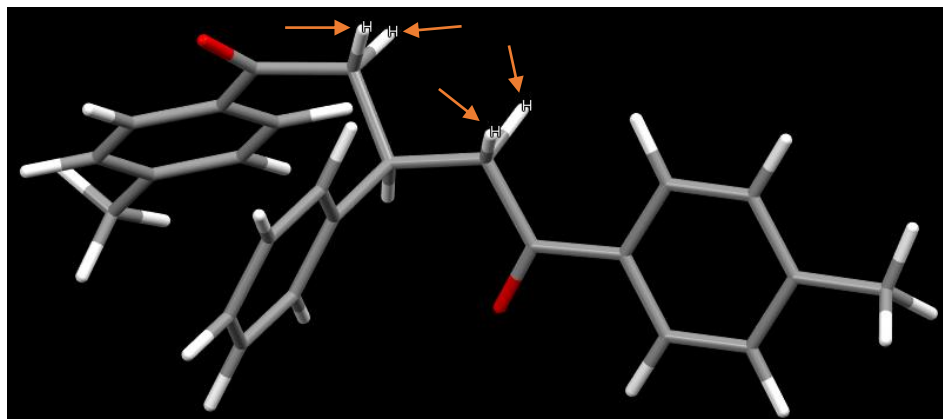
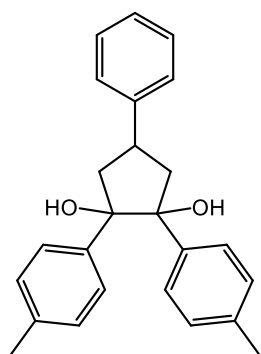


Figure S1.1. Optimised geometry of compound **1a** (M06-2X/def2svp level of theory).

Figure S1.1 shows that the most stable conformer of **1a** has two CH_2 groups (indicated by arrows) with considerably different electronic environment. As a result, the protons of the two CH_2 groups are having different chemical shift values. The CH_2 group, *cis* to the adjacent carbonyl group have a more de-shielded chemical shift (3.45 ppm), whereas the *trans* CH_2 protons have comparatively upfield chemical shift (3.31 ppm) in the 1H NMR spectrum.

Step-2: Synthesis of 4-phenyl-1,2-di-*para*-tolylcyclopentane-1,2-diol (2a**):** The

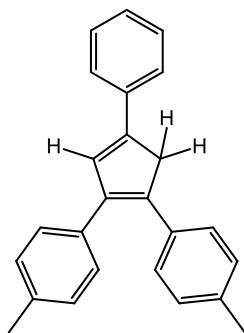


compounds **1a** (18.68 g, 52.47 mmol) and Zn-dust (17.155 g, 262.35 mmol) were taken in a 500 mL round bottom flask, to this 200 mL of glacial acetic acid was added. The reaction mixture was stirred and refluxed at 90-100 °C for 4 h. After completion of the reaction, as monitored by TLC, the un-reacted Zn-dust was removed through filtration. The resultant filtrate

was added dropwise into the crushed ice with vigorous stirring to produce the yellow solid. Thereafter, the solid was filtered and washed several times with distilled water in order to remove excess acetic acid and finally extracted in ethyl acetate. The organic layer was separated from water using a separating funnel. After removing ethyl acetate using rotary evaporator under reduced pressure, the resultant crude solid, 4-phenyl-1,2-di-*para*-tolylcyclopentane-1,2-diol (**2a**) was

purified further by washing several times with *n*-hexane. Finally, the white solid of **2a** was dried in a temperature controlled hot air oven at 65 °C for 24 h. The weight of the isolated compound was 7.4 g (40% Yield). **¹H NMR** (400 MHz, CDCl₃, 298 K) δ ppm: 7.39 (d, 4H, *J* = 8.0 Hz, ArH), 6.94 (d, 4H, *J* = 8.0 Hz, ArH), 6.85-6.79 (m, 5H, ArH), 4.10-4.01 (m, 1H, methine), 3.40 (s, 2H, hydroxyl), 2.76 (dd, 2H, *J* = 12 Hz & 16 Hz, -CH₂), 2.57 (dd, 2H, *J* = 8 Hz, 16 Hz, -CH₂), 2.19 (s, 6H, ArCH₃), **¹³C NMR** (101 MHz, CDCl₃, 298 K) δ ppm: 144.36, 140.22, 136.28, 128.50, 127.99, 127.05, 126.19, 126.10, 85.42, 45.44, 38.22, 20.90. **HRMS** (ESI-TOF) *m/z* calculated for C₂₅H₂₇O₂ [M+H]⁺: 359.2006; found: 359.1654.

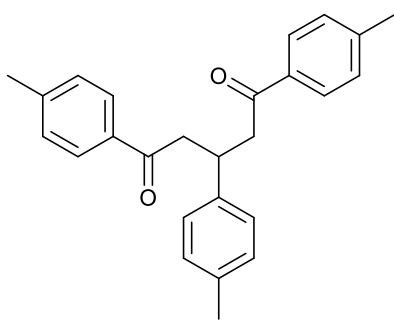
Step-3: Synthesis of 4,4'-(4-phenylcyclopenta-1,3-diene-1,2-diyl)bis(methylbenzene) (1):



Compound **2a** (11.25 g, 31.38 mmol) was dissolved in 60 mL of ethanol, to this 6 mL of concentrated hydrochloric acid (30%) was added dropwise with vigorous stirring. The reaction mixture was stirred and refluxed until the complete conversion of **2a** to the yellow solid **1**. After completion of the reaction, as monitored by TLC, the resultant yellow solid 4,4'-(4-phenylcyclopenta-1,3-diene-1,2-

diyl)bis(methylbenzene) (**1**) was filtered and dried in a temperature controlled hot air oven at 65 °C for 24 h. Further, **1** was purified by column chromatography using EtOAc/hexane (2%) as eluents. The weight of the isolated compound was 7.0 g (70% Yield). **¹H NMR** (400 MHz, CDCl₃, 298 K) δ ppm: 7.55 (d, 2H, *J* = 8.0 Hz, ArH), 7.35-7.28 (m, 4H, ArH), 7.23-7.18 (m, 3H, ArH), 7.13 (d, 2H, *J* = 8.0 Hz, ArH), 7.02 (t, 3H, *J* = 8.00 Hz, ArH), 3.89 (s, 2H, Cp-CH₂), 2.35 (s, 3H, Ar-CH₃), 2.30 (s, 3H, Ar-CH₃); **¹³C NMR** (100 MHz, CDCl₃) δ ppm: 144.45, 141.31, 138.88, 136.75, 136.17, 135.86, 134.29, 134.13, 132.02, 129.16, 128.96, 128.65, 128.24, 127.60, 126.77, 124.84, 44.90, 21.27, 21.18.

Synthesis of 4,4',4''-(cyclopenta-1,3-diene-1,2,4-triyl)tris(methylbenzene) (2): Following the general procedures described for **1**, the compound **2** was synthesized as follows:

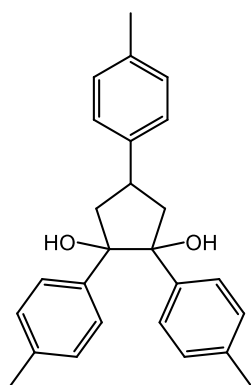


Step-1: Synthesis of 1,3,5-tri-p-tolylpentane-1,5-dione (1b): Following the general procedure of **1a**, using 4-methyl benzaldehyde (10 g, 83.23 mmol), 4-methyl acetophenone (23.45 g, 174.79 mmol) and NaOH (13.31 g, 332.94 mmol) as starting materials, **1b** was achieved as a white solid. The weight of the

isolated compound was 24.34g (79% Yield). $^1\text{H NMR}$ (400 MHz, CDCl_3 , 298 K) δ ppm: 7.85 (d, 4H $J = 8.0$ Hz, ArH), 7.23 (d, 4H, $J = 8.0$ Hz, ArH), 7.16 (d, 2H, $J = 8.0$ Hz, ArH), 7.07 (d, 2H, $J = 8.0$ Hz, ArH), 4.05-3.97 (m, 1H, methine), 3.43 (dd, 2H, $J = 8.0$ Hz & 16 Hz, $-\text{CH}_2$, *cis* to carbonyl), 3.20 (dd, 2H, $J = 8.0$ Hz, 16.0 Hz, $-\text{CH}_2$, *trans* to carbonyl), 2.39 (s, 6H, ArCH_3), 2.28 (s, 3H, ArCH_3); $^{13}\text{C NMR}$ (101 MHz, CDCl_3 , 298 K) δ ppm: 198.40, 143.82, 140.93, 134.47, 129.29, 129.27, 128.32, 127.31, 45.01, 37.02, 21.66, 21.05.

The most stable conformer of **1b** has two CH_2 groups (indicated by arrows) with considerably different electronic environment. As a result, the protons of the two CH_2 groups are having different chemical shift values. The CH_2 group, *cis* to the adjacent carbonyl group have a more de-shielded chemical shift (3.43 ppm), whereas the *trans* CH_2 protons have comparatively upfield chemical shift (3.20 ppm) in the $^1\text{H NMR}$ spectrum.

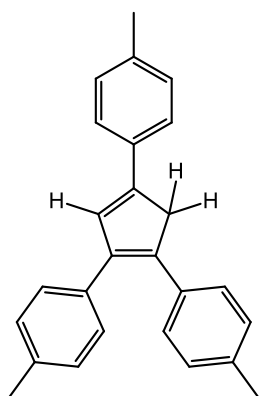
Step-2: Synthesis of 1,2,4-tri-p-tolylcyclopentane-1,2-diol (2b): Following the general procedure of **2a**, using **1b** (24.34 g, 65.69 mmol) and Zn dust (21.47 g, 328.48 mmol) as starting materials, **2b** was



achieved as a white solid. The weight of the isolated compound was 11.7 g (48% Yield). $^1\text{H NMR}$ (400 MHz, CDCl_3 , 298 K) δ ppm: 7.29 (d, 2H, $J = 8.0$ Hz, ArH), 7.20 (d, 2H, $J = 8.0$ Hz, ArH), 6.94 (d, 2H, $J = 8.0$ Hz, ArH), 6.84 (d, 2H, $J = 8.0$ Hz, ArH), 3.97- 4.06 (m, 1H, methine), 3.37 (s, 2H, hydroxyl), 2.74 (dd, 2H, $J = 10$ Hz & 14 Hz, $-\text{CH}_2$), 2.54 (dd, 2H, $J = 9.2$ Hz, 14 Hz, $-\text{CH}_2$), 2.38 (s, 3H, ArCH_3), 2.19 (s, 6H, ArCH_3); $^{13}\text{C NMR}$ (101 MHz, CDCl_3 , 298 K)

δ ppm: 141.30, 140.33, 136.29, 135.62, 129.23, 128.02, 126.97, 126.24, 85.50, 45.61, 37.90, 21.06, 20.94.

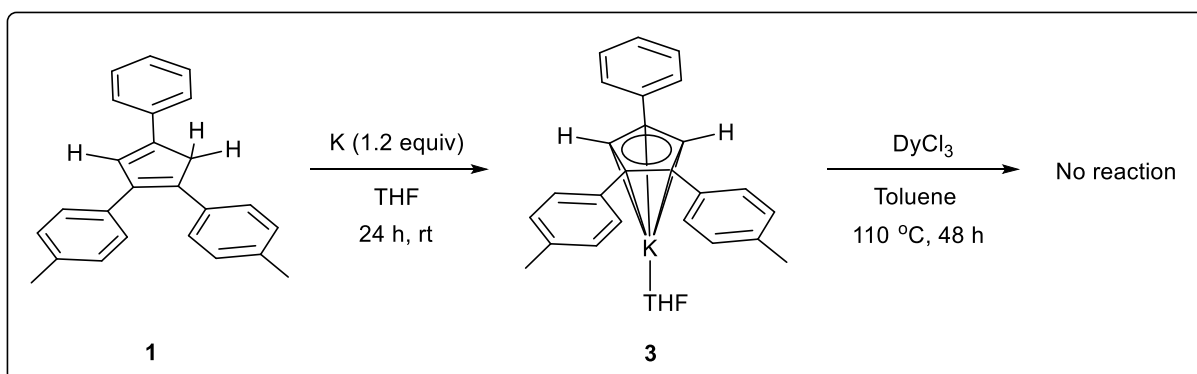
Step 3: Synthesis of 4,4',4''-(cyclopenta-1,3-diene-1,2,4-triyl)tris(methylbenzene) (2):



Following the general procedure of **1**, using **2b** (11.0 g, 29.53 mmol) and 30% HCl (6mL) as starting materials, **2** was synthesized as a yellow solid. The weight of the isolated compound was 8.5 g (86% Yield). $^1\text{H NMR}$ (400 MHz, CDCl_3 , 298 K) δ ppm: 7.46 (d, 2H, $J = 8.0$ Hz, ArH), 7.29 (d, 2H, $J = 8.0$ Hz, ArH), 7.21 (d, 2H, $J = 8$ Hz, ArH), 7.14 (t, 4H, $J = 8.0$ Hz, ArH), 7.03 (d, 2H, $J = 8.00$ Hz, ArH), 6.96 (s, 1H, CpH), 3.88 (s, 2H, Cp- CH_2), 2.36-2.31 (m, 9H, Ar CH_3); $^{13}\text{C NMR}$ (101 MHz, CDCl_3 , 298 K) δ ppm: 144.60, 141.39, 138.39, 136.75, 136.60, 136.010, 134.44, 134.27, 133.19, 131.23, 129.40, 129.20, 129.00, 128.31, 127.63, 124.83, 44.97, 21.34, 21.28, 21.24; **HRMS** (ESI-TOF) m/z calculated for $\text{C}_{26}\text{H}_{25}$ $[\text{M}+\text{H}]^+$: 337.1951; found: 337.1950.

S3. Syntheses and characterization of potassium cyclopentadienide salts **3** and **4**

S3.1 Synthesis of potassium 1-phenyl-3,4-di-*para*-tolylcyclopenta-2,4-dien-1-ide (**3**)



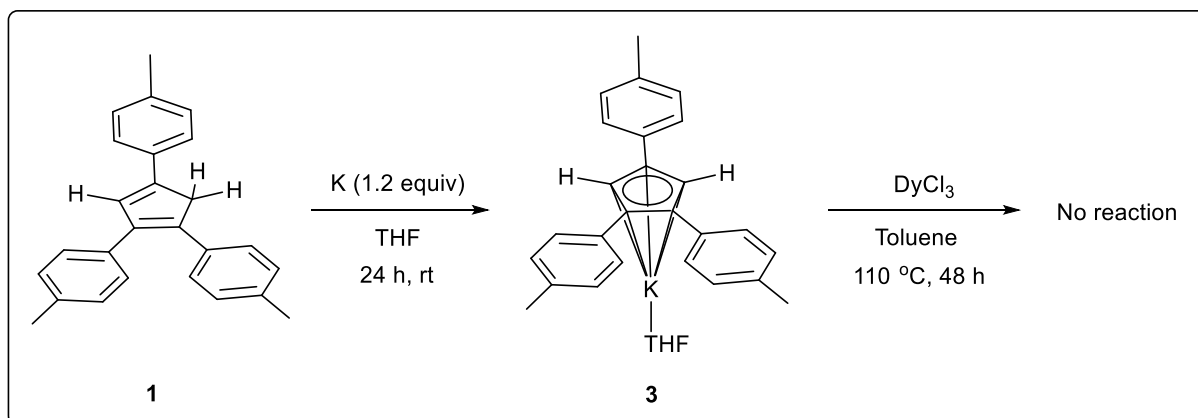
Scheme S1. Synthetic route for **3** and its reactivity with Dy(III)Cl_3 .

The compound 4,4'-(4-phenylcyclopenta-1,3-diene-1,2-diyl)bis(methylbenzene) (**1**) (2.5 g, 7 mmol) was taken in an oven dried 100 mL Schlenk flask, to this freshly distilled dry THF (15 mL) was added. Thereafter, the potassium (0.36 g, 9.2 mmol) pieces were added portion wise to the reaction mixture over a period of 10 min with

vigorous stirring. Further, the reaction was allowed for stirring at RT under argon atmosphere for 24 h. During the reaction, the color of the reaction mixture was slowly converted from yellow to deep-blue. After completion of the reaction (monitored by the disappearance of the metallic potassium), the resultant deep-blue solution was filtered and the residual solvent was removed subsequently under vacuum followed by drying the resultant solid mass of potassium 1-phenyl-3,4-di-*para*-tolylcyclopenta-2,4-dien-1-ide (**3**) as a pale-yellow solid. Several attempts to crystallize **3** from various solvents, e.g., *n*-hexane/ THF/ toluene were failed. **3** was isolated in 78% yield as a pale-yellow solid. ¹H NMR (400 MHz, C₆D₆) spectrum was found to be very broad in C₆D₆.

Further, the reaction between potassium 1-phenyl-3,4-di-*para*-tolylcyclopenta-2,4-dien-1-ide (**3**) (2 mmol) and anhydrous DyCl₃ (1 mmol) in 2:1 molar ratio in anhydrous toluene (10 mL) at 110 °C under argon atmosphere for 24 h was failed to produce the corresponding K-Dy-Cp complex **5**. A longer reaction time (more than 48 h) also showed the similar results indicating poor reactivity of **3** towards DyCl₃.

S3.2 Synthesis of potassium 1,3,4-tri-*para*-tolylcyclopenta-2,4-dien-1-ide (**4**)



Scheme S2. Synthetic route for **4** and its reactivity with Dy(III)Cl₃.

The compound, 4,4',4''-(cyclopenta-1,3-diene-1,2,4-triyl)tris(methylbenzene) (**2**) (3.0 g, 9.0 mmol) was taken in an oven dried 100 mL Schlenk flask, to this freshly distilled dry THF (15 mL) was added. Thereafter, the potassium (0.42 g, 11.0 mmol) pieces were added portion wise to the reaction mixture over a period of 10 min followed by

subsequent stirring the reaction mixture at RT under argon atmosphere for 24 h. After completion of the reaction, the formation of yellow precipitates was observed which was separated via filtration and thoroughly dried under high vacuum. The resultant yellow solid of potassium 1,3,4-tri-*para*-tolylcyclopenta-2,4-dien-1-ide (**4**) was obtained in 69% yield. δ ppm: ^1H NMR (400 MHz, benzene- d_6) δ ppm: The spectrum was found to be very broad in C_6D_6 .

The reaction of potassium 1,3,4-tri-*para*-tolylcyclopenta-2,4-dien-1-ide (**4**) (2 mmol) with anhydrous DyCl_3 (1 mmol) in anhydrous toluene (10 mL) at 110 °C under argon atmosphere for 24 h was failed similarly as the reaction of **3**. Even a longer reaction time (more than 48 h) could not produce the corresponding K-Dy-Cp complex **6**, indicating the poor reactivity of **4** towards anhydrous DyCl_3 .

S3.3 Syntheses of potassium-dysprosium sandwich complexes **5** and **6**

S3.3.1 Synthesis of $[(\text{Me}_2\text{Cp})_4\text{Dy}^{\text{III}}_2\text{Cl}_4\text{K}_2]\cdot 3(\text{C}_7\text{H}_8)$ (**5**):

A mixture of anhydrous DyCl_3 (1 mmol, 268 mg), $\text{Me}_2\text{Cp-H}$ (**1**) (2 mmol, 644 mg) and potassium (2 mmol, 80 mg) were taken in a 50 mL oven dried Schlenk flask, to this freshly distilled 10 mL of dry toluene was transferred through cannula at 0°C under argon atmosphere. Further, the reaction mixture was stirred at RT for 10 min followed by refluxing at 110°C for 48 h. After completion of the reaction, the yellow turbid reaction mixture was filtered-off to obtain a yellow clear filtrate. Finally, the resultant clear filtrate was concentrated closely to 3 mL under high vacuum and stored at -40 °C in a freezer for 3 days to obtain light yellow block shaped crystals of $[(\text{Me}_2\text{Cp})_4\text{Dy}^{\text{III}}_2\text{Cl}_4\text{K}_2]\cdot 3(\text{C}_7\text{H}_8)$ (**5**) in 71% yield. The suitable single crystal of **5** was picked up from the mother liquor (concentrated toluene solution) for single crystal X-ray diffraction studies.

S3.3.2 Synthesis of $[(\text{Me}_3\text{Cp})_4\text{Dy}^{\text{III}}_2\text{Cl}_4\text{K}_2]\cdot 3(\text{C}_7\text{H}_8)$ (**6**):

Following the general synthetic procedure of **5**, using anhydrous DyCl_3 (1 mmol, 268 mg), $\text{Me}_3\text{Cp-H}$ (**2**) (2 mmol, 672 mg) and potassium (2 mmol, 80 mg) as starting materials, the potassium-dysprosium mixed metallocene complex $[(\text{Me}_3\text{Cp})_4\text{Dy}^{\text{III}}_2\text{Cl}_4\text{K}_2]\cdot 3(\text{C}_7\text{H}_8)$ (**6**) was obtained as faint yellow block shaped crystals from the mother liquor (concentrated toluene solution). The crystals of **6** were isolated in 72% yield.

S4. Investigation of photophysical properties of ligands 1-2

S4.1 UV-vis spectra of ligands 1 and 2 in different solvents

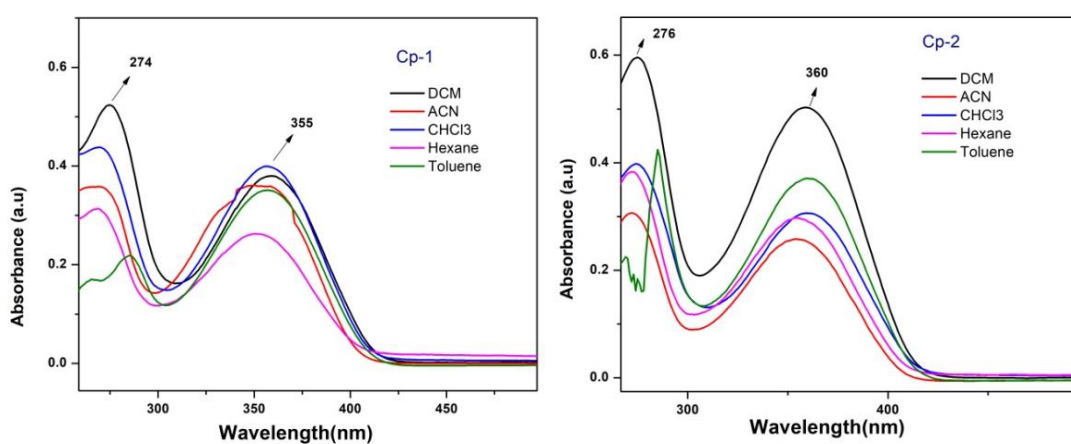


Figure S1.2. UV-visible absorption spectra of **1** (left) and **2** (right) in different solvents.

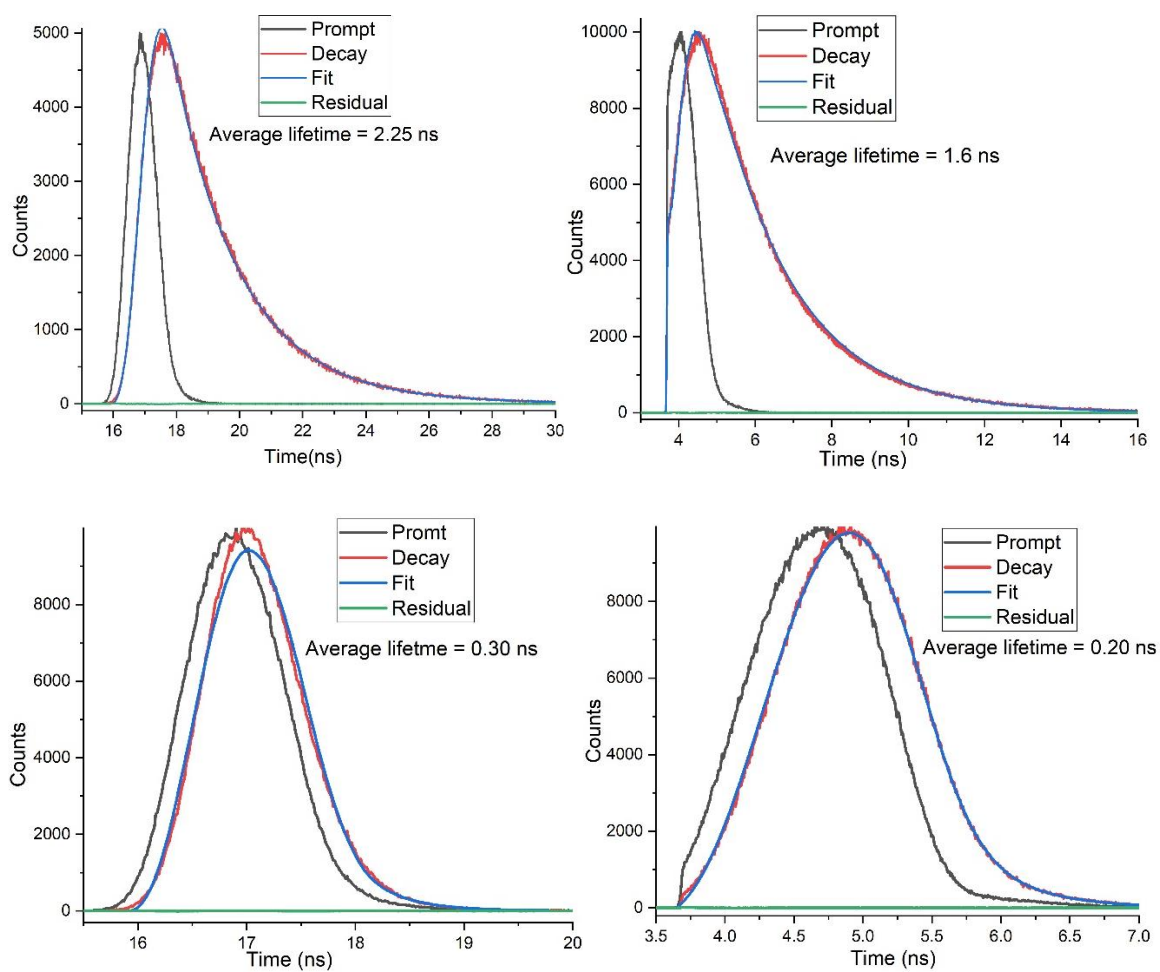
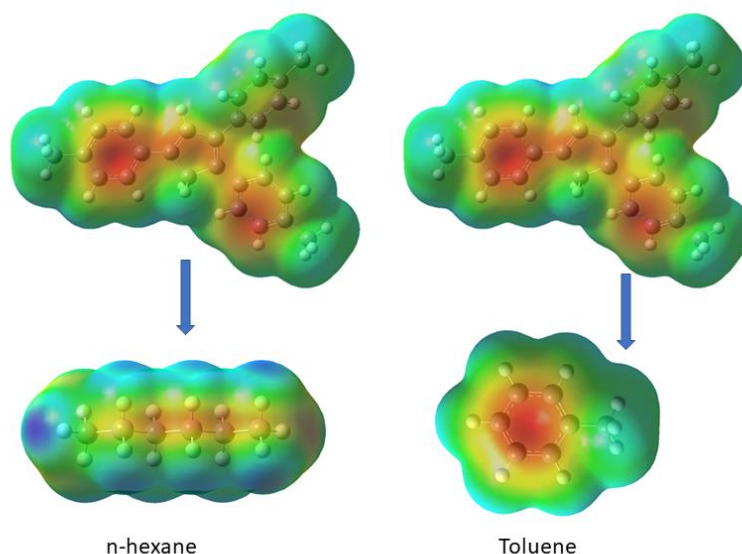


Figure S2. PL decay curves after excitation of **1** (left) and **2** (right) in solid state (top) and also in solution (bottom) with laser pulse.

Both the ligands **1** and **2** in different solvents displayed similar absorptions bands at around 274 nm and 360 nm (Figures S1-S2) which is probably due to the π - π^* transitions of conjugated aromatic phenyl moieties substituted on the cyclopentadienyl core.⁷

M06/def2TZVP level of theory was used to generate the fchk files for generating these MEP plots.



Weak electrostatic dipolar interactions with Me₃CP-H (**2**) ligand and non-polar non-coordinating solvents (hexane, toluene)

Figure S3. The electrostatic interaction between ligand **2** and solvents (*n*-hexane or toluene).

S4.2 AIEE studies of compounds **1** and **2** in different solvents

S4.2.1 AIEE studies of compounds **1** and **2** in THF:water mixture

In order to explore the AIEE properties of these compounds, their fluorescent behaviour was studied in THF:water mixture by sequential addition of different fractions of water into THF. In the present study we have used most commonly preferred solvent pair i.e. THF:water to explore the AIEE characteristics. The compounds **1** and **2** are insoluble in water, hence their absorption and emissions can be readily altered due to the formation of molecular nano-aggregates in the miscible solvent pair caused by the addition of different fractions of water into THF. As shown in Figures 3a-b, the fluorescence intensity of **1** and **2** was enhanced with the increasing water content which in turn reflects their AIEE phenomenon. Considering **1** as an example, the drastic change of fluorescence intensity and photoluminescence was noticed with the increase of water fraction from 0 to 20% (Figure 3a), afterwards, the slight enhancement of emission was observed when the water fraction reaches 50%. The maximum intensity was observed when the water fraction was nearly 60%. The increase of fluorescence intensity can be attributed to AIEE effect caused by the formation of the molecular nano-aggregates in the

miscible solvent pair, which can restrict the intermolecular rotations of molecules resulting increased fluorescence emission. Interestingly, fluorescence intensity drops down when the water fraction reaches 70-90%. This might be due to the decreasing number of emissive molecules located at the surface of the molecular aggregates due to increasing water content. In other words, the size of the nano-aggregates formed in the solution increases with the increasing water content. On the other hand, **2** displayed gradual increase of fluorescence emission with the increase of water fraction from 0 to 80% as shown in Figure 3b. However, the fluorescence intensity drops down when the water fraction exceeds 90%. The AIEE properties of these compounds were also studied in acetone:water mixture and the results (Figure S7 and S8) obtained from these studies are quite similar to that of THF:water system. Based on the data obtained from these studies we conclude that compounds **1** and **2** exhibit moderate AIEE properties under the given experimental conditions.

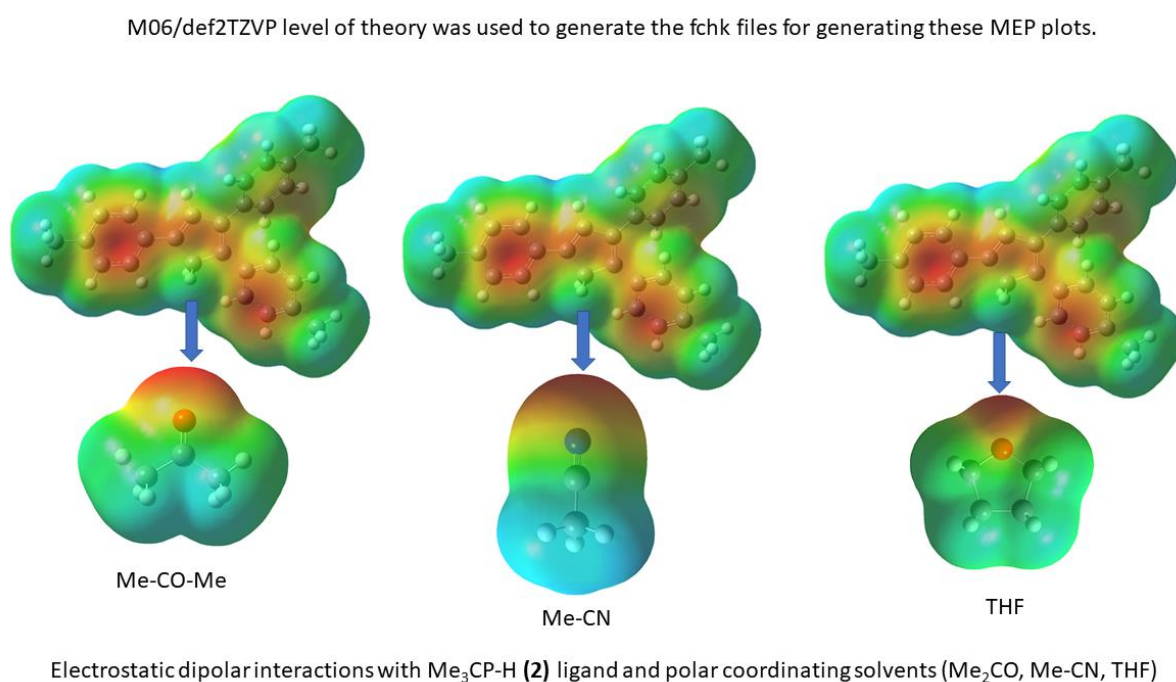
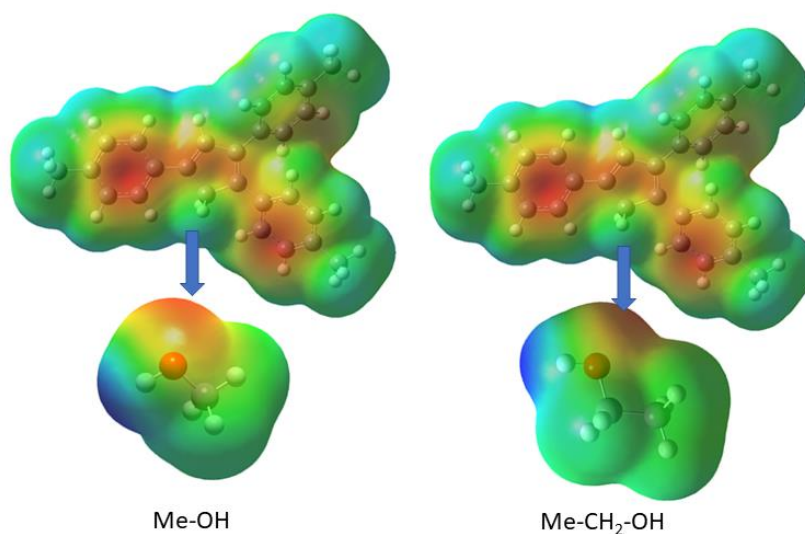


Figure S4. The electrostatic interaction between ligand **2** and acetone or MeCN or THF.

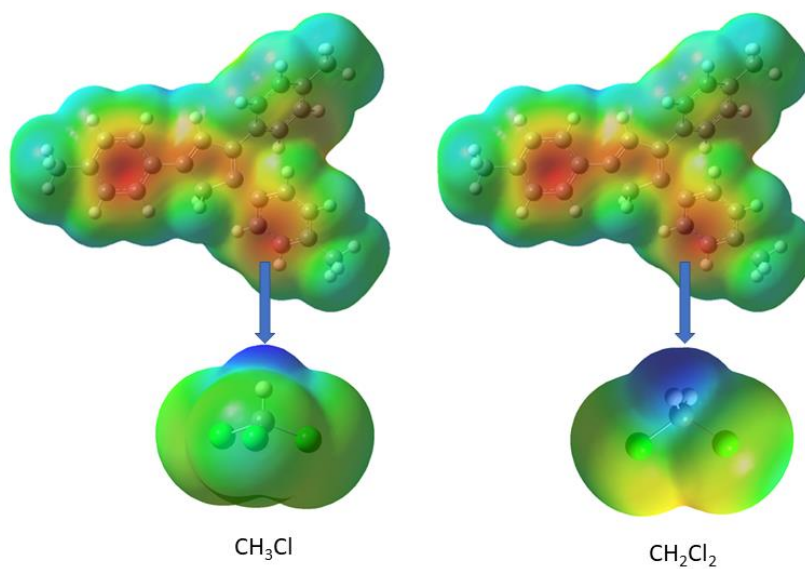
M06/def2TZVP level of theory was used to generate the fchk files for generating these MEP plots.



Electrostatic dipolar interactions with Me₃CP-H (**2**) ligand and polar coordinating solvents (Me-OH, EtOH)

Figure S5. The electrostatic interaction between ligand **2** and MeOH or EtOH.

M06/def2TZVP level of theory was used to generate the fchk files for generating these MEP plots.



Electrostatic dipolar interactions with Me₃CP-H (**2**) ligand and polar non-coordinating solvents (CH₃Cl, DCM)

Figure S6. The electrostatic interaction between ligand **2** and CHCl₃ or DCM.

S4.2.2 AIEE studies of compounds 1 and 2 acetone:water mixture:

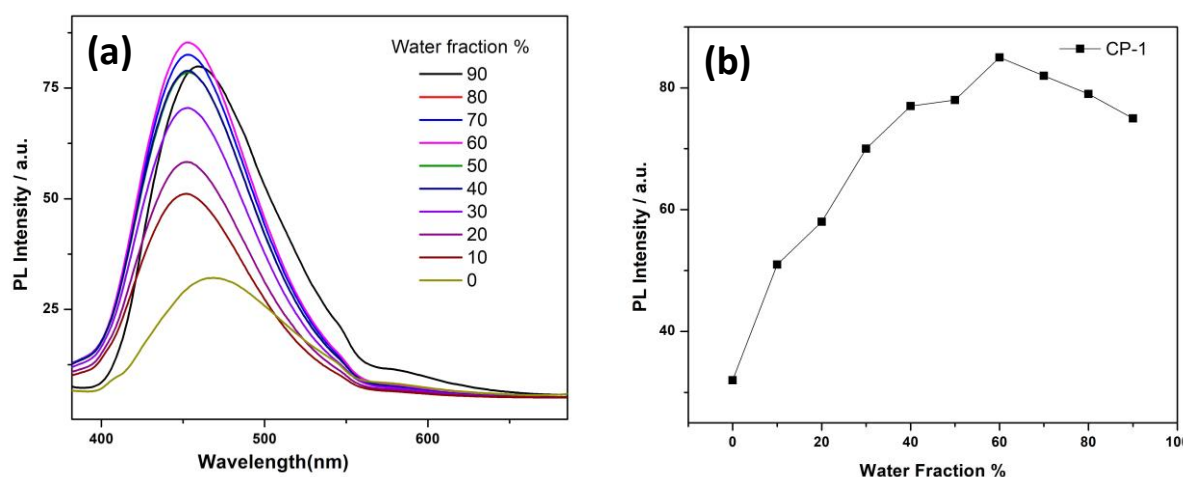


Figure S7. (a) AIEE studies of **1** in acetone:water mixture with the increase of water fractions from 10-90%; (b) The image showing change in the PL intensity of **1** with the addition of different fractions of water (10-90%) into the acetone.

The enhancement of PL intensity observed for **1** with the continuous addition of water fractions till 60% in the acetone:water mixture due to Aggregation Induced Emission Enhancement (AIEE) phenomenon. Afterwards, PL intensity decreases when the water fractions reached about 60-90%. This is due to decreasing the number of emissive molecules located at the surface of the molecular aggregates with the increasing water content. In other words, the size of the nano-aggregates formed in the acetone:water mixture increases further with the increasing water content.

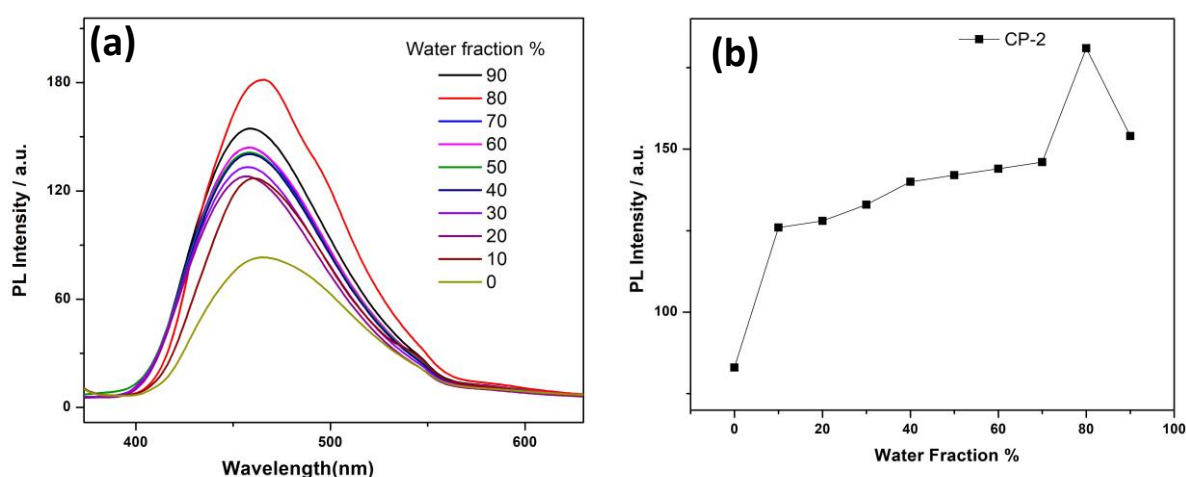


Figure S8. (a) AIEE studies of **2** in acetone:water mixture with the increase of water fractions from 10-90%; (b) The image showing change in the PL intensity of **2** with the addition of different fractions of water (10-90%) into the acetone.

As shown in Figure S8(a)-(b), the sudden jump in the emission enhancement observed for **2** when the 10% water added to acetone, thereafter, slight enhancement in the PL intensity noticed upon increasing water fractions from 20-70%. The gradual enhancement of the emission with the increasing water content attributes the AIEE phenomenon of **2**. The maximum emission noticed for **2** in the acetone:water mixture when the water fractions reaches about 80% and the emission intensity decreases afterwards with the increase of water content from 80-90%. Moreover, the AIEE phenomenon of **1** and **2** in acetone: water mixture matched well with the similar studies performed in THF:water mixture.

S4.3 Quantum yield calculation for ligands 1, 2, complexes 3, 4, 5 and 6

The fluorescence quantum yields (Φ) have been calculated for the ligands **1**, **2** and complexes **3**, **4**, **5**, **6** using the following equation (quinine sulphate has been used as the reference).

$$\phi_F = \phi_R \frac{I_F A_F \eta_F^2}{I_R A_R \eta_R^2}$$

In the above equation, Φ_F and Φ_R represents the quantum yields of the unknown fluorescent sample and the standard reference (quinine sulphate), respectively. I_F and I_R are the integrated fluorescence intensities (area under the fluorescence spectral curve) for the unknown sample and the reference, respectively. A_F and A_R are the respective absorbance values of the unknown sample and the reference. η_F , η_R are the refractive indices of acetonitrile and water, respectively.

S5. Crystallographic details for compounds 1 and 2

CCDC reference numbers: 2006636, 2006639 contains the supplementary crystallographic data for complexes **5** and **6**, respectively.

Table S1. Crystal data and structure refinement for 1 and 2 .		
Identification code	1	2
Empirical formula	C ₂₅ H ₂₂	C ₂₆ H ₂₄
Formula weight	322.42	336.45
Temperature	296(2) K	296(2) K
Wavelength	0.71076 Å	0.71073 Å
Crystal system	Monoclinic	Orthorhombic
Space group	Cc	Iba2
Unit cell dimensions	$a = 12.834(9) \text{ \AA}; \alpha = 90^\circ.$ $b = 18.991(10) \text{ \AA}; \beta = 113.36(3)^\circ.$ $c = 8.136(6) \text{ \AA}; \gamma = 90^\circ.$	$a = 22.059(2) \text{ \AA}; \alpha = 90^\circ.$ $b = 22.2927(12) \text{ \AA}; \beta = 90^\circ.$ $c = 7.6696(3) \text{ \AA}; \gamma = 90^\circ.$
Volume	$V = 1820(2) \text{ \AA}^3$	$V = 3771.5(4) \text{ \AA}^3$
Z	4	8
Density (calculated)	1.176 Mg/m ³	1.185 Mg/m ³
Absorption coefficient	0.066 mm ⁻¹	0.067 mm ⁻¹
F(000)	688	1440
Crystal size	0.300 x 0.250 x 0.250 mm ³	0.280 x 0.220 x 0.100 mm ³
Theta range for data collection	3.915 to 36.454°.	1.846 to 26.245°.
Index ranges	-21 ≤ h ≤ 21, - 31 ≤ k ≤ 31, -12 ≤ l ≤ 13	-26 ≤ h ≤ 27, - 27 ≤ k ≤ 25, -9 ≤ l ≤ 7
Reflections collected	32565	14443
Independent reflections	8555 [<i>R</i> (int) = 0.0383]	3393 [<i>R</i> (int) = 0.0280]
Completeness to theta =	99.5 %	99.9 %

25.243°		
Refinement method	Full-matrix least-squares on F ²	Full-matrix least-squares on F ²
Data / restraints / parameters	8555 / 2 / 226	3393 / 1 / 238
Goodness-of-fit on F ²	1.050	1.040
Final R indices [<i>I</i> > 2σ(<i>I</i>)]	R1 = 0.0786, wR2 = 0.1879	R1 = 0.0386, wR2 = 0.0952
R indices (all data)	R1 = 0.1106, wR2 = 0.2075	R1 = 0.0473, wR2 = 0.1011
Absolute structure parameter	2.0(10)	-2.1(10)
Extinction coefficient	n/a	n/a
Largest diff. peak and hole	0.409 and -0.414 e.Å ⁻³	0.219 and -0.208 e.Å ⁻³

Till date, various mechanisms have been proposed to understand the AIEE phenomenon of organic solid-state emitters including restriction of intermolecular rotations, formation of j-type aggregates, inhibition of photo-cyclization/photo-isomerisation, blockage of non-radiative relaxation pathways of the excited species etc. To understand the mechanism for fluorescence emission of compounds **1** and **2**, we have investigated the relationship between their structure and photophysical properties. Along this direction, we have grown suitable single crystals of **1** and **2** (Figures S9, S13) in *n*-hexane by a slow evaporation method. The molecular structure and packing patterns of these compounds were well-studied using single crystal X-ray diffraction analysis. **1** crystallizes in a monoclinic crystal system *Cc* space group with *Z* = 4. While **2** crystallizes in an orthorhombic crystal system *Iba2* space group with *Z* = 8. Both of these compounds adopt non-coplanar geometry and possess different packing patterns in the crystal lattice as shown in Figures S12 and S16. The crystal data and structure refinement for compounds **1** and **2** are given in Table S1. The dihedral angle measured between the cyclopentadienyl core and a substituted phenyl moiety on them is one of the parameters considered to rationalize the packing features of molecules in the solid state, which in turn directly influences the electronic and photophysical properties in their solid/aggregated state. The selected dihedral angles measured between the planes of central cyclopentadienyl

ring and aromatic phenyl moieties of **1** and **2** are given in Table S2 and Figures S10 and S15. Taking **1** as an example, planes of two 4-methyl phenyl moieties (II and III) are twisted away from the plane of the cyclopentadiene core (I) with the corresponding dihedral angles of 35.71° and 34.24° which indicates the negligible co-facial π - π stacking between the individual molecules. In contrast, the torsion angle between the planes of cyclopentadiene core (I) and phenyl ring (IV) is 6.58°, indicating its slight non-planar orientation (see Table S2). **1** displays strong C-H \cdots π interactions with its adjacent molecule; where *ortho*-hydrogen of one of the 4-methylphenyl moieties of **1** underwent strong π interactions with the electron cloud of cyclopentadienyl core which is next to **1**. The short C-H \cdots π distance 2.870 Å suggested that the strong packing features could be possible between the molecules when compared to few similar type molecules reported with measured distances C-H \cdots π in the range of 3.16-3.30 Å. This weak bonding interaction led to J-type aggregation of molecules in column as shown in Figure S11. Further, every individual molecule in the column underwent weak H \cdots H interactions with their adjacent molecules located in the next column, which led to 1D arrangement of molecules in the solid state (Figure S11 and Figure S12). The approximate distance between two independent 1D chains is 3.970 Å. This observation helped us conclude that molecules are tightly packed inside the crystal lattice due to weak bonding forces (C-H \cdots π and H \cdots H interactions) exerted between them, as a result of which, the intermolecular rotations between them are hindered hence enhanced PL intensity was observed. This conclusion is supported by the experimental observed high emission intensity of **1** in solid and aggregated states than compared to in their THF solutions.

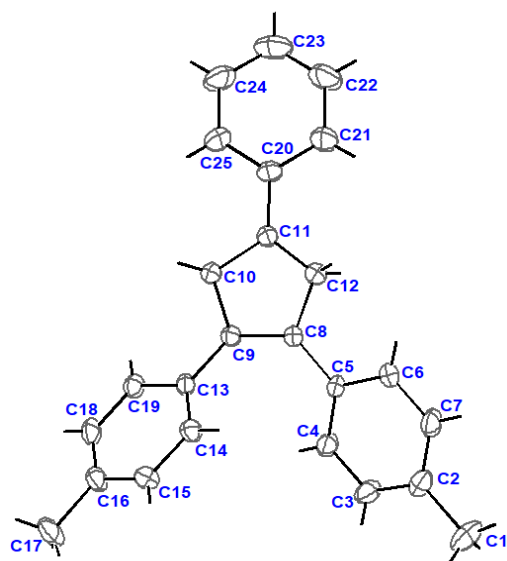


Figure S9. Molecular structure of **1** (ORTEP view). All the atoms are drawn at 50% probability level.

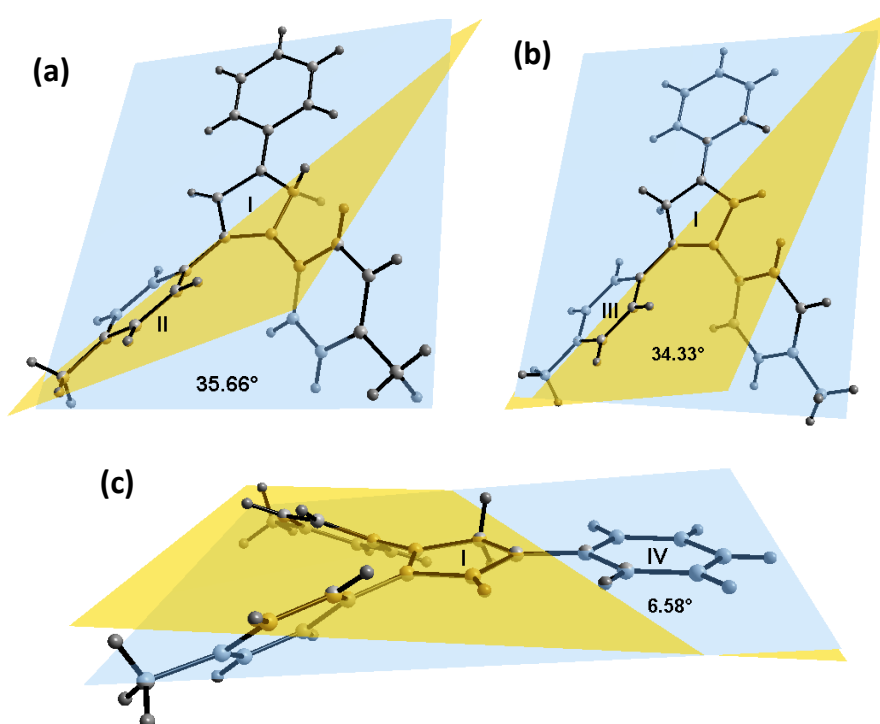


Figure S10. The molecular planes passed through the atoms of cyclopentadienyl core (I) and substituted aromatic phenyl moieties (II, III and IV) in the molecular structure of **1**. The measured torsion angle between the planes of I-II, I-III and I-IV in **1** are 35.66°, 34.33° and 6.58°, respectively.

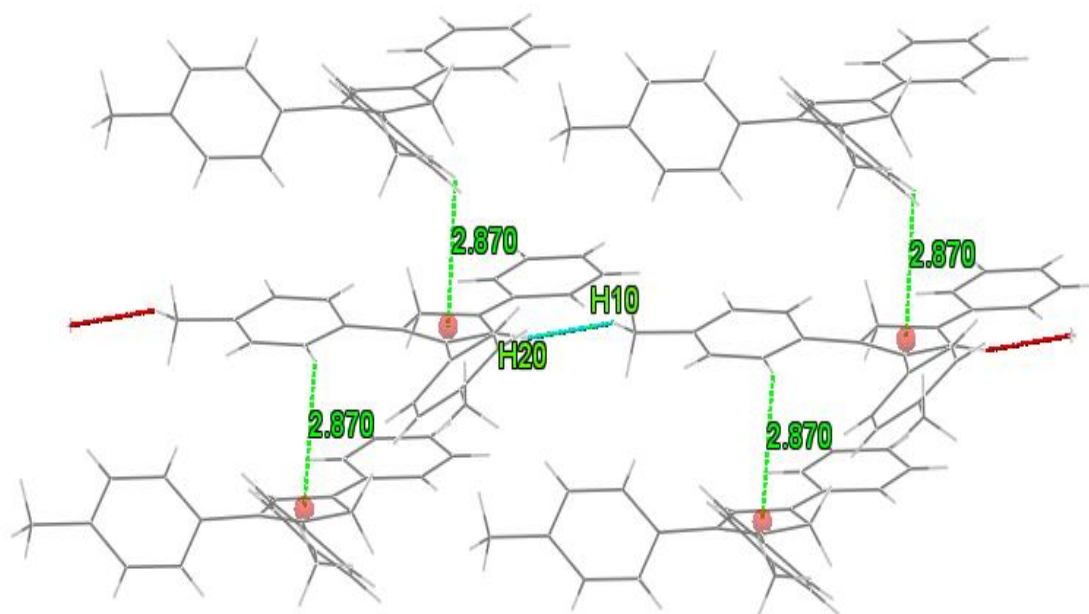


Figure S11. The figure showing weak H \cdots H and CH \cdots π bonding interactions exerted between the adjacent molecules of **1** in the horizontal and vertical direction respectively, led to 1D-chain like assembly in the crystal lattice. The measured CH \cdots π distance between the molecules of **1** is 2.870Å.

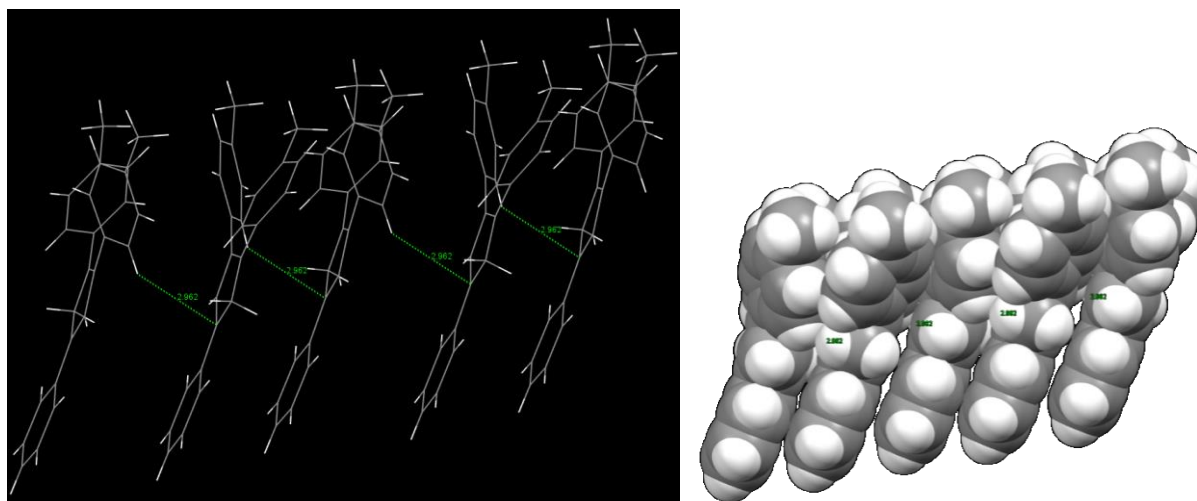


Figure S12. Indirect [C-H of five membered phenyl-ring \cdots π of five membered Cp ring] for Me₂Cp-H (**1**) along a propagating 1D chain. The space filling model along 1D chain (right; grey: C; white: H).

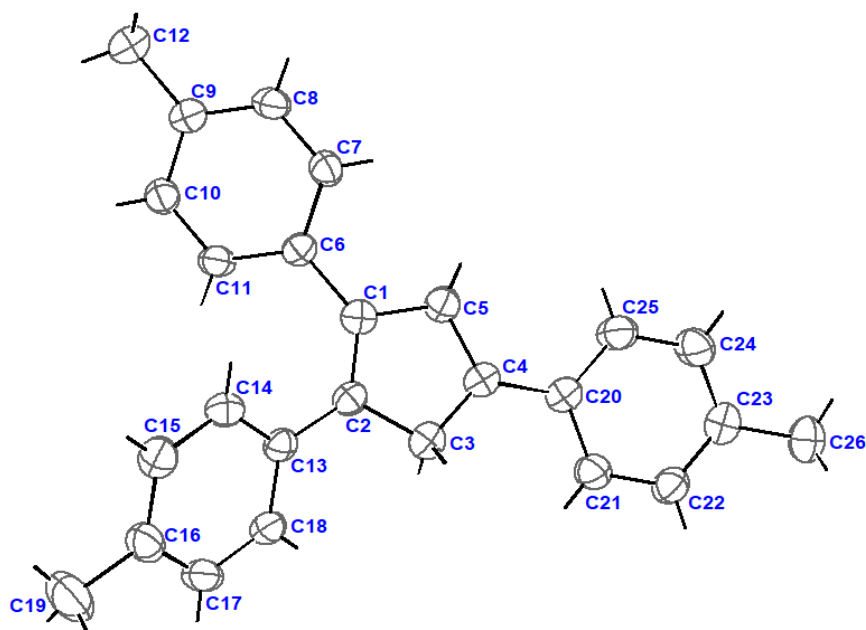


Figure S13. The molecular structure of **2** (ORTEP view). All the atoms are drawn at 50% probability level.

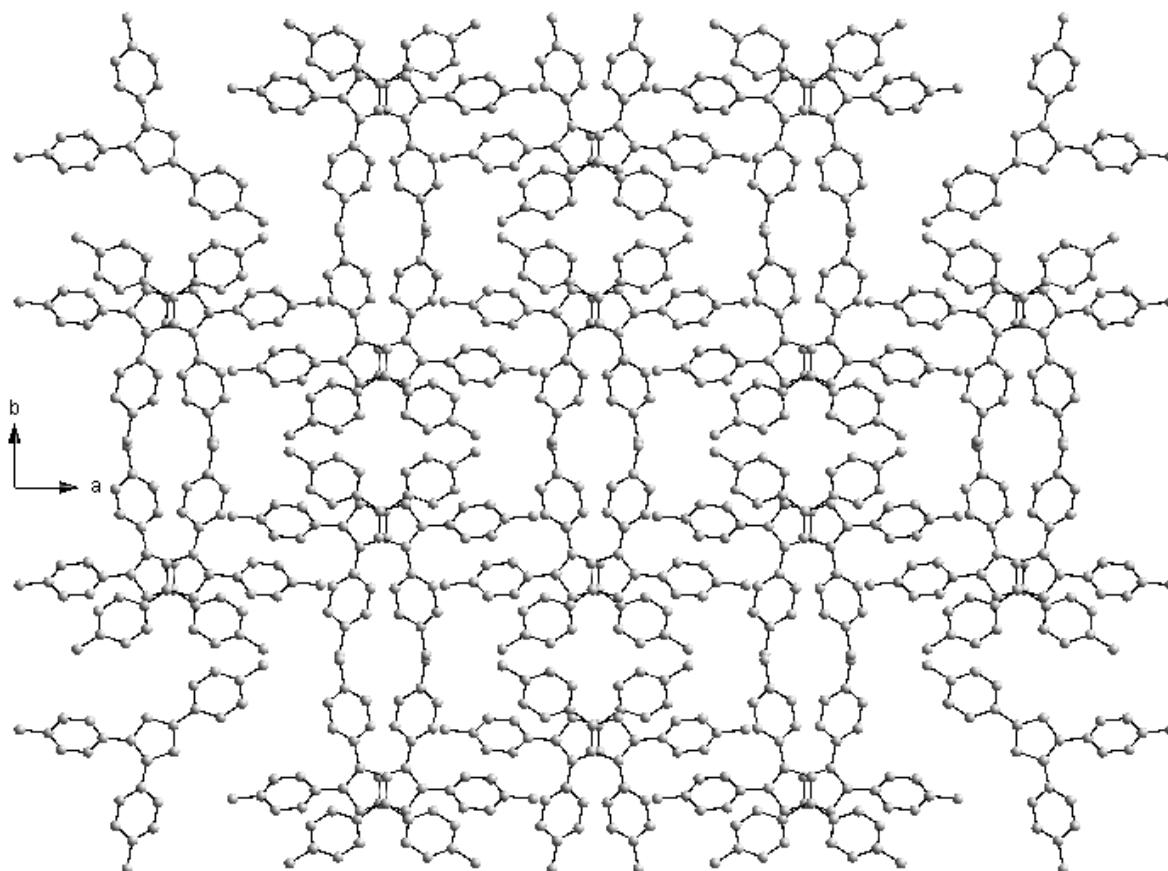


Figure S14. Packing patterns of **2** (View along c-axis). Hydrogen atoms are omitted for the clarity.

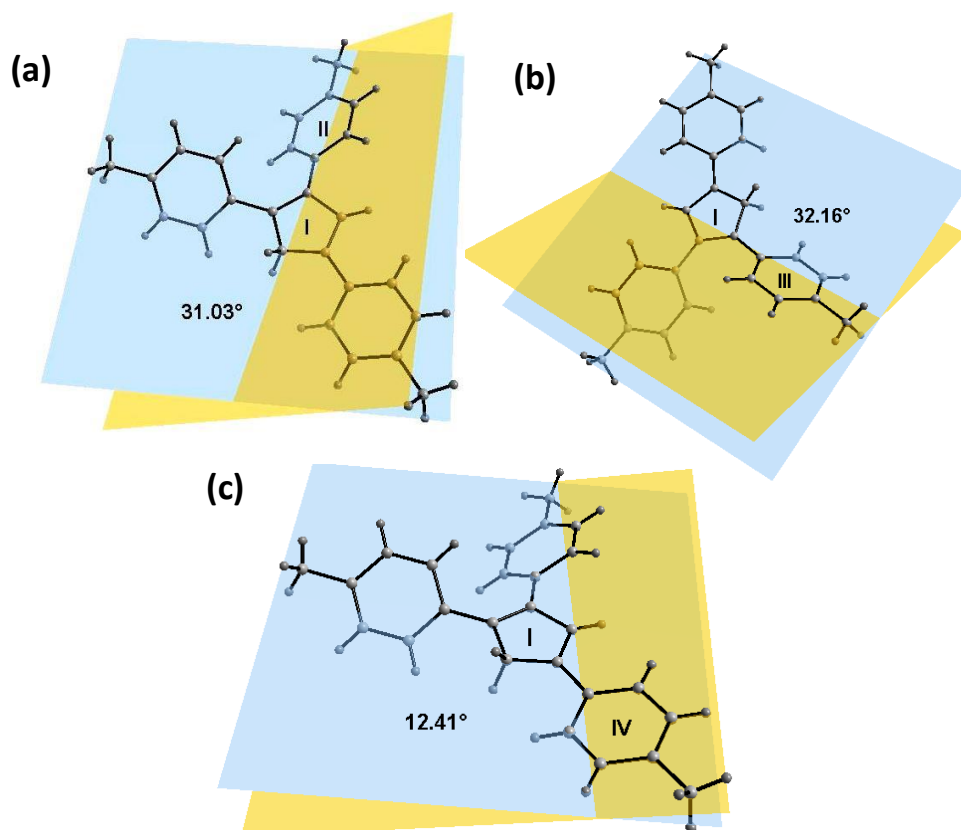
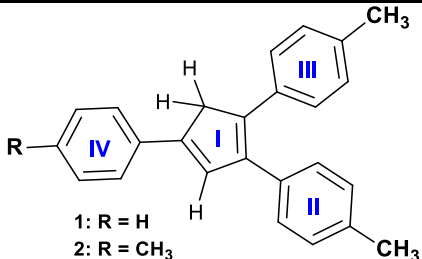


Figure S15. The molecular planes passed through the atoms of cyclopentadienyl core (I) and substituted 4-methyl phenyl moieties (II, III and IV) in the molecular structure of **2**. The measured torsion angle between the planes of I-II, I-III and I-IV in **2** are 31.03°, 32.16° and 12.41°, respectively.

Table S2. Selected torsion angle between the planes of cyclopentadienyl core and substituted aromatic phenyl moieties of **1** and **2** in the single crystal.

 1: R = H 2: R = CH ₃	Torsion angle(°)		
	I-II	I-III	I-IV
1	35.66°	34.33°	6.58°
2	31.03°	32.16°	12.41°

The molecular structure **2** also adopts twisted conformation like **1** as shown in Figure S15. The planes of 4-methyl phenyl moieties (II and III, see ESI) substituted at C1 and C2 positions of the cyclopentadiene are twisted out with dihedral angles of 31.03° and 32.14° respectively, which are comparatively lower than those in **1** (Table S3). While C4 substituted 4-methyl phenyl moiety (IV) has largely deviated from the planer Cp ring (I) as found out from its dihedral angle 12.41° , which is significantly higher than those in **1**. The dimeric structure of **2** was given in Figure S18, whereas the distance between two independent Cp molecules are separated with a centroid distance of 4.1672 \AA . The sequential packing of these dimeric species in the crystal lattice further lead to butterfly-like molecular columns as shown in Figure S18b. Moreover, the packing arrangement of **2** viewed along the *c* axis is given in Figure S18. It is worth mentioning that the dimeric species in the molecular column is stabilized by the way of C-H $\cdots\pi$ interactions (I': 3.067 - 3.564 \AA and II'': 3.502 \AA) exerted between them, which means intermolecular motions are not free between the molecules (Figure S16). Due to the strong packing features of molecules at their solid state are might be beneficial to the enhancement of PL intensity of **2** revealed from their fluorescence/AIEE investigations.

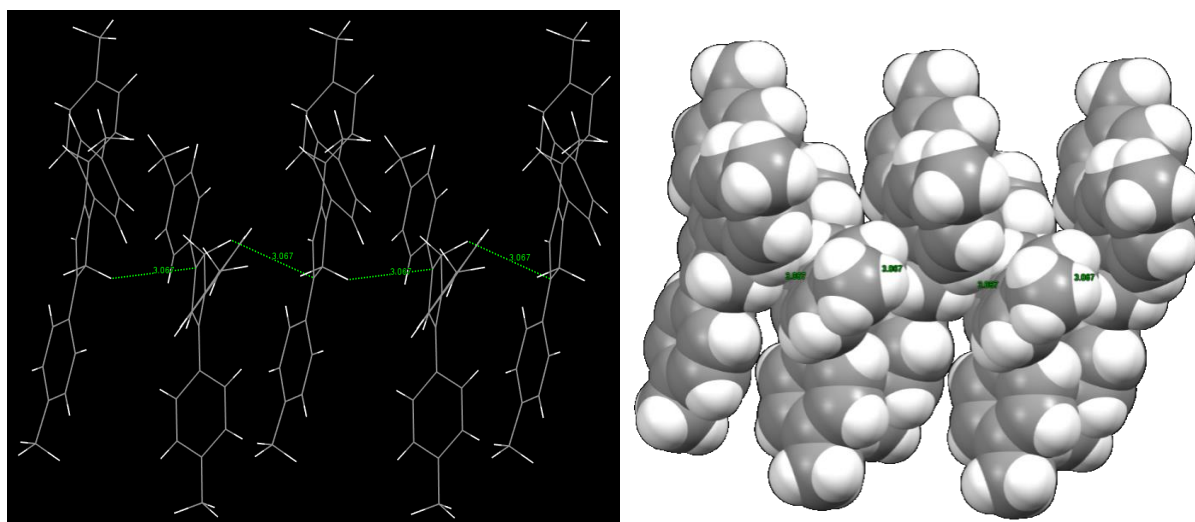


Figure S16. C-H of five membered Cp-ring $\cdots\pi$ of five membered ring of another Me₃Cp-H along 1D chain (left). So, the electrostatic C-H $\cdots\pi$ interactions are different in these two (**1**, **2**) compounds. Cp-ring to Cp-ring interaction is direct in Me₃Cp-H (**2**) and it is indirect for Me₂Cp-H (**1**) along a propagating 1D chain. The space filling model along 1D chain (right; grey: C; white: H).

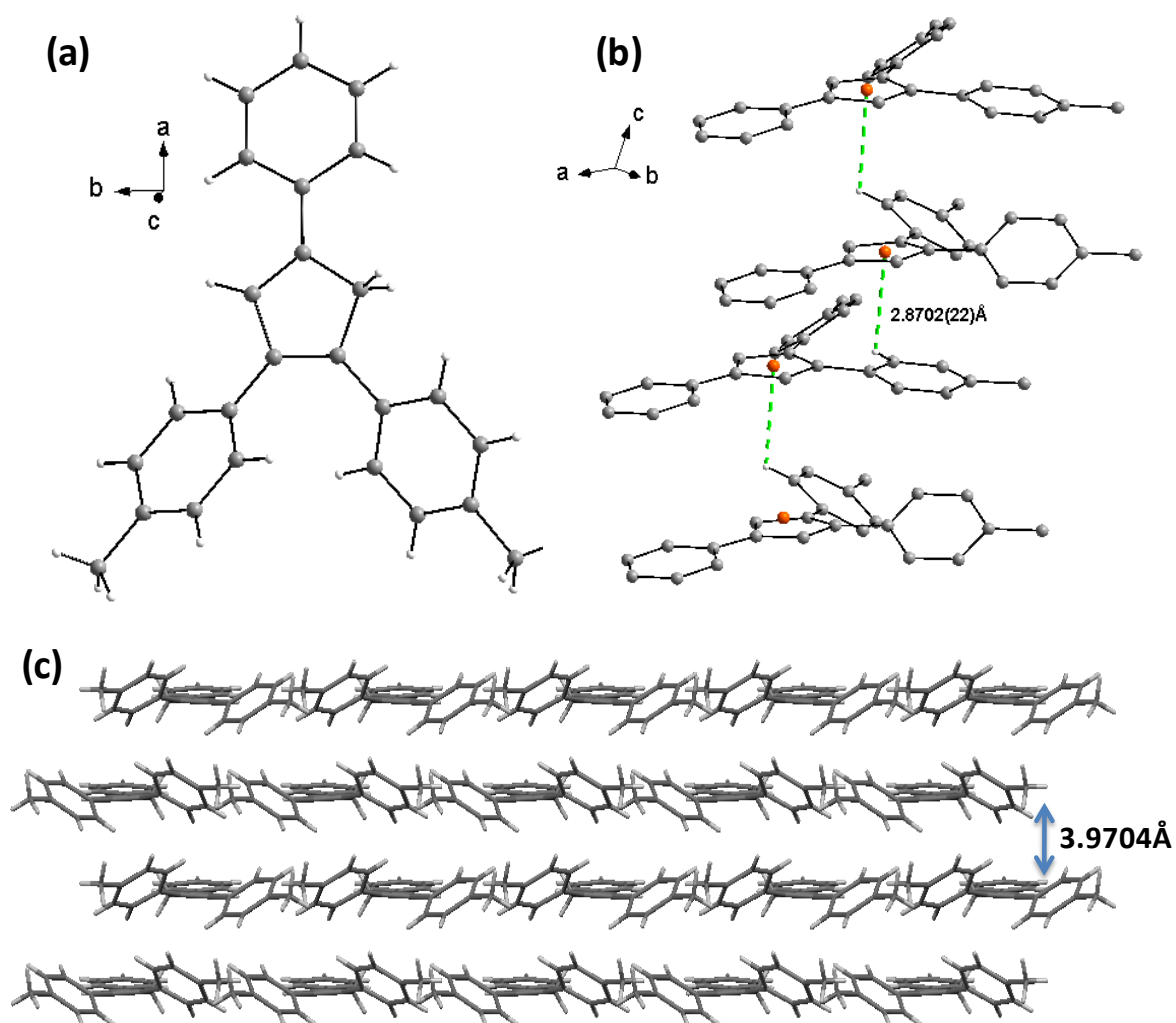


Figure S17.(a) Molecular structure of **1**; (b) stacking arrangement of **1**, where the CH... π distance between the molecules within the molecular column is 2.870 Å (hydrogen atoms are omitted for the clarity except the hydrogen atom which is involved in bonding); (c) The H...H interactions between the molecules of **1** led to 1D arrangement (view along *a* axis) and the distance between two independent 1D chains is 3.970 Å. Color code: carbon: grey; hydrogen: white.

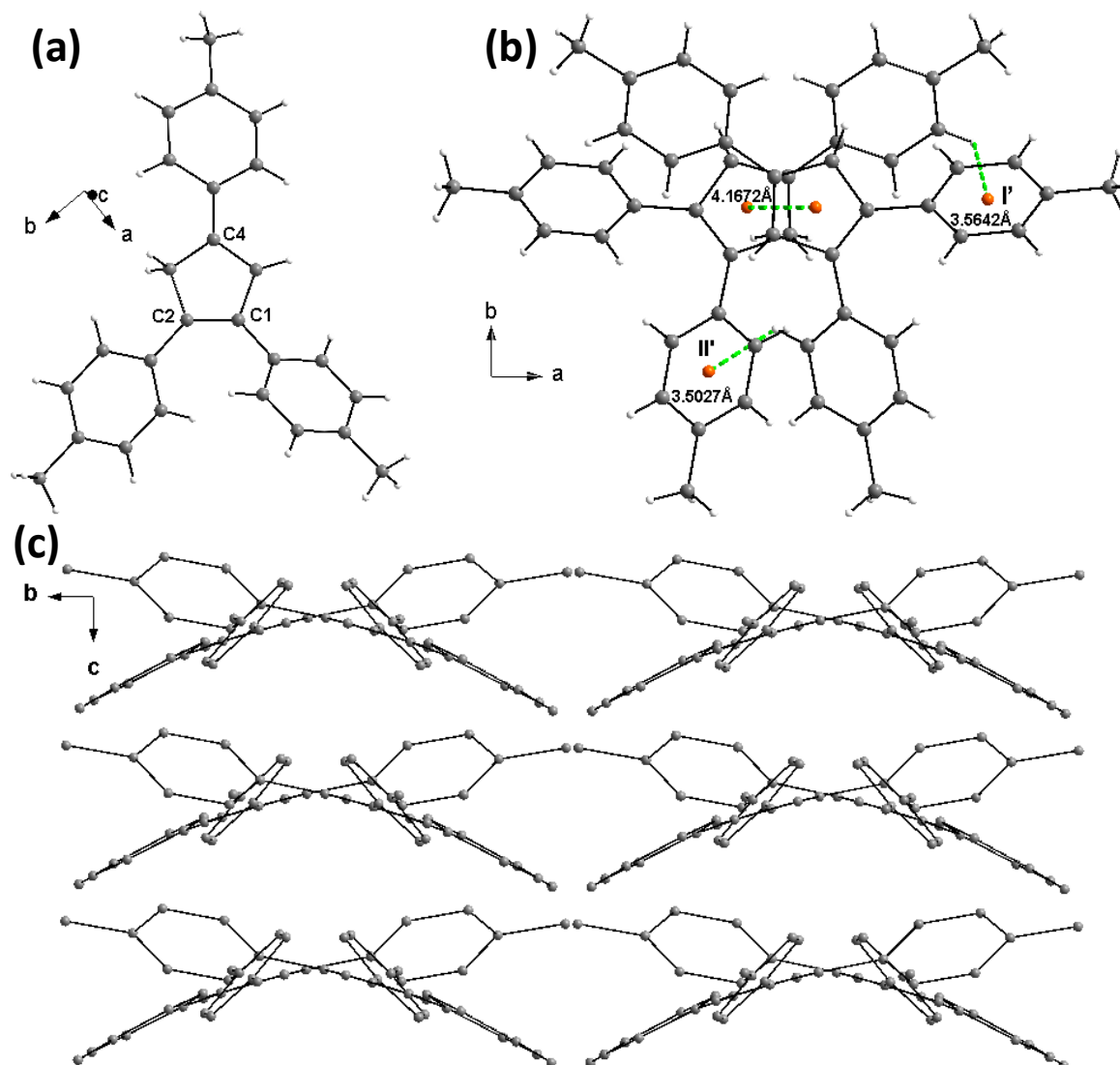


Figure S18. (a) Molecular structure of **2**; (b) The image showing dimeric structure of **2** (view along *c* axis) and the measured centroid distance between them is 4.167 Å. The CH... π interaction distances for interactions I' and II' in the dimeric form of **2** are 3.5642 Å and 3.5027 Å respectively; (c) butterfly-like packing features of **2** (view along *a* axis). Color code: carbon: grey; hydrogen: white.

S6. Computational details

S6.1. General remarks:

All DFT calculations on Me₂Cp-H (**1**) and Me₃Cp-H (**2**) were carried out using Gaussian 09 program suite.⁹ Geometry optimisations were performed at BP86¹⁰/def2TZVP¹¹ level of theory alongwith Grimme's dispersion correction (GD3).¹² Vibrational frequency analysis was carried out at BP86(GD3)/def2TZVP level of

theory to verify the obtained structures as true minima (absence of imaginary frequency). NBO analysis¹³ was carried out on the optimised structures at M06-2X¹⁴ (GD3)/def2TZVP level of theory. TDDFT analysis was carried out on the optimised structures at M06-2X(GD3)/def2TZVP level of theory with default salvation model (SMD) in solvents: acetone and chloroform.

S6.2. Geometry optimization and NBO calculations for Me₂Cp-H (1) and Me₃Cp-H (2):

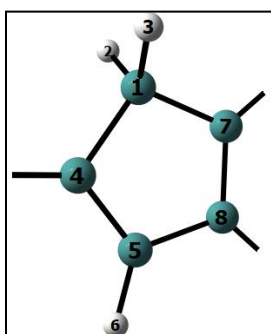


Figure S19: Cyclopentadiene core with aryl substitutions at C4, C7 and C8. The atoms C1, H2, H3, C4, C5, C7 and C8 mentioned in the below tables are shown here.

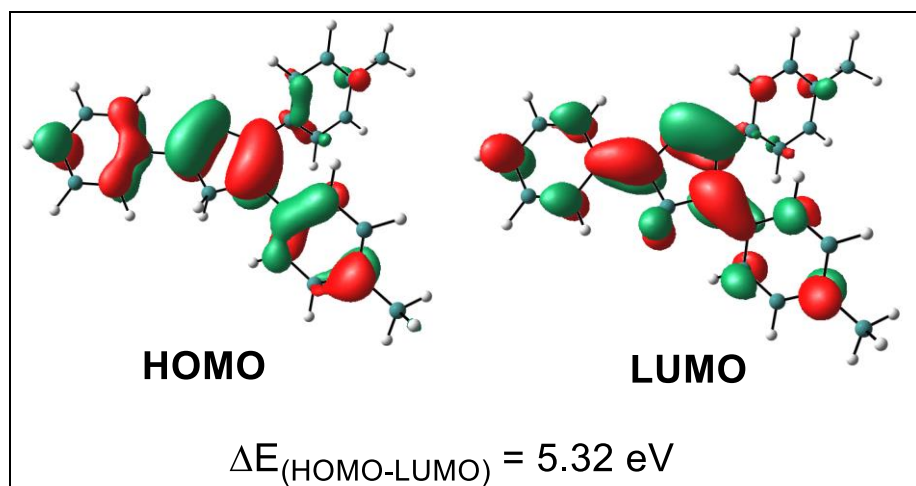


Figure S20. Frontier Molecular Orbitals of **1**.

1 and **2** were further studied by DFT calculations. The optimised geometries of **1** and **2** are similar to their respective molecular structure determined by X-Ray Diffraction (Table S3). NBO analysis reveals a slightly lower WBI value (1.69 and 1.63) for double bonds in the cyclopentadienyl core than expected (1.8-2.1), presumably due

to the extensive conjugation (Tables S4 and S5). HOMO of **1** and **2** is predominantly of the π -symmetry of the two double bonds of the cyclopentadienyl core while the LUMO is formed majorly by the π^* molecular orbitals (Figure S21). Both compounds feature a very high HOMO-LUMO energy gap, pegged at 5.32 eV for **2**. TDDFT analysis of **1** indicates two absorption bands (π to π^* class): one at 275 nm due to the electronic transition between HOMO and LUMO+1 and the other at 378 nm due to the electronic transition between HOMO and LUMO (Figures S21 and S23). **2** also display similar UV-Vis absorption characteristics (Figure S24-S26). The predicted absorption spectra match well with that of the experimental spectra (within the error limit of ± 20 nm).

Table S3: Comparison of experimental bond lengths of cyclopentadienyl core with those in the computationally optimised structure (predicted).

Bond	Me ₂ Cp-H (1)		Me ₃ Cp-H (2)	
	Predicted (Å)	Experimental (Å)	Predicted (Å)	Experimental (Å)
C1-H2	1.104	0.9697(27)	1.104	0.9691(23)
C1-H3	1.105	0.9703(30)	1.105	0.9703(23)
C1-C4	1.510	1.3799(38)	1.510	1.4344(32)
C1-C7	1.512	1.4722(40)	1.512	1.4898(33)
C7-C8	1.380	1.3666(33)	1.380	1.3704(31)
C4-C5	1.367	1.4791(37)	1.367	1.4150(34)
C5-C8	1.458	1.5045(40)	1.458	1.4807(33)

Table S4: NBO analysis (important bonds only) of Me₃Cp-H (**2**) and Me₂Cp-H (**1**) at M06-2X(GD3)/def2TZVP level of theory.

Bond of 1	Occupancy	Atomic contribution	WBI
C1-H2	1.954	C (sp ^{3.5}) - 62%, H - 38%	0.888
C1-H3	1.948	C (sp ^{3.6}) - 62%, H - 38%	0.884
C4-C5	1.980	C4 (sp ^{1.8}) - 51%, C5 (sp ^{1.7}) - 49%,	1.692
C4-C5	1.839	C4 (p) - 50%, C5 (p) - 50%,	
C7-C8	1.973	C7 (sp ^{1.8}) - 50%, C9 (sp ^{1.8}) - 50%,	1.631
C7-C8	1.818	C4 (p) - 50%, C5 (p) - 50%,	
Bond of 2	Occupancy	Atomic contribution	WBI
C1-H2	1.954	C (sp ^{3.5}) - 62%, H - 38%	0.888
C1-H3	1.948	C (sp ^{3.6}) - 62%, H - 38%	0.884
C4-C5	1.979	C4 (sp ^{1.8}) - 51%, C5 (sp ^{1.7}) - 49%,	1.691
C4-C5	1.839	C4 (p) - 50%, C5 (p) - 50%,	1.691
C7-C8	1.972	C7 (sp ^{1.8}) - 50%, C9 (sp ^{1.8}) - 50%,	1.691
C7-C8	1.819	C4 (p) - 50%, C5 (p) - 50%,	1.631

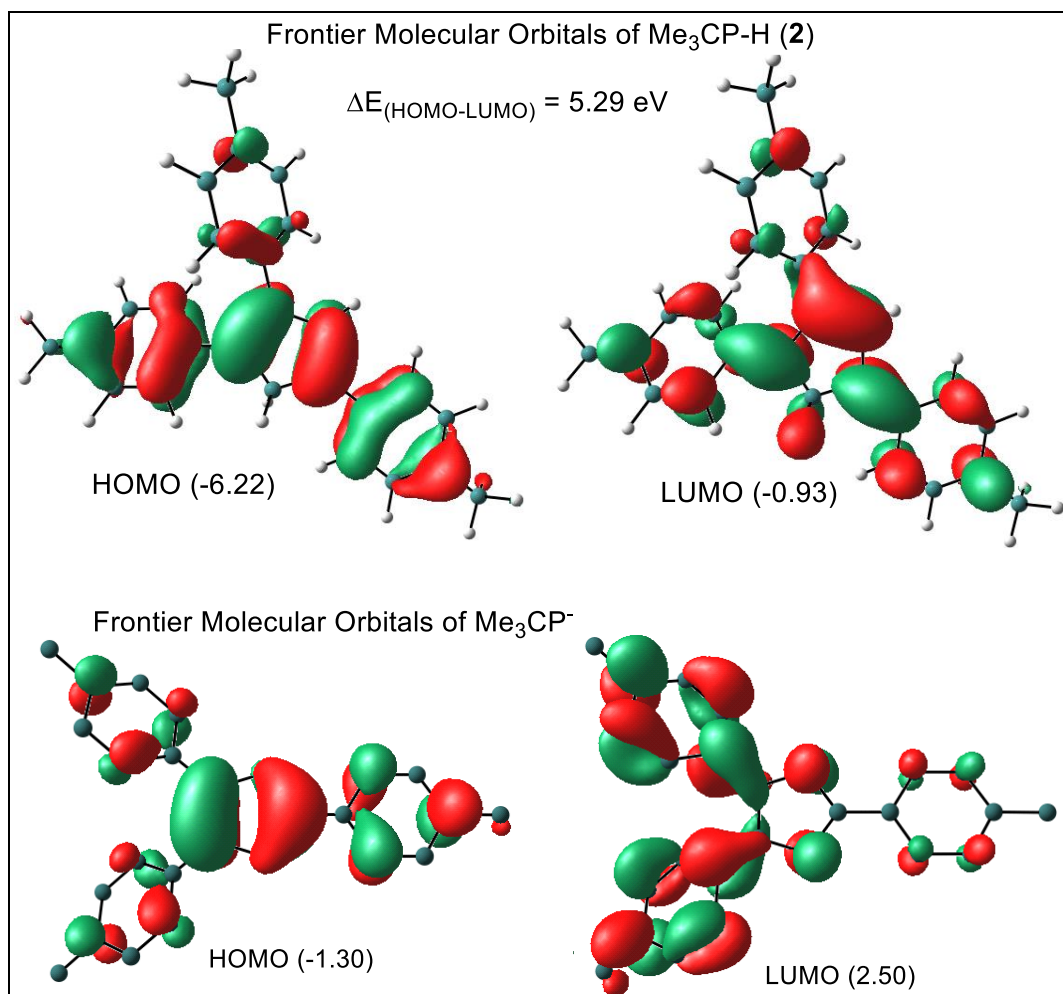


Figure S21. Frontier Molecular Orbitals of Me₃Cp-H (2) and Me₃Cp⁻ anion.

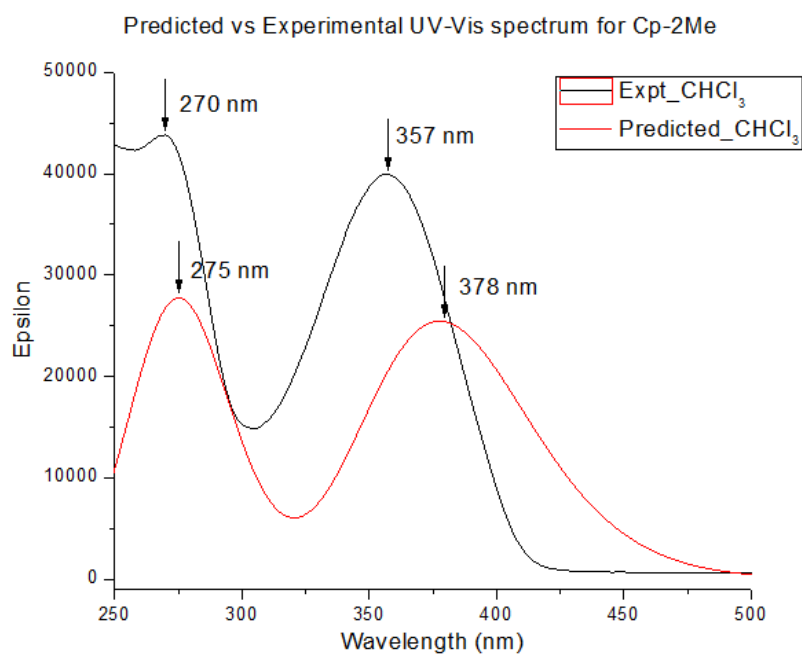


Figure S22. Predicted vs Experimental UV/vis spectrum for Me₂Cp-H (1) in chloroform.

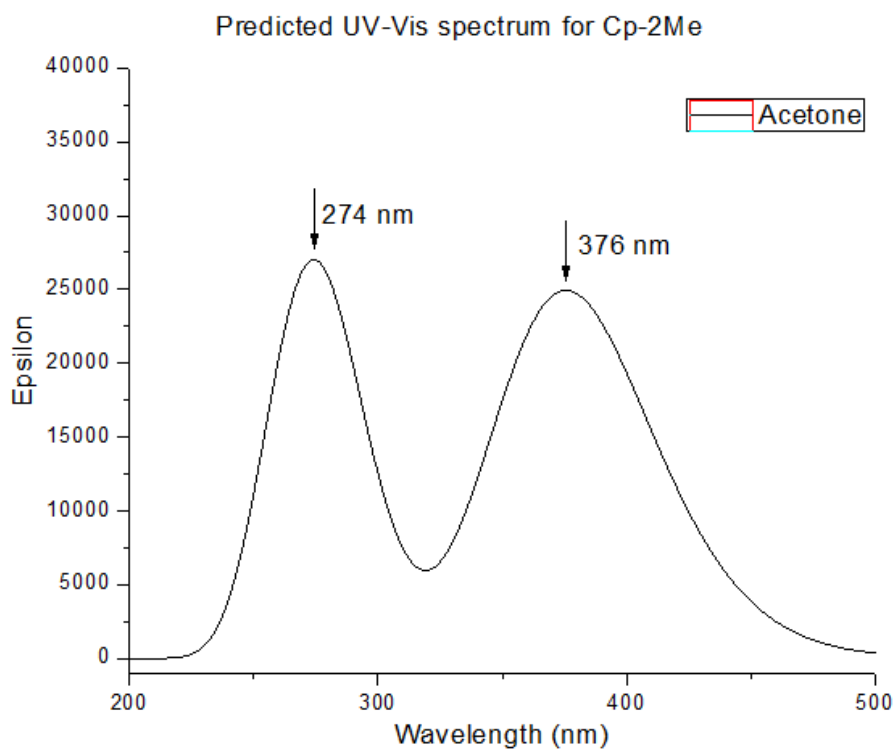


Figure S23. Predicted UV-Vis spectrum for Me₂Cp-H (1) in acetone.

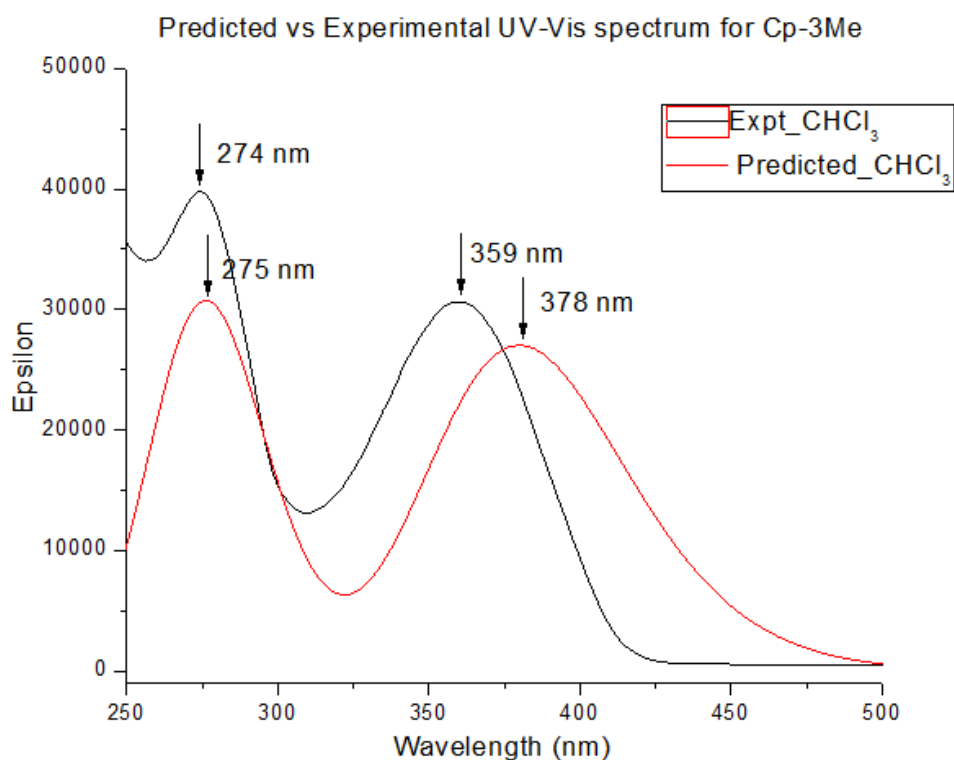


Figure S24. Predicted vs Experimental UV-Vis spectrum for Me₃Cp-H (2) in chloroform.

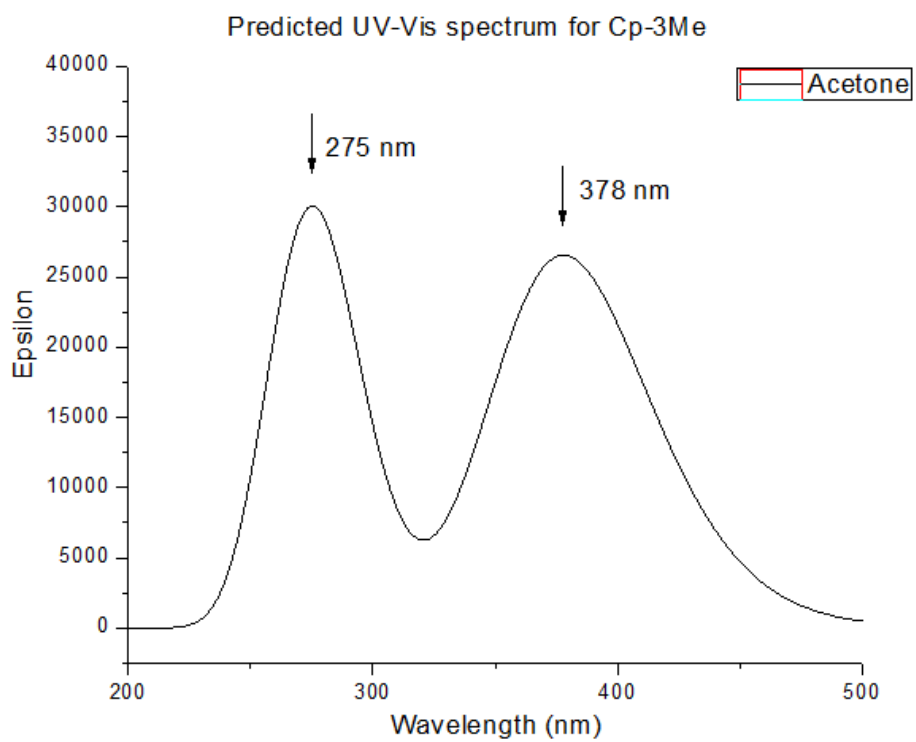


Figure S25. Predicted UV/vis spectrum for Me₃Cp-H (**2**) in acetone.

Orbitals involved in transitions occurring in UV-Vis spectrum for Me₃Cp-H (2):

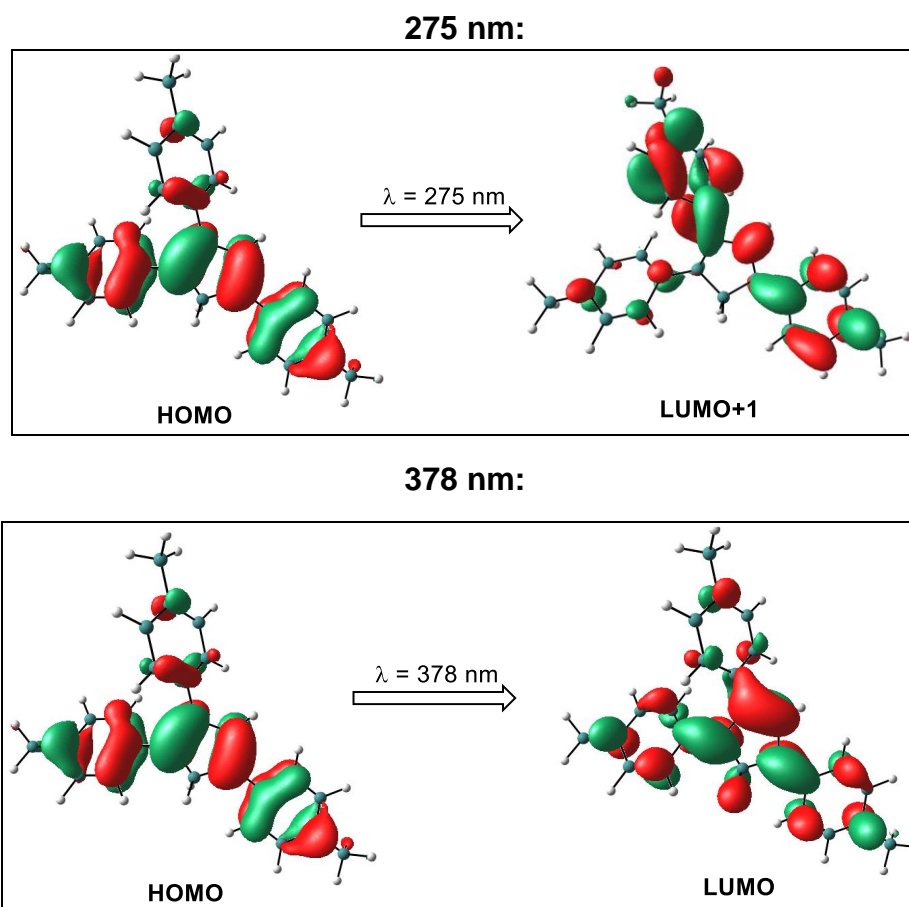


Figure S26. Both Me₂Cp-H (1) and Me₃Cp-H (2) show similar UV-vis spectrum with the same frontier orbitals involved in the transitions. Only the frontier orbitals for Me₃Cp-H (2) involved in transition is shown here. The solvent dependence is also similar for both Me₂Cp-H (1) and Me₃Cp-H (2) without any effect on the orbitals involved in transitions.

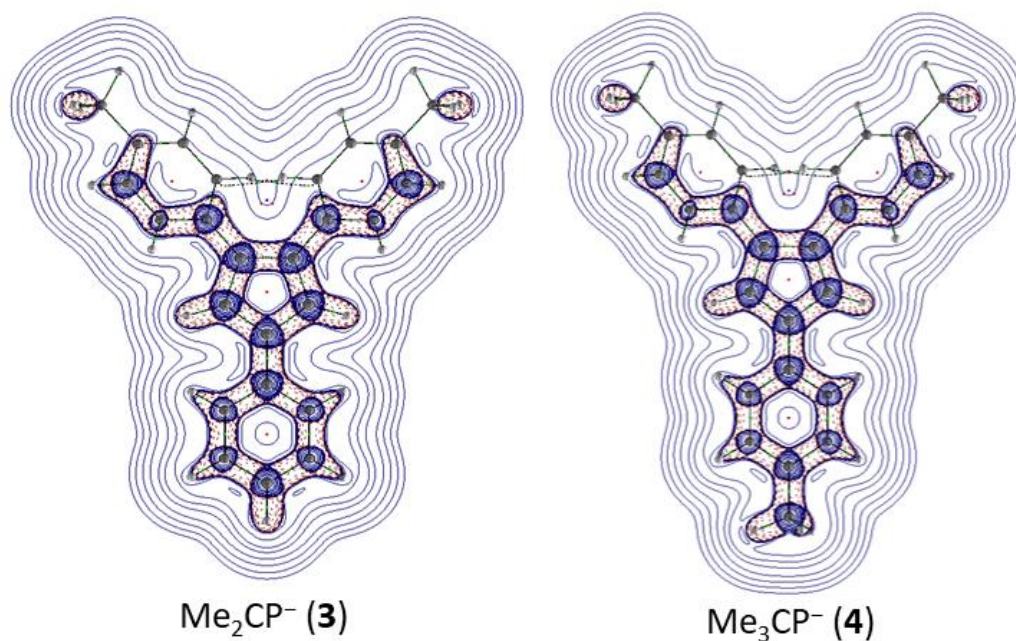


Figure S27. Laplacian contour plots of Me_2Cp^- (**3**) and Me_3Cp^- (**4**).

Table S5. AIM results of the C(Cp) - C(Ph) bond of **1-4** at the M06/def2TZVPP level of theory.

Ligand	$\rho(r)$	$\nabla^2\rho(r)$	$H(r)$	$V(r)$	$G(r)$	ϵ
1	0.279	-0.780	-0.73	-0.341	0.268	0.079
2	0.279	-0.782	-0.74	-0.342	0.268	0.080
3	0.281	-0.784	-0.78	-0.352	0.274	0.107
4	0.281	-0.782	-0.78	-0.351	0.273	0.106

Table S6: NBO analysis (important bonds only) of Me₂Cp⁻ anion at M06(GD3)/def2TZVP level of theory.

Bond	Occupancy	Atomic contribution	WBI
C1-H2	1.98	C1 (sp ^{2.3}) - 59%, H2 - 41%	0.94
C1-C3	1.97	C1 (sp ^{1.9}) - 49%, C3 (sp ^{2.0}) - 51%	1.32
C1-C6 (1)	1.97	C1 (sp ^{1.8}) - 49%, C6 (sp ^{2.0}) - 51%	1.41
C1-C6 (2)	1.77	C1 (p) - 51%, C6 (p) - 49%	
C3-C4 (1)	1.97	C3 (sp ^{2.0}) - 51%, C4 (sp ^{1.9}) - 49%	1.32
C3-C4 (2)	1.70	C3 (p) - 51%, C4 (p) - 49%	
C4-H5	1.98	C4 (sp ^{2.3}) - 59%, H5 - 41%	0.94
C4-C7	1.97	C4 (sp ^{1.8}) - 49%, C7 (sp ^{2.0}) - 51%	1.41
C6-C7	1.96	C6 (sp ^{1.8}) - 50%, C7 (sp ^{2.0}) - 50%	1.22

Table S7. Comparison of absolute energies of HOMO and LUMO of Me_nCp-H and their corresponding anions at M06(GD3)/def2TZVP level of theory (gas phase).

Compound	Me ₂ Cp-H	Me ₂ Cp ⁻	Me ₃ Cp-H	Me ₃ Cp ⁻
HOMO (eV)	-6.30	-1.33	-6.22	-1.30
LUMO (eV)	-0.99	2.49	-0.93	2.50

S6.3. Geometry optimization and NBO analysis of the singlet biradical state (excited state) of Me₂Cp-H (1)

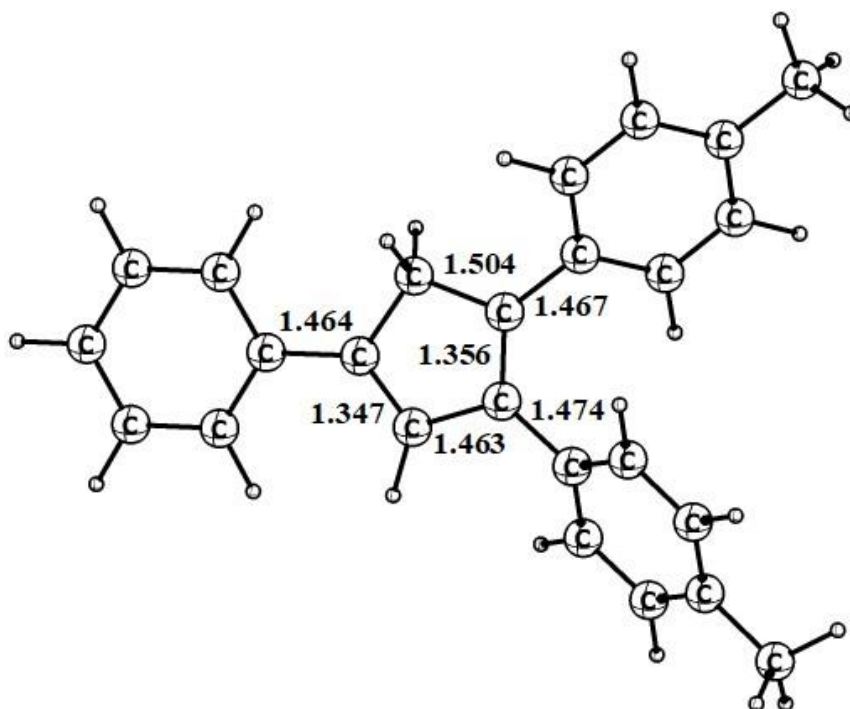


Figure S28. Optimized geometry of Me₂Cp-H (1) in singlet biradical state at UM062x/Def2TZVPP//BP86/def2TZVPP level of theory.

The of Me₂Cp-H (1) molecule has been optimized at UM062x/Def2TZVPP//BP86/def2TZVPP level of theory. Molecular orbital analysis has been performed to confirm the formation of singlet biradical. The different orientation of molecular orbitals at α and β SOMO's as shown in Figure S60 indicates the formation of singlet biradical. The calculations predict that singlet state is more stable than singlet biradical state by 70.58 kcal/mol. Molecular orbitals of α-

and β - states from SOMO-1 to SOMO-5 (Figures S28-S29) shows the π electron delocalization of electrons over the substituted aromatic rings. SOMO-6 indicates the π electron delocalization of electrons from aromatic rings to Cp ring while SOMO-7 represents the π electron delocalization in Cp ring of **1**.

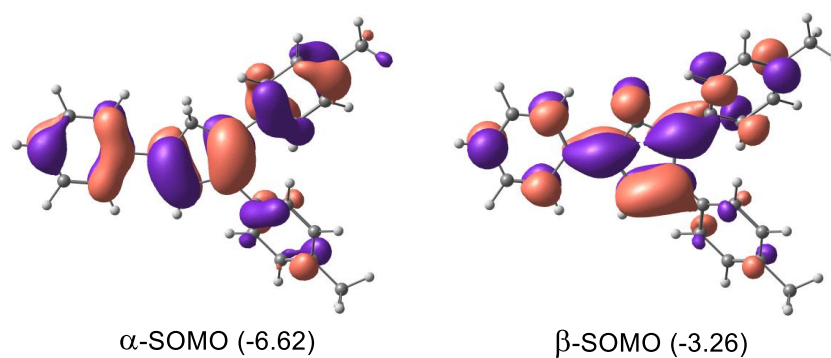


Figure S29. α - and β -SOMO of Me₂Cp-H (**1**) singlet biradical state at UM062x/Def2TZVPP//BP86/def2TZVPP level.

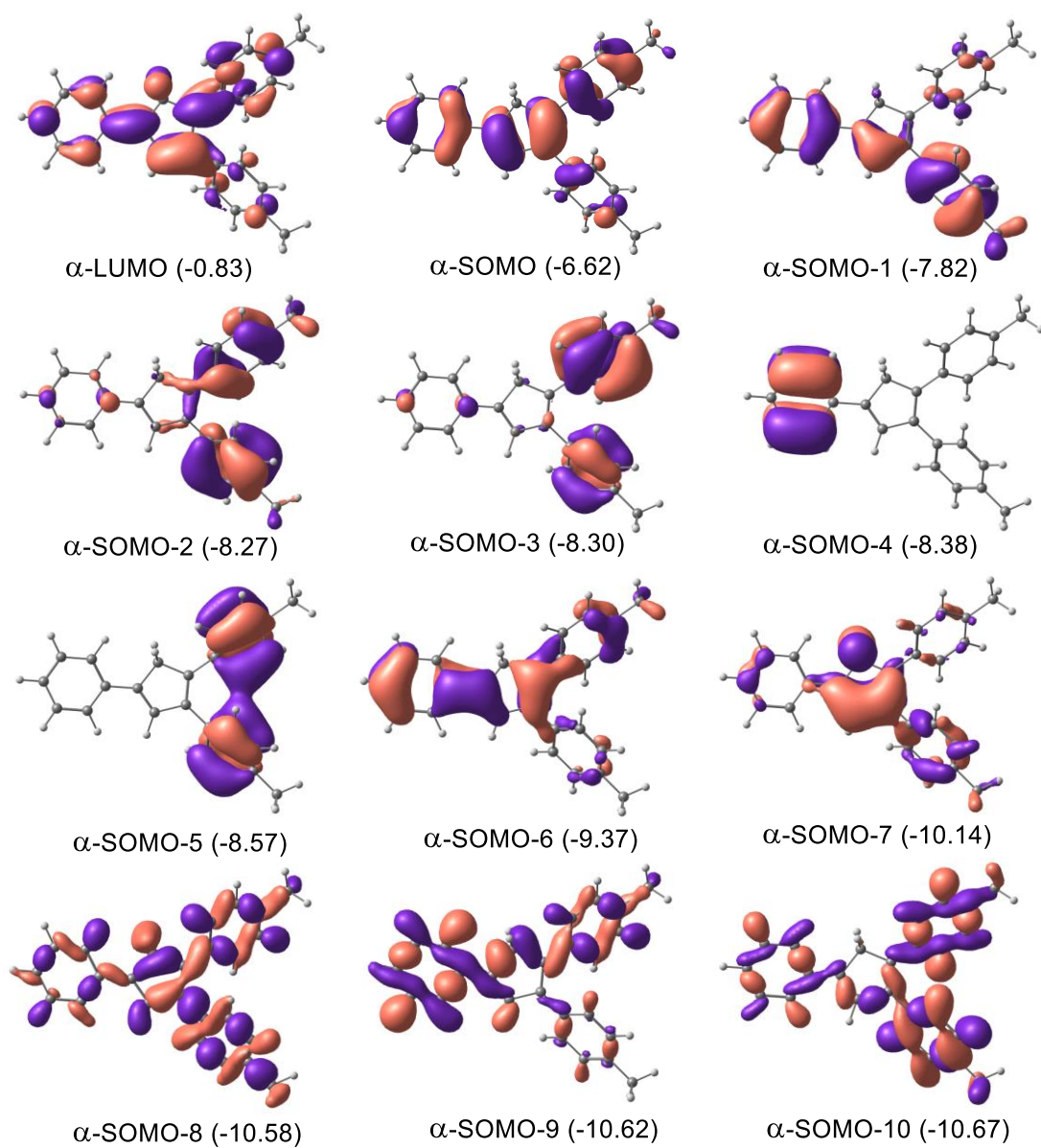


Figure S30. α -MOs of Me₂Cp-H (1) singlet biradical state at UM062x/Def2TZVPP//BP86/def2TZVPP level.

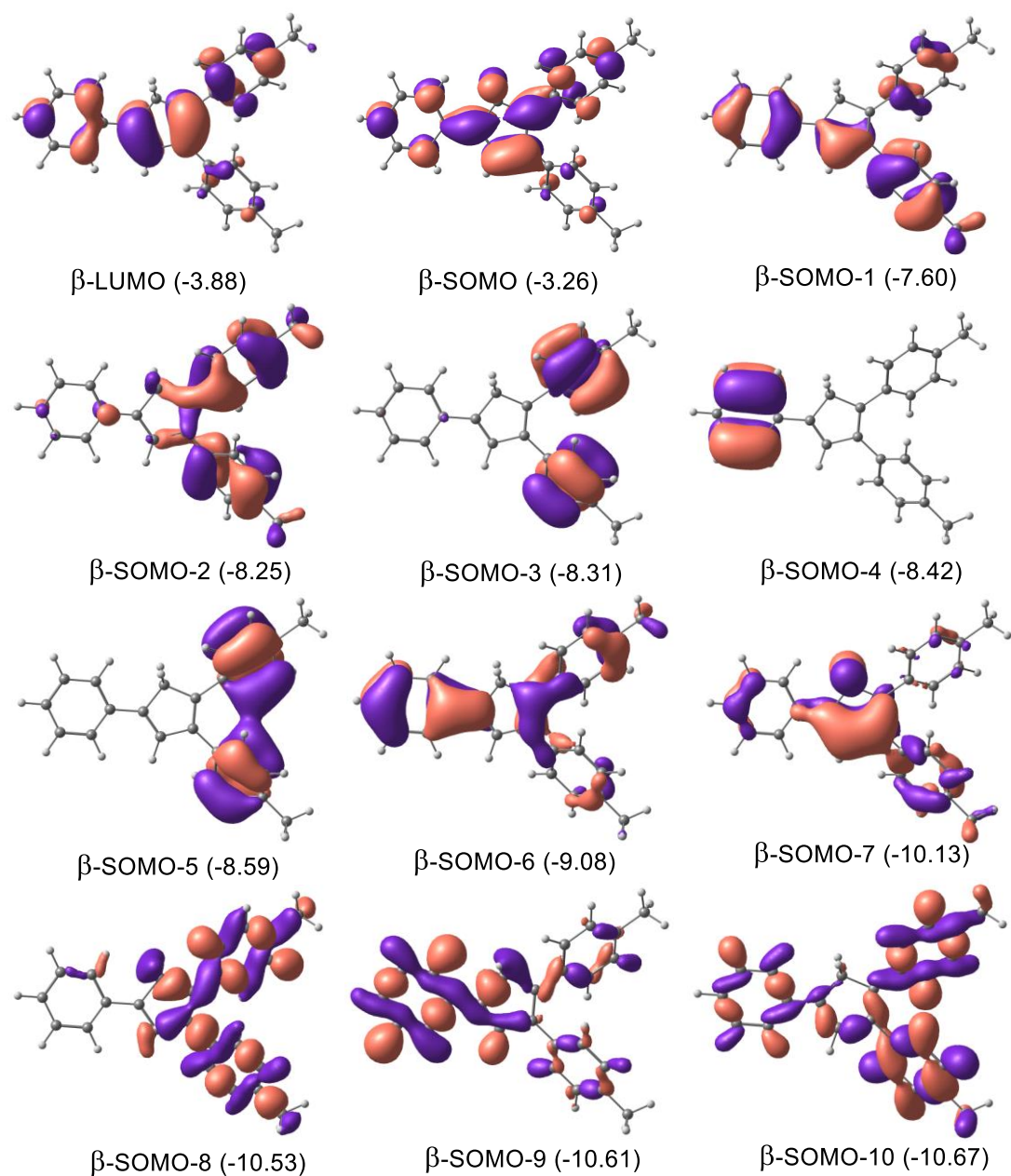


Figure S31. β -MO's of Me₂Cp-H (1) singlet biradical state at UM062x/Def2TZVPP//BP86/def2TZVPP level.

S6.4. Optimized coordinates

Me₂Cp-H (1):

6	-1.464379000	-1.215753000	-0.048586000
1	-1.663097000	-1.909819000	0.786054000
1	-1.669025000	-1.785692000	-0.973271000
6	-2.319034000	0.026834000	0.016837000
6	-1.470485000	1.098241000	0.055485000

1	-1.759526000	2.149280000	0.065558000
6	-0.039615000	-0.711981000	-0.017318000
6	-0.078613000	0.667184000	0.019858000
6	1.039765000	1.626113000	-0.035833000
6	1.058559000	2.762518000	0.790614000
6	2.102337000	1.455461000	-0.944211000
6	2.109998000	3.680558000	0.726043000
1	0.248926000	2.916813000	1.507853000
6	3.144498000	2.376056000	-1.007741000
1	2.101143000	0.585220000	-1.602799000
6	3.171638000	3.506839000	-0.172269000
1	2.104874000	4.549531000	1.389256000
1	3.955470000	2.219600000	-1.724327000
6	1.104699000	-1.619351000	0.036523000
6	1.051441000	-2.890007000	-0.573463000
6	2.289108000	-1.289678000	0.734554000
6	2.131215000	-3.771932000	-0.509892000
1	0.157169000	-3.186725000	-1.125317000
6	3.360428000	-2.174611000	0.794829000
1	2.356636000	-0.327949000	1.243993000
6	3.308750000	-3.434396000	0.171547000
1	2.058025000	-4.743859000	-1.005172000
1	4.259145000	-1.887572000	1.347855000
6	-3.777595000	0.016126000	0.007391000
6	-4.493497000	-1.195001000	-0.118431000
6	-4.530116000	1.207334000	0.126476000
6	-5.888816000	-1.214977000	-0.129518000
1	-3.949249000	-2.136716000	-0.211480000
6	-5.922301000	1.186316000	0.114736000
1	-4.013043000	2.162473000	0.234512000

6	-6.613775000	-0.025321000	-0.014229000
1	-6.413548000	-2.167502000	-0.229843000
1	-6.476154000	2.122885000	0.208722000
6	4.298493000	4.505554000	-0.263740000
1	5.279148000	4.005654000	-0.241025000
1	4.247518000	5.073443000	-1.207160000
1	4.265696000	5.229060000	0.562969000
6	4.472161000	-4.389581000	0.260840000
1	5.421863000	-3.888715000	0.017037000
1	4.574234000	-4.794872000	1.281147000
1	4.349702000	-5.239968000	-0.424587000
1	-7.705083000	-0.039860000	-0.022999000

Me₃Cp-H (2):

6	-1.093333000	-1.213658000	-0.041887000
1	-1.292487000	-1.907740000	0.792631000
1	-1.300039000	-1.782649000	-0.966644000
6	-1.946659000	0.030036000	0.024997000
6	-1.096719000	1.100571000	0.063898000
1	-1.384449000	2.151954000	0.074666000
6	0.332461000	-0.711735000	-0.012025000
6	0.294551000	0.667379000	0.026105000
6	1.413664000	1.625377000	-0.032044000
6	1.435837000	2.761447000	0.794800000
6	2.473108000	1.454875000	-0.944134000
6	2.487359000	3.679206000	0.726981000
1	0.628536000	2.915724000	1.514660000
6	3.515352000	2.375170000	-1.010944000
1	2.469267000	0.584849000	-1.603000000
6	3.545754000	3.505629000	-0.175165000

1	2.484823000	4.547966000	1.390520000
1	4.323763000	2.218734000	-1.730455000
6	1.475694000	-1.620370000	0.039192000
6	1.418469000	-2.892344000	-0.567870000
6	2.663789000	-1.291286000	0.731575000
6	2.497513000	-3.775507000	-0.507449000
1	0.521238000	-3.189334000	-1.114752000
6	3.734459000	-2.177162000	0.788315000
1	2.734661000	-0.329016000	1.239535000
6	3.678731000	-3.438037000	0.167455000
1	2.420654000	-4.748487000	-1.000173000
1	4.635944000	-1.890126000	1.336887000
6	-3.404315000	0.020064000	0.014810000
6	-4.126090000	-1.185228000	-0.110763000
6	-4.160033000	1.210025000	0.128622000
6	-5.521498000	-1.199494000	-0.127236000
1	-3.588358000	-2.130939000	-0.202705000
6	-5.549726000	1.188807000	0.111393000
1	-3.645839000	2.167148000	0.234249000
6	-6.264457000	-0.016439000	-0.017558000
1	-6.045534000	-2.153516000	-0.230425000
1	-6.100528000	2.129452000	0.199694000
6	4.672594000	4.504086000	-0.270319000
1	5.653265000	4.004122000	-0.248582000
1	4.620057000	5.070515000	-1.214545000
1	4.641420000	5.228868000	0.555347000
6	4.842642000	-4.393166000	0.251377000
1	5.787560000	-3.898614000	-0.022626000
1	4.966318000	-4.778245000	1.277043000
1	4.705023000	-5.256568000	-0.414639000

6	-7.772081000	-0.023734000	-0.020981000
1	-8.170434000	-1.012692000	-0.287928000
1	-8.172850000	0.241559000	0.971293000
1	-8.174406000	0.709962000	-0.736916000

Me₂Cp-H in Singlet Biradical state (UM062x/Def2TZVPP)

Energy: -965.7235639

6	1.461261000	-1.214741000	0.035419000
1	1.653287000	-1.882243000	-0.810565000
1	1.665426000	-1.794117000	0.942990000
6	2.306642000	0.026139000	-0.008035000
6	1.478737000	1.088324000	-0.023691000
1	1.768251000	2.130367000	-0.018991000
6	0.047230000	-0.701847000	0.018624000
6	0.082341000	0.653539000	0.003848000
6	-1.036761000	1.610678000	0.055807000
6	-1.028568000	2.750518000	-0.744315000
6	-2.114737000	1.422035000	0.923194000
6	-2.073627000	3.662978000	-0.694976000
1	-0.203129000	2.915578000	-1.426807000
6	-3.151043000	2.336428000	0.971659000
1	-2.131767000	0.547565000	1.561699000
6	-3.150758000	3.472901000	0.162568000
1	-2.050631000	4.536859000	-1.335569000
1	-3.977460000	2.170803000	1.653619000
6	-1.105684000	-1.606892000	-0.038327000
6	-1.081461000	-2.835334000	0.622081000
6	-2.245179000	-1.295573000	-0.789893000
6	-2.159531000	-3.707100000	0.556048000
1	-0.213784000	-3.110952000	1.208571000

6	-3.314511000	-2.168563000	-0.853079000
1	-2.279782000	-0.362565000	-1.337331000
6	-3.295635000	-3.389410000	-0.177530000
1	-2.114479000	-4.651236000	1.086271000
1	-4.182403000	-1.904541000	-1.447045000
6	3.770082000	0.010872000	-0.005236000
6	4.469013000	-1.194195000	0.098541000
6	4.512044000	1.192719000	-0.109568000
6	5.855953000	-1.219507000	0.102735000
1	3.921579000	-2.124964000	0.178131000
6	5.894902000	1.168405000	-0.104863000
1	3.997281000	2.140478000	-0.199570000
6	6.576277000	-0.039041000	0.002156000
1	6.374280000	-2.166229000	0.185103000
1	6.447178000	2.095803000	-0.186921000
6	-4.273964000	4.469008000	0.241931000
1	-5.243278000	3.969147000	0.233140000
1	-4.213646000	5.048064000	1.165922000
1	-4.241736000	5.167687000	-0.593069000
6	-4.471443000	-4.322816000	-0.252244000
1	-5.358617000	-3.868264000	0.192910000
1	-4.714523000	-4.562930000	-1.288687000
1	-4.269689000	-5.254791000	0.273953000
1	7.658151000	-0.056677000	0.005136000

S7. Crystallographic details for complexes 5 and 6

CCDC reference numbers: 2006659, 2007965 contains the supplementary crystallographic data for complexes **5** and **6**, respectively.

S7.1 Crystallographic details for compounds 5 and 6

Table S8. crystal data and structure refinement for compounds **5** and **6**

Complex	5	6
Formula	C ₁₂₁ H ₁₀₈ Cl ₄ Dy ₂ K ₂	C ₁₂₅ H ₁₁₆ Cl ₄ Dy ₂ K ₂
Fw (g mol ⁻¹)	2107.07	2163.17
Temperature (K)	200(2)	200(2)
Wavelength (Å)	0.71073	0.71073
Crystal system	Triclinic	Triclinic
Space group	<i>P</i> -1	<i>P</i> -1
<i>a</i> (Å)	15.0406(5)	17.1088(7)
<i>b</i> (Å)	18.9527(6)	17.7780(8)
<i>c</i> (Å)	21.4668(8)	20.6046(9)
α (°)	65.2020(10)	69.756(2)
β (°)	78.557(2)	79.617(2)
γ (°)	67.6990(10) ^o	62.673(2)
Volume(Å ³)	5134.0(3)	5222.1(4)
<i>Z</i>	2	2

$\rho_{cal}(\text{mg}/\text{m}^3)$	1.363	1.376
μ (mm^{-1})	1.678	1.652
Reflections collected	88738	74623
Independent reflections	22712	[R_{int} = 19755 [R_{int} = 0.0521] 0.0362]
Data/restraints/parameters	22712 / 139 / 1162	19755 / 195 / 1198
GOOF (all data)	1.066	1.019
$R_1, wR_2[I > 2\sigma(I)]$	0.0334, 0.0810	0.0391, 0.0839
$R_1, wR_2(\text{all data})$	0.0451, 0.0854	0.0633, 0.0946
$\Delta\rho$ ($\text{e} \cdot \text{\AA}^{-3}$)	1.171 and -0.912	1.316 and -0.961

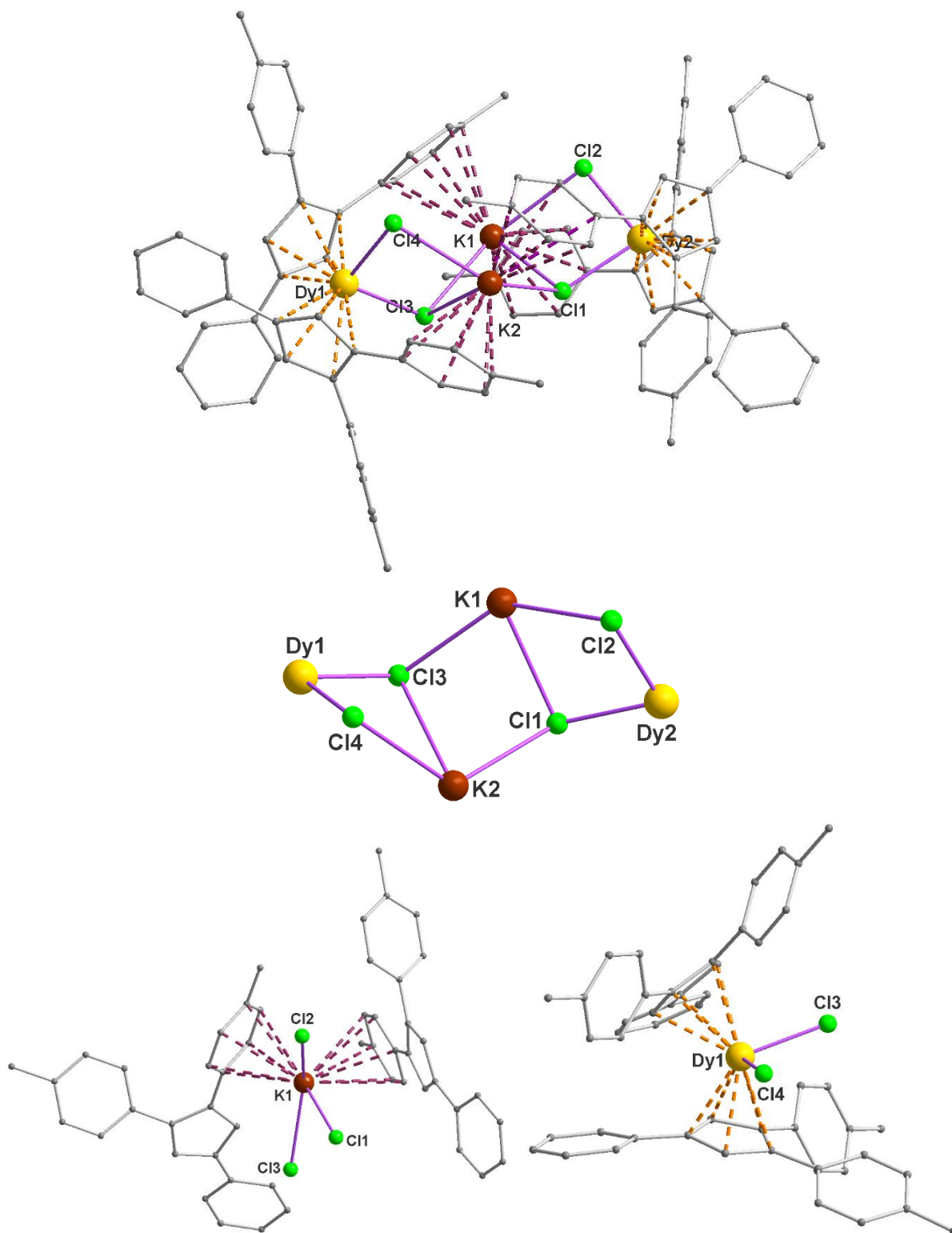


Figure S32. Molecular structure of **5** (top); Ladder-type assembly of $K_2Cl_4Dy_2$ core constructed by K_2Cl_2 unit together with two $\mu\text{-Cl}^-$ ions and two Dy^{III} ions (middle); Bonding scenario in K-sandwich constructed by the π -electronic cloud of two 4-methyl phenyl moieties shared by two individual Cp units (bottom, left); Dy^{III} ions stabilized between the π -electron clouds of two independent Cp units and its bonding scenario (bottom, right). The hydrogen atoms are omitted for the clarity.

S7.2 Structure description of complex $[(\text{Me}_3\text{Cp})_4\text{Dy}^{\text{III}}_2\text{Cl}_4\text{K}_2]\cdot 3(\text{C}_7\text{H}_8)$ (**6**):

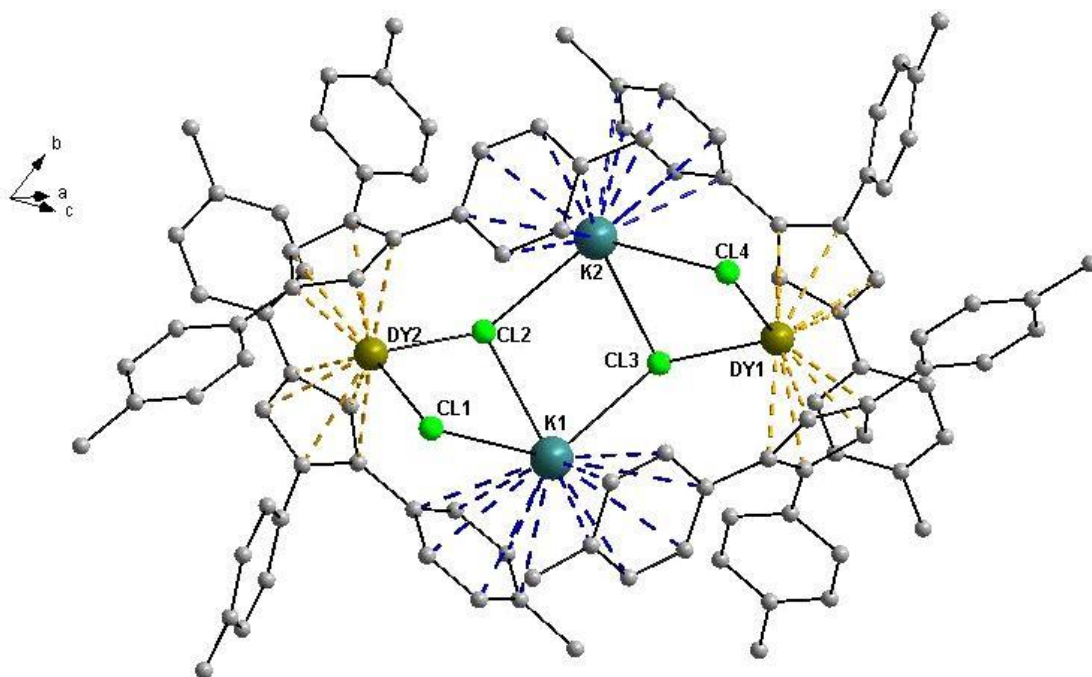


Figure S33. Molecular structure of **6** (hydrogen atoms and toluene molecules are omitted for the clarity).

The compound $[(\text{Me}_3\text{Cp})_4\text{Dy}^{\text{III}}_2\text{Cl}_4\text{K}_2]\cdot 3(\text{C}_7\text{H}_8)$ (**6**) also crystallizes in a triclinic crystal system with $P-1$ space group. The molecular structure of **6** was shown in Figure S28. The structure and bonding scenario of **6** is similar to **5**. For **6**, the $\text{Cp}_{\text{cen1}}\cdots\text{Dy}\cdots\text{Cp}_{\text{cen2}}$ and $\text{Aryl}_{\text{cen1}}\cdots\text{K}\cdots\text{Aryl}_{\text{cen2}}$ angles are in the range of 129.70° – 130.74° and 115.70° – 113.92° respectively. In addition, the measured Dy–Cl and K–Cl distances are in the range of 2.586–2.611 Å and 3.043–3.239 Å, respectively. For the better understanding, the selected bond lengths and bond angles of compounds **5** and **6** were given in the Table S5. The bonding modes of Dy^{III} and K⁺ ions in the molecular structure of **6** were given in the Figures S39–S40. Finally, the weak H \cdots H bonding interactions exerted between the molecules of **6** displayed a 1D chain like assembly in the crystal lattice. Further each of these independent 1D chains form a supramolecular 2D network by connecting each other through C–H \cdots π interactions (Figure S36).

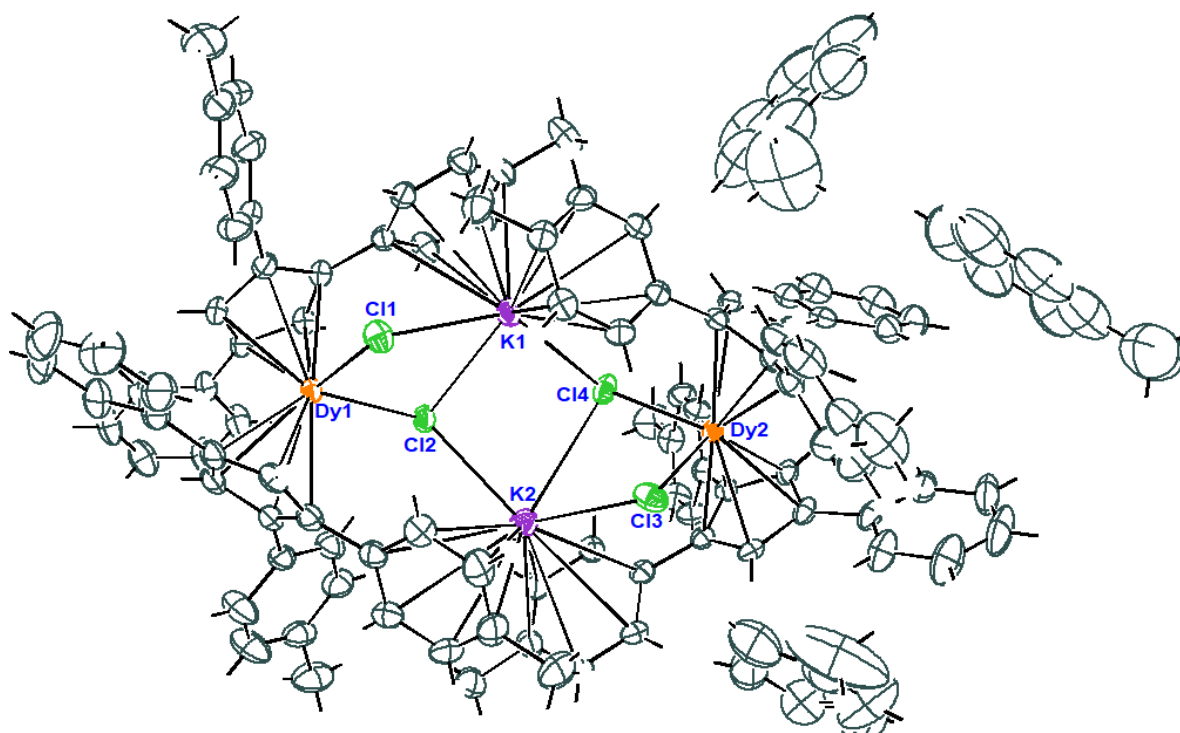


Figure S34. Asymmetric unit of **5** (ORTEP view). All the atoms are drawn at 50% probability level.

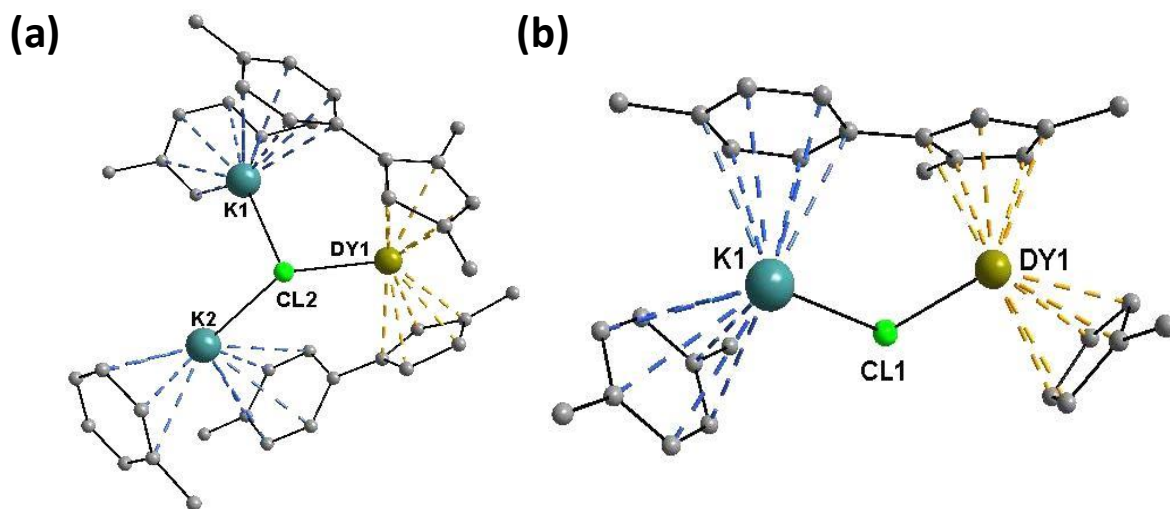


Figure S35. Bridging modes of μ_3 -chloride (a) and μ -chloride (b) ions in the molecular structure **5**.

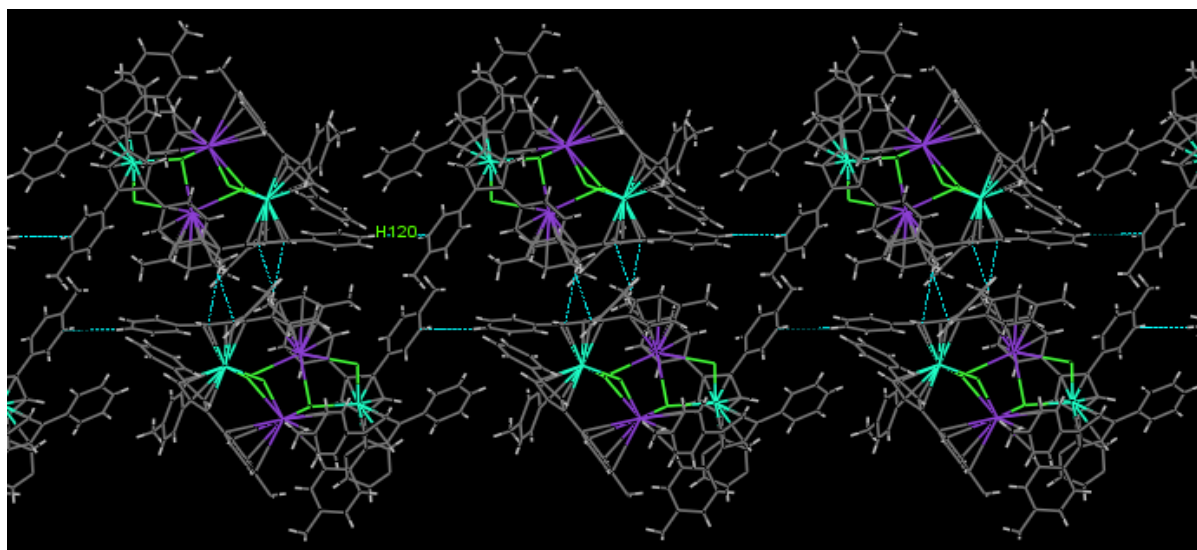
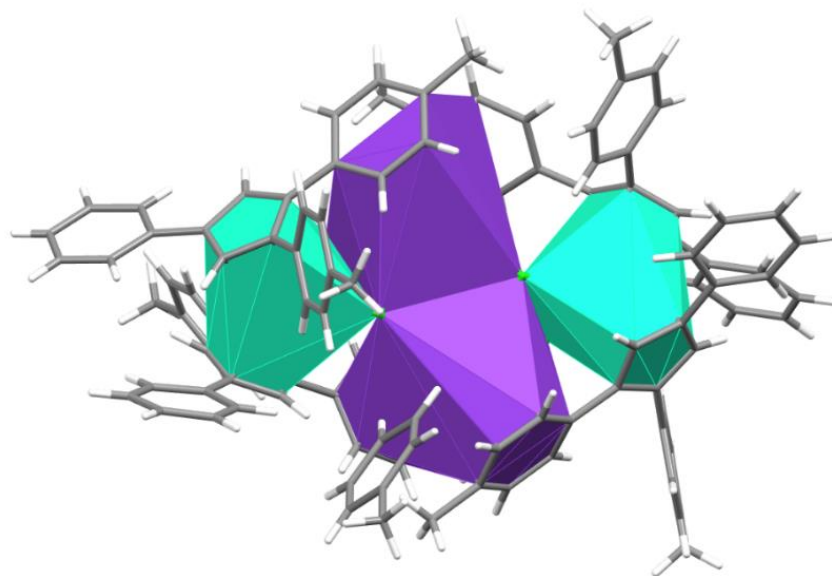


Figure S36. Polyhedral view of K- (green) and Dy-ions (purple) (top) of **5**. The image (mercury view) showing weak C-H... π interactions exerted between the molecules of **5** led to supramolecular 2D-network in the crystal lattice (bottom).

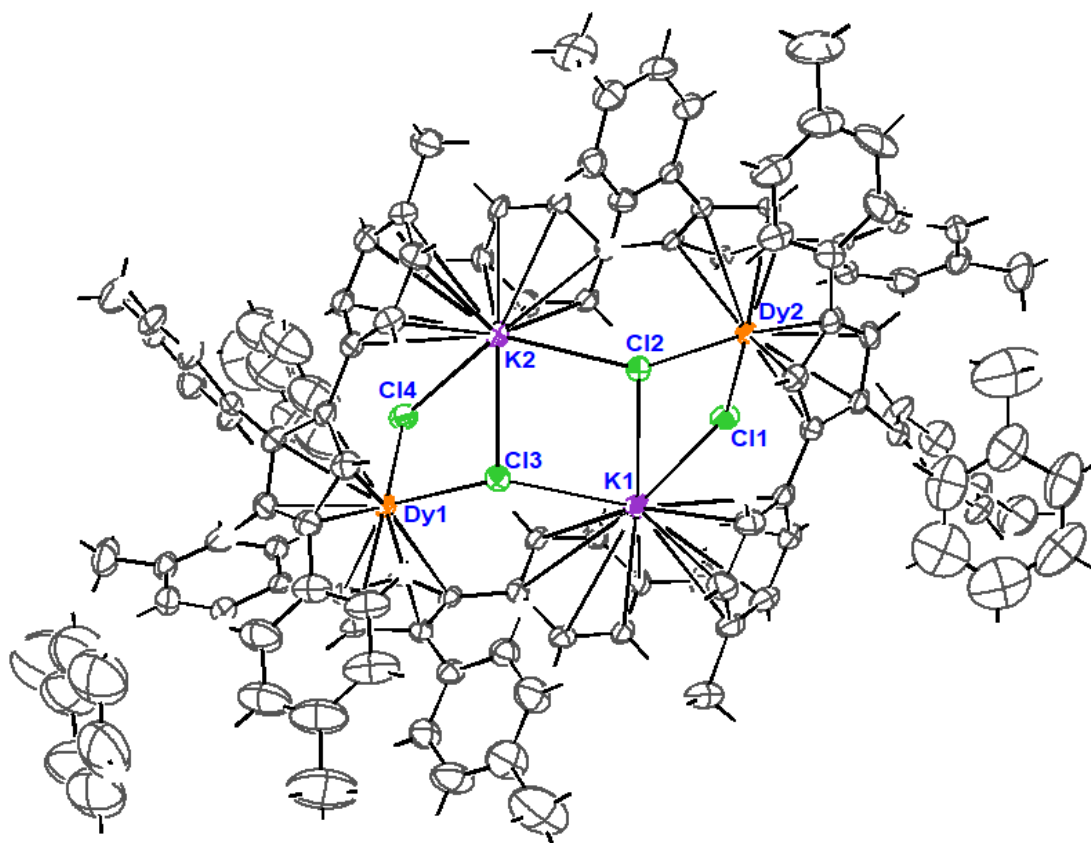


Figure S37. Asymmetric unit of **6** (ORTEP view). All the atoms are drawn at 50% probability level.

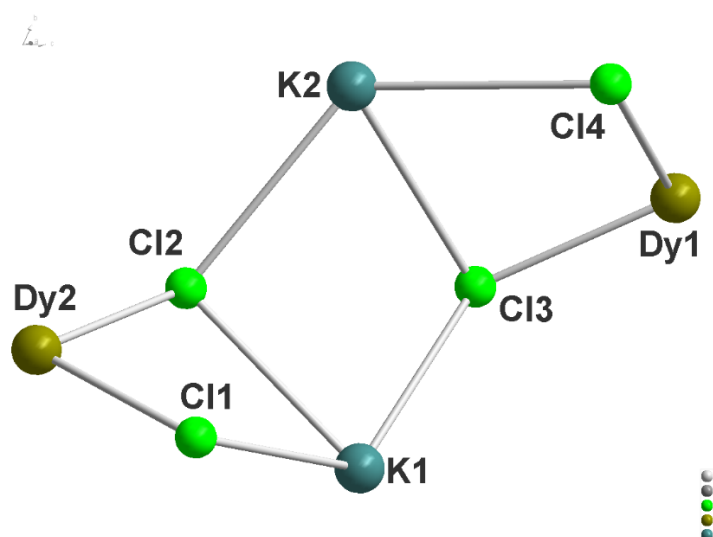


Figure S38. The $K_2Cl_4Dy_2$ core of **6**.

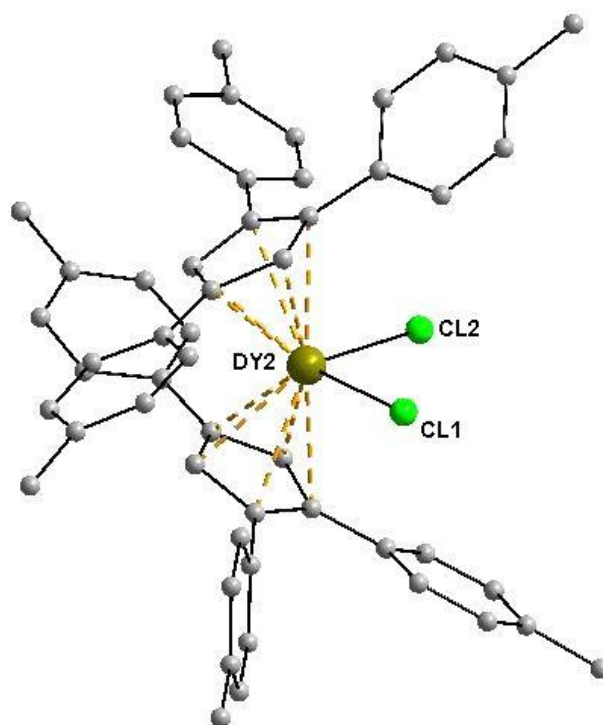


Figure S39. Bridging modes of Dy^{III} in the complex **6**. Hydrogen atoms are omitted for the clarity.

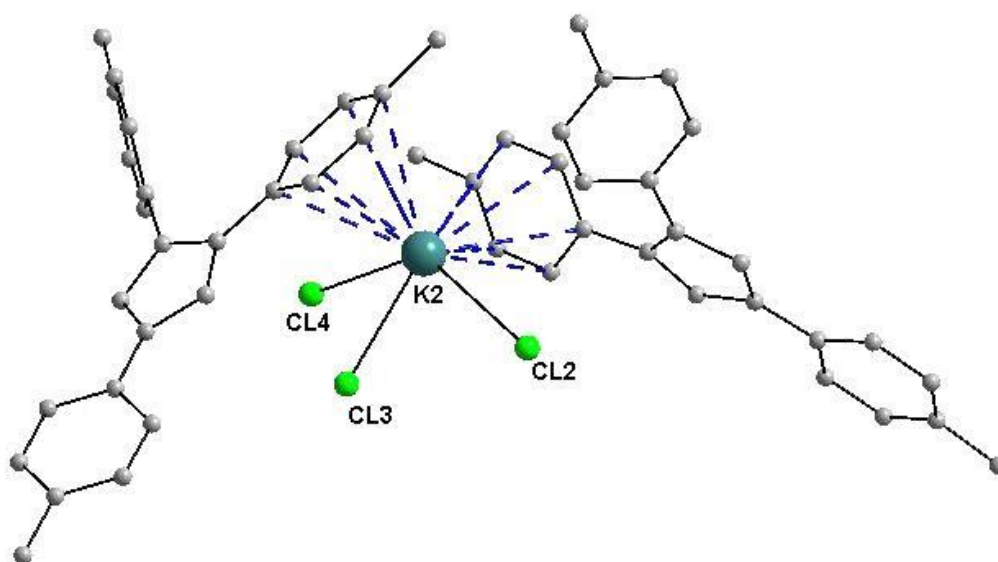


Figure S40. Bridging modes of K ion in the complex **6**. Hydrogen atoms are omitted for the clarity.

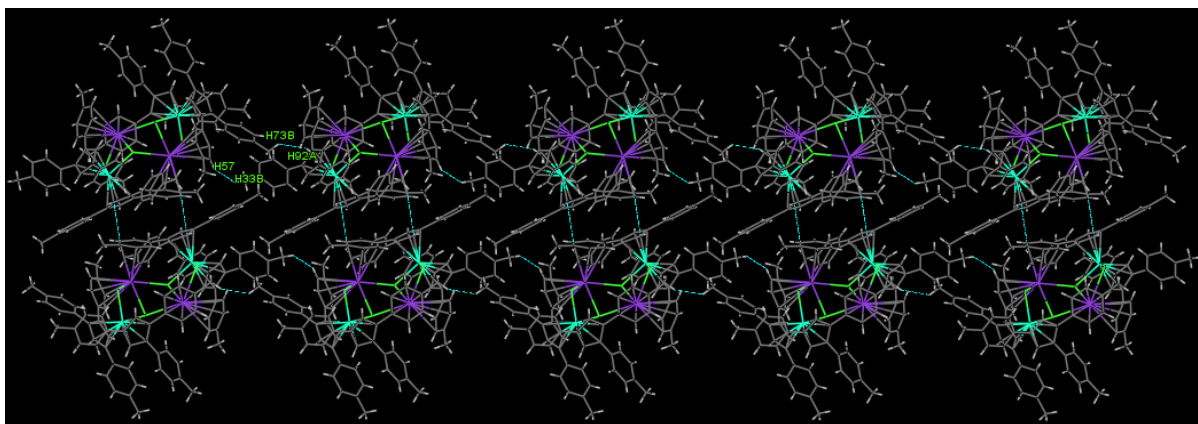


Figure S41. The compound **6** showing 2D supramolecular network in the solid state caused due to weak H...H and C-H... π bonding interactions exerted between the independent molecules of **6**.

Table S9. Comparison between the bond parameters of complexes **5** and **6**

5		6	
type of bond	bond length (Å)/angle(°)	type of bond	bond length (Å)/angle(°)
Cl1—Dy2	2.6185 (8)	Cl1—Dy2	2.5927 (11)
Cl2—Dy2	2.5874 (8)	Cl2—Dy2	2.6099 (10)
Cl3—Dy1	2.5993 (8)	Cl3—Dy1	2.6112 (11)
Cl4—Dy1	2.5903 (8)	Cl4—Dy1	2.5861 (11)
Cl1—K1	3.0559 (11)	Cl1—K1	3.2389 (15)
Cl1—K2	3.0279 (12)	Cl2—K1	3.0431 (14)
Cl2—K1	3.1805 (11)	Cl2—K2	3.1146 (14)
Cl4—K2	3.0972 (12)	Cl3—K2	3.0930 (15)
Cl3—K1	3.1404 (12)	Cl3—K1	3.1134 (14)
Cl3—K2	3.4657 (12)	Cl4—K2	3.2265 (16)
Cp _{cen1} —Dy1	2.414	Cp _{cen1} —Dy1	2.388
Cp _{cen2} —Dy1	2.427	Cp _{cen2} —Dy1	2.392
Cp _{cen1} —Dy2	2.391	Cp _{cen1} —Dy2	2.397

Cp _{cen2} -Dy2	2.397	Cp _{cen2} -Dy2	2.396
Cp _{cen1} -K1	2.978	Cp _{cen1} -K1	2.976
Cp _{cen2} -K1	2.988	Cp _{cen2} -K1	3.012
Cp _{cen1} -K2	3.013	Cp _{cen1} -K2	2.985
Cp _{cen2} -K2	3.015	Cp _{cen2} -K2	3.000
Cp _{cen1} -Dy1-Cp _{cen2}	130.85°	Cp _{cen1} -Dy1-Cp _{cen2}	129.70°
Cp _{cen1} -Dy2-Cp _{cen2}	129.73°	Cp _{cen1} -Dy2-Cp _{cen2}	130.74°
Cp _{cen1} -K1-Cp _{cen2}	113.98°	Ar _{cen1} -K1-Ar _{cen2}	115.70°
Cp _{cen1} -K2-Cp _{cen2}	116.81°	Ar _{cen1} -K2-Ar _{cen2}	113.92°

Table S10. Selected bond lengths (Å) and Bond angles (°) for the complex **5**.

C29—Dy2	2.644 (3)	C71—K1	3.346 (3)
C77—Dy1	2.658 (3)	C73—K1	3.306 (3)
C7—Dy2	2.655 (3)	C70—K1	3.279 (3)
C8—Dy2	2.650 (3)	C72—K1	3.342 (3)
C75—Dy1	2.768 (3)	C30—K2	3.502 (3)
C9—Dy2	2.728 (3)	C31—K2	3.450 (4)
C10—Dy2	2.718 (3)	C32—K2	3.277 (4)
C76—Dy1	2.758 (3)	C35—K2	3.336 (4)
C11—Dy2	2.662 (3)	C34—K2	3.172 (4)
C78—Dy1	2.665 (3)	C33—K2	3.158 (4)
C79—Dy1	2.694 (3)	C114—K1	3.299 (3)
C25—Dy2	2.644 (3)	C115—K1	3.216 (3)
C26—Dy2	2.672 (3)	C116—K1	3.241 (4)
C27—Dy2	2.723 (3)	C121—K1	3.264 (3)
C28—Dy2	2.703 (3)	C117—K1	3.309 (4)
C46—Dy1	2.759 (3)	C119—K1	3.322 (4)
C43—Dy1	2.662 (3)	C118—K1	3.325 (4)

C44—Dy1	2.654 (3)		
C45—Dy1	2.733 (3)	Cl1—K1	3.0559 (11)
C47—Dy1	2.678 (3)	Cl1—K2	3.0279 (12)
		Cl2—K1	3.1805 (11)
Cl1—Dy2	2.6185 (8)	Cl4—K2	3.0972 (12)
Cl2—Dy2	2.5874 (8)	Cl3—K1	3.1404 (12)
Cl3—Dy1	2.5993 (8)	Cl3—K2	3.4657 (12)
Cl4—Dy1	2.5903 (8)		
C57—K2	3.536 (4)	C58—K2	3.387 (4)
C55—K2	3.278 (3)	C56—K2	3.486 (4)
		C59—K2	3.137 (4)
		C69—K1	3.232 (3)
Dy2—Cl1—K2	129.24 (3)	Dy1—Cl3—K2	89.69 (3)
Dy2—Cl1—K1	97.95 (3)	K1—Cl3—K2	82.48 (3)
K2—Cl1—K1	91.61 (3)	Dy1—Cl4—K2	98.49 (3)
Dy2—Cl2—K1	95.57 (3)	Cl4—Dy1—Cl3	91.62 (3)
Dy1—Cl3—K1	116.05 (3)		

Table S11. Selected bond lengths (Å) and Bond angles (°) for the complex **6**.

C76—Dy2	2.645 (4)	C1—K1	3.465 (4)
C77—Dy2	2.638 (4)	C2—K1	3.275 (4)
C78—Dy2	2.653 (4)	C3—K1	3.160 (5)
C75—Dy2	2.723 (4)	C4—K1	3.192 (4)
C51—Dy1	2.646 (4)	C6—K1	3.444 (4)
C50—Dy1	2.640 (4)	C56—K1	3.334 (4)
C22—Dy1	2.702 (4)	C86—K2	3.362 (4)
C23—Dy1	2.713 (4)	C87—K2	3.346 (4)
C89—K2	3.256 (5)	C88—K2	3.289 (4)
C25—Dy1	2.652 (4)	C34—K2	3.268 (4)

C26—Dy1	2.656 (4)	C90—K2	3.209 (5)
C101—Dy2	2.667 (4)	C36—K2	3.350 (5)
C103—Dy2	2.716 (4)	C37—K2	3.405 (4)
C104—Dy2	2.648 (4)	C38—K2	3.326 (4)
C102—Dy2	2.739 (4)	C55—K1	3.331 (5)
C100—Dy2	2.637 (4)	C39—K2	3.250 (4)
C48—Dy1	2.715 (4)	C53—K1	3.270 (4)
C52—Dy1	2.735 (4)	C58—K1	3.229 (4)
C49—Dy1	2.646 (4)	C54—K1	3.312 (5)
		C57—K1	3.266 (4)
CI1—Dy2	2.5927 (11)	CI1—K1	3.2389 (15)
CI2—Dy2	2.6099 (10)	CI2—K1	3.0431 (14)
CI3—Dy1	2.6112 (11)	CI2—K2	3.1146 (14)
CI4—Dy1	2.5861 (11)	CI3—K2	3.0930 (15)
		CI3—K1	3.1134 (14)
		CI4—K2	3.2265 (16)

S9 Spectral data of compounds 1a, 2a, 1, 1b, 2b, 2, 7, 8

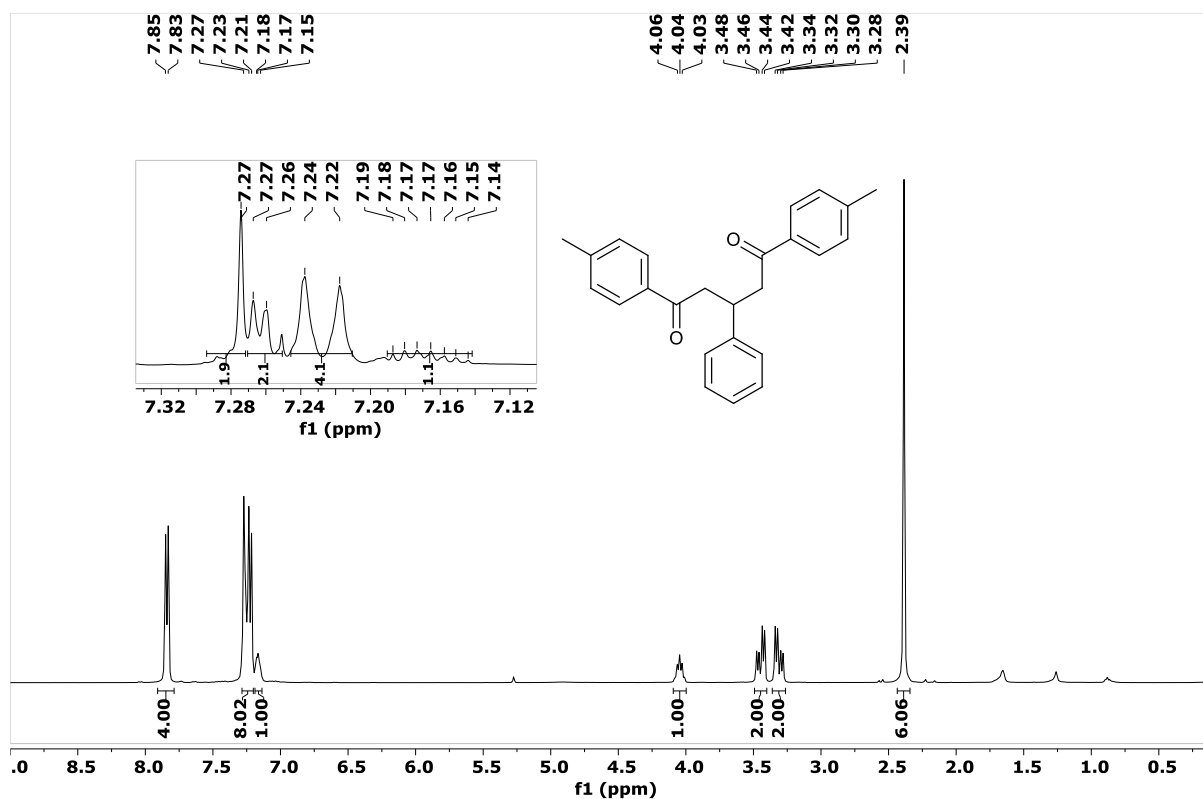


Figure S42. ¹H NMR Spectrum of compound 1a in CDCl₃ at 298 K.

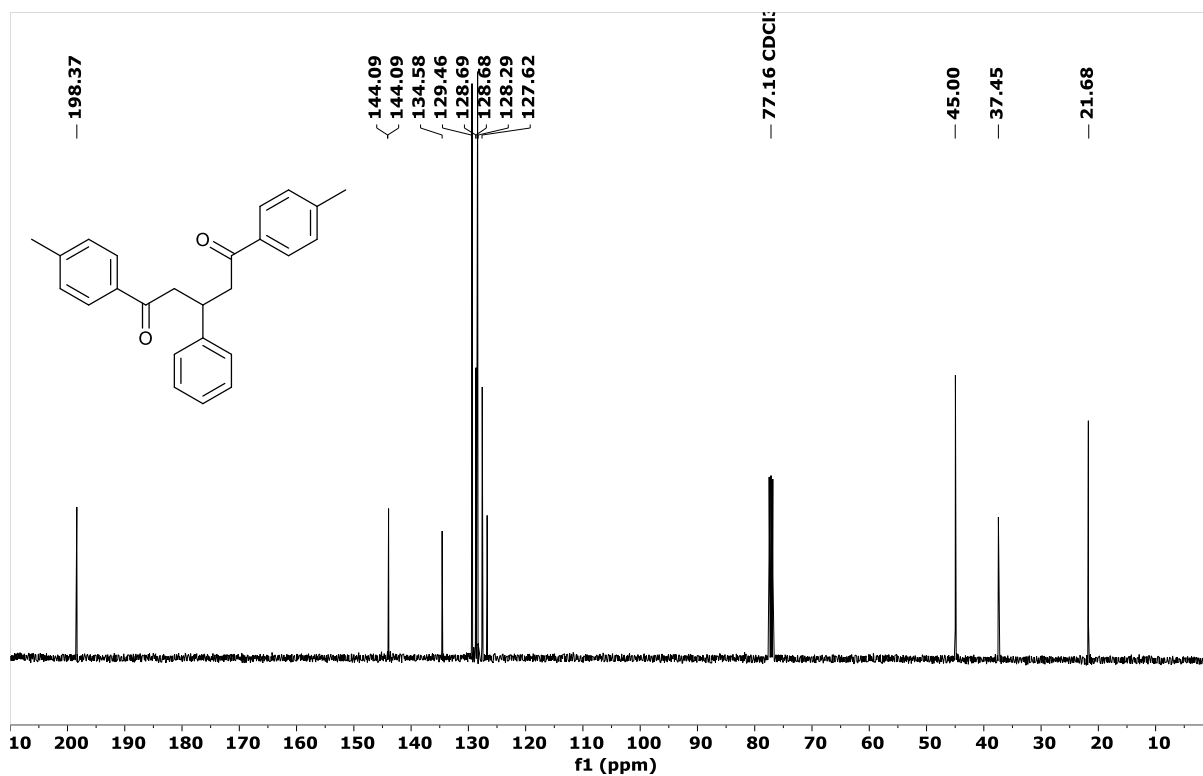


Figure S43. ¹³C NMR Spectrum of compound 1a in CDCl₃ at 298 K.

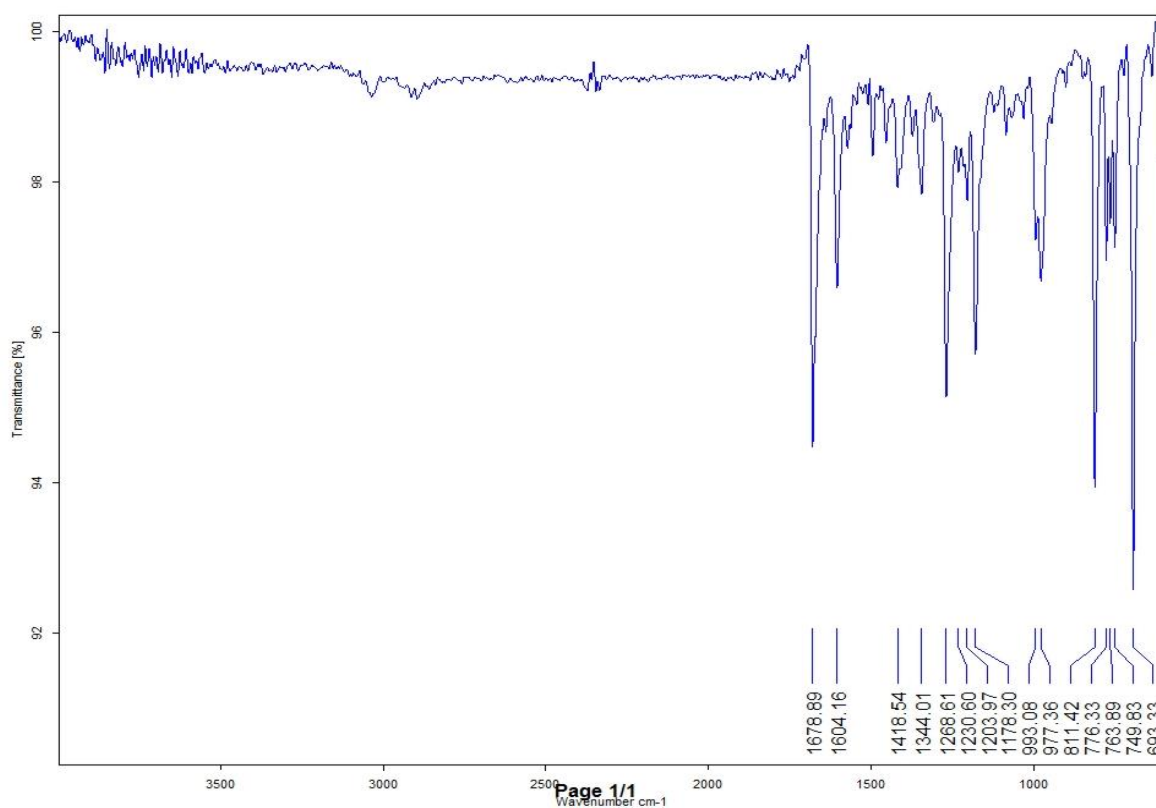
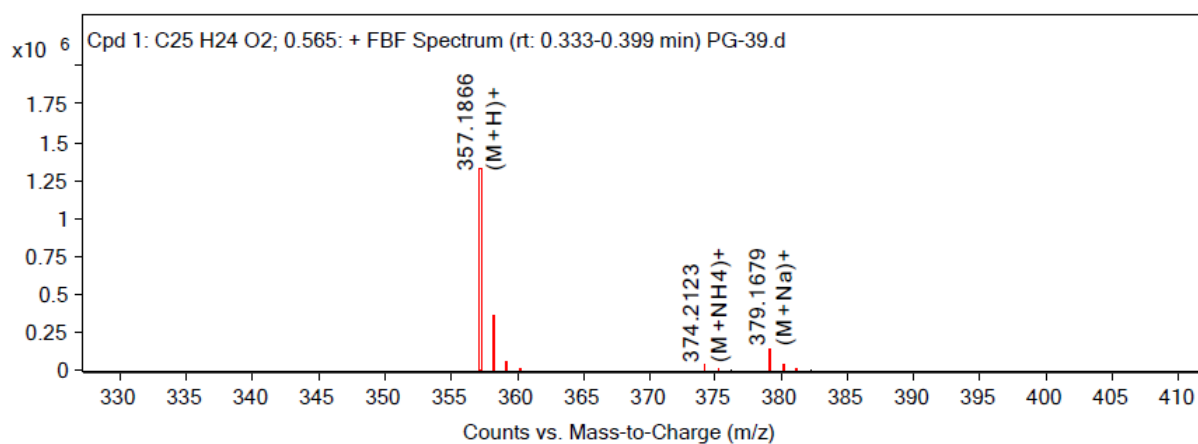


Figure S44. FT-IR spectrum of compound 1a



MS Spectrum Peak List

<i>m/z</i>	<i>z</i>	Abund	Ion
357.1866	1	1319639.75	(M+H)+
358.1898	1	307979.09	(M+H)+
359.1921	1	35338.97	(M+H)+
360.195	1	3512.05	(M+H)+
374.2123	1	32477.94	(M+NH4)+
375.215	1	8567.57	(M+NH4)+
376.2174	1	1257.43	(M+NH4)+
379.1679	1	136425.16	(M+Na)+
380.1709	1	30726.65	(M+Na)+
381.1739	1	4128.08	(M+Na)+

Figure S40. ESI-MS of compound 1a.

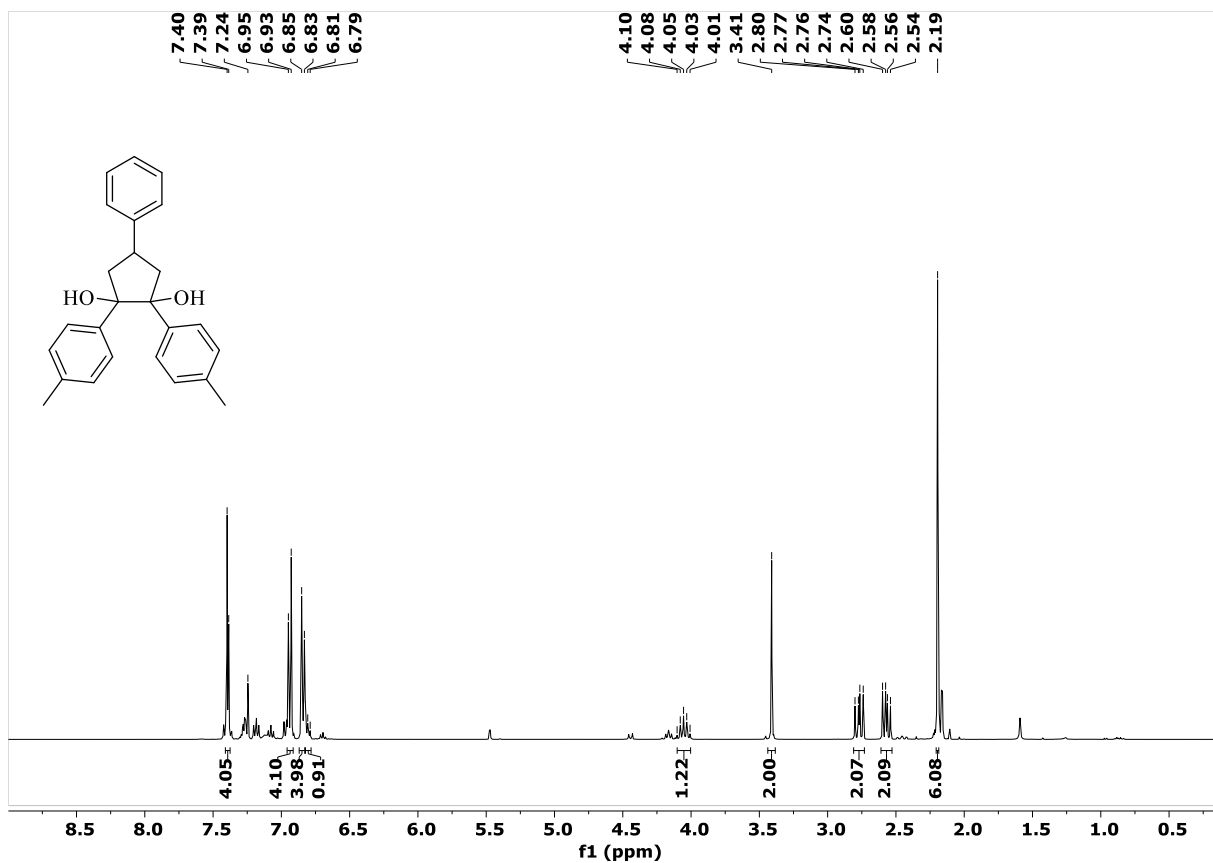


Figure S45. ¹H NMR spectrum of compound **2a** in CDCl₃ at 298 K.

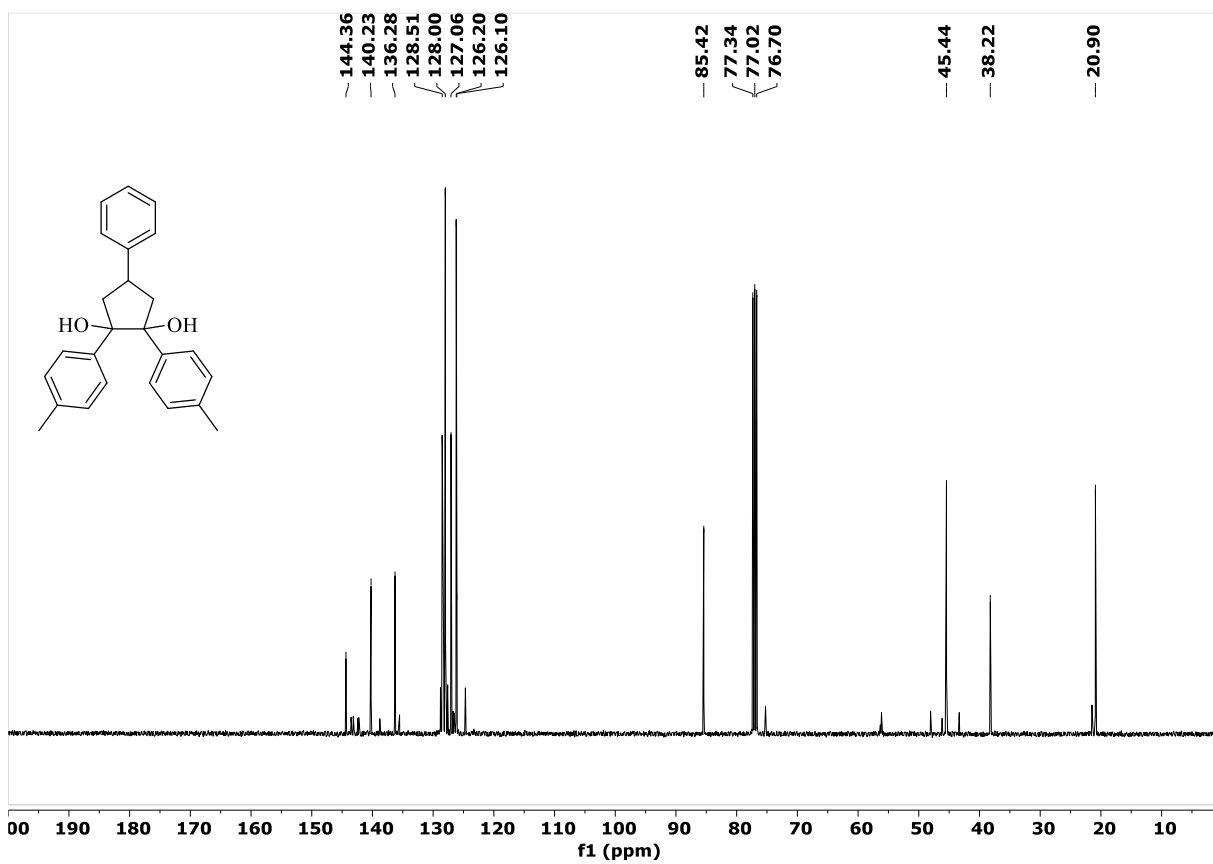


Figure S46. ¹³C NMR spectrum of compound **2a** in CDCl₃ at 298 K.

MS Zoomed Spectrum

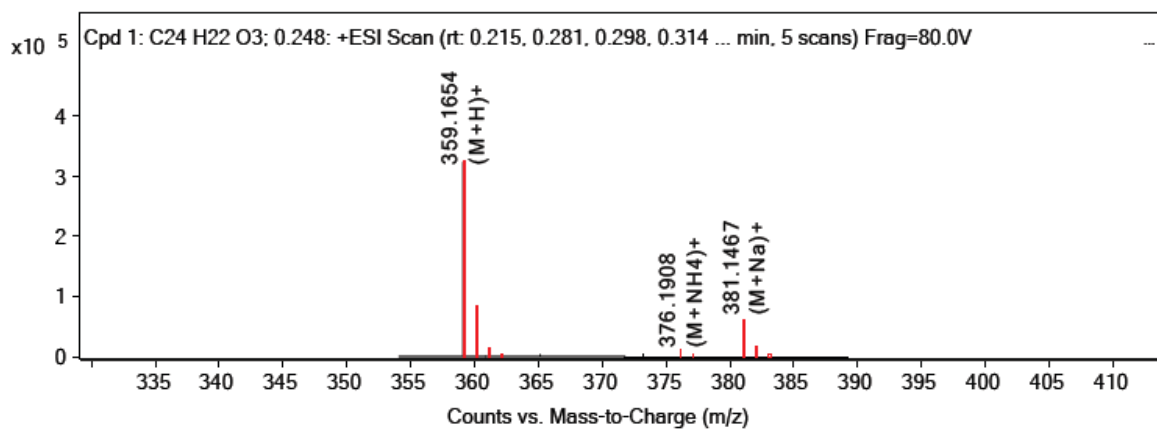


Figure S47. ESI-MS spectrum of compound **2a**.

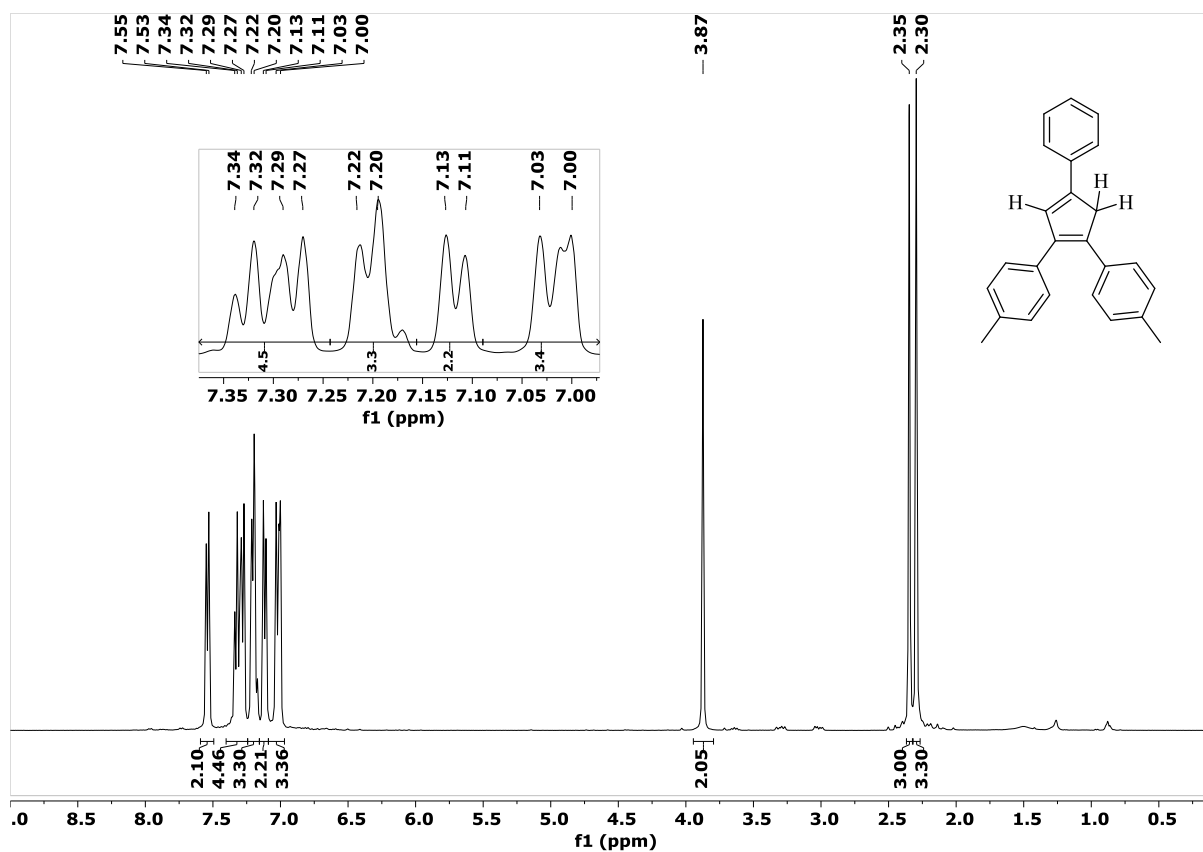


Figure S48. ¹H NMR spectrum of compound 1 in CDCl₃ at 298 K.

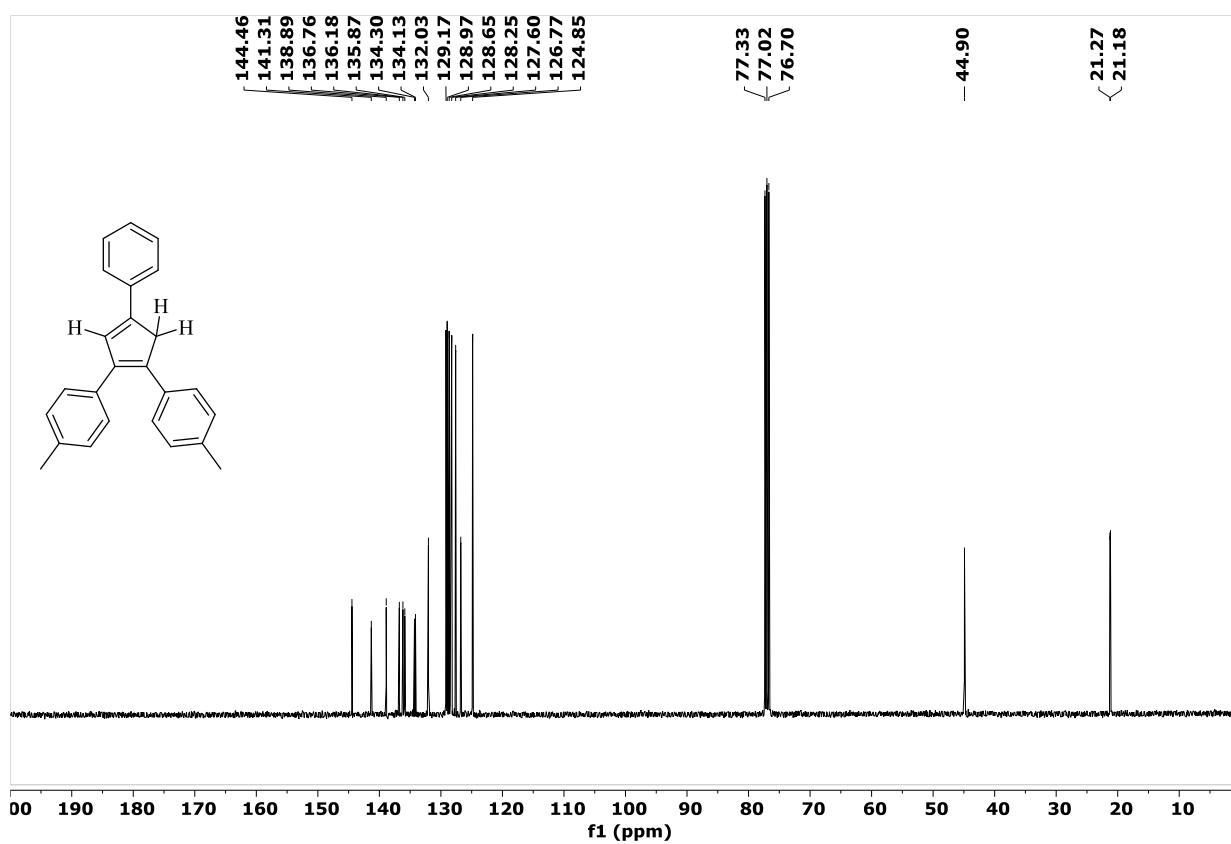


Figure S49. ¹³C NMR spectrum of compound 1 in CDCl₃ at 298 K.

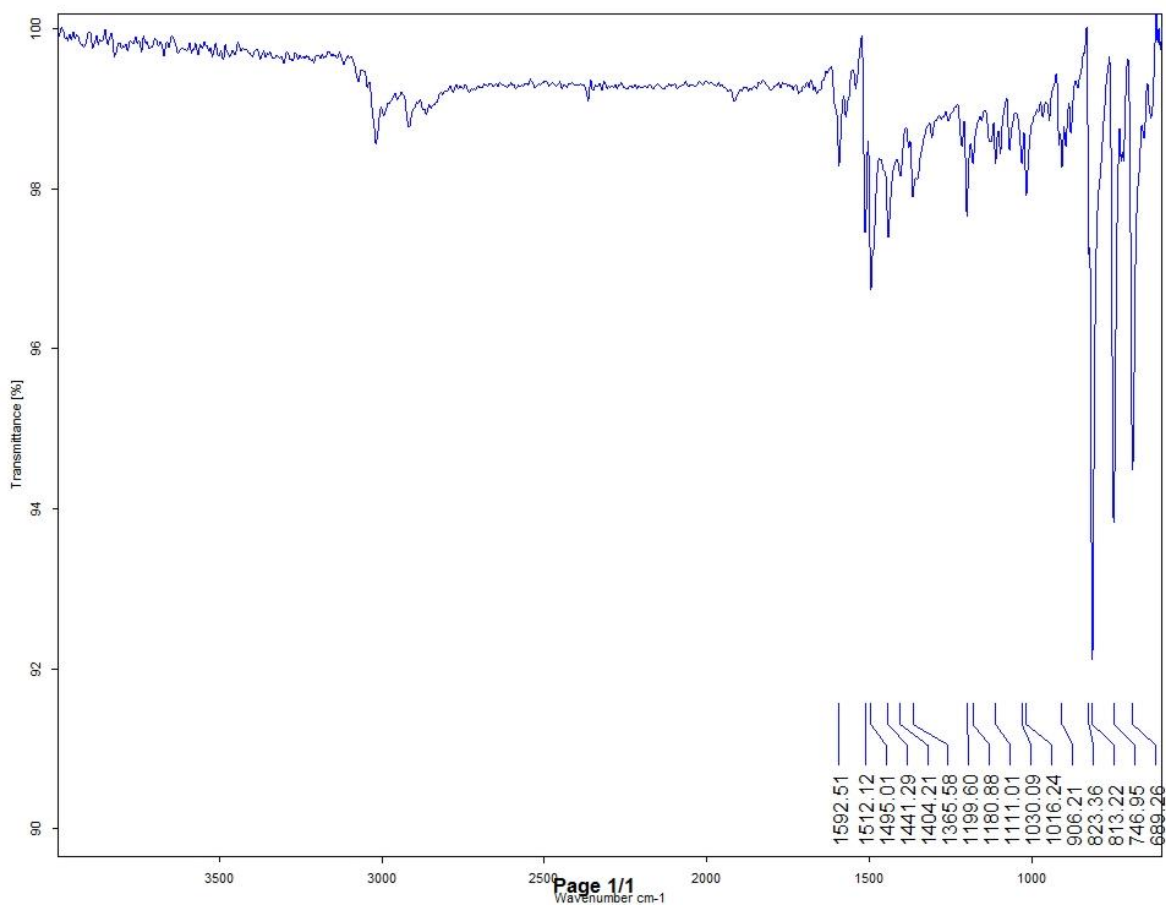


Figure S50. FT-IR spectrum of 1.

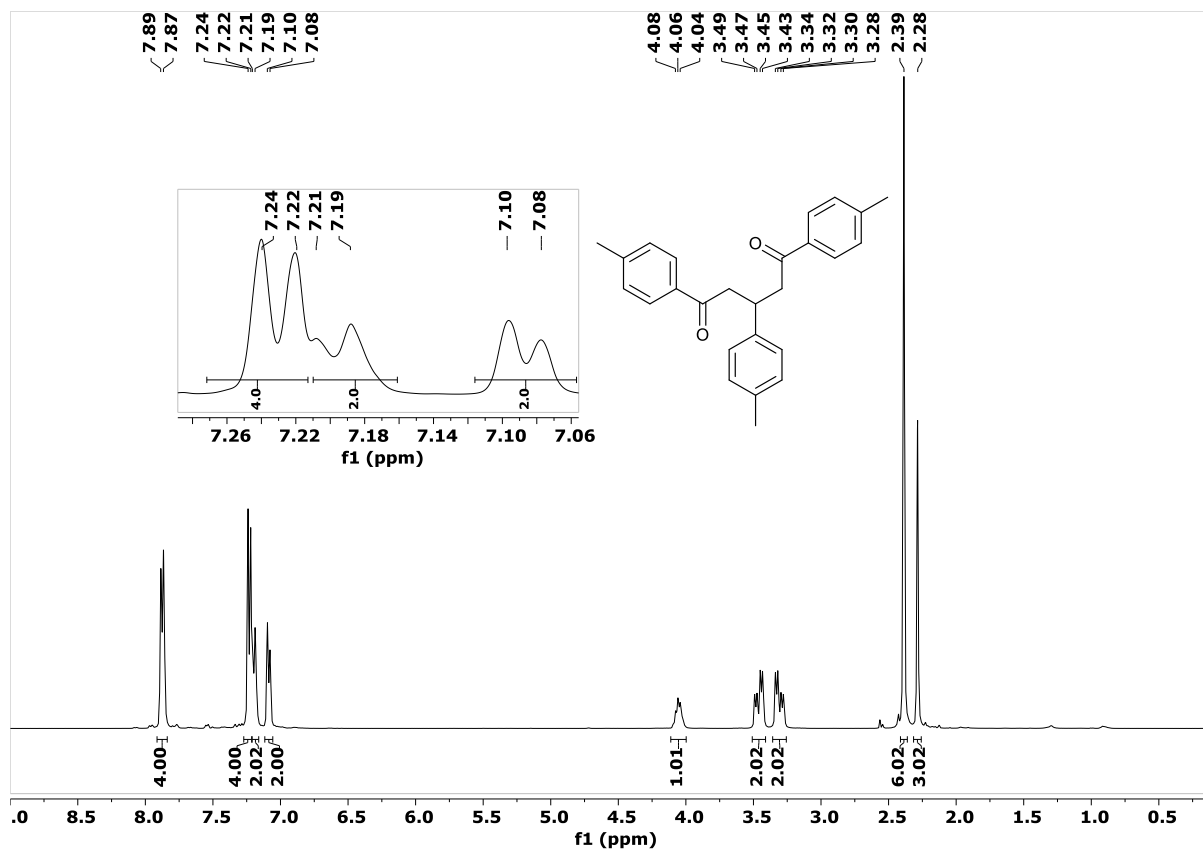


Figure S51. ¹H NMR spectrum of compound **1b** in CDCl₃ at 298 K.

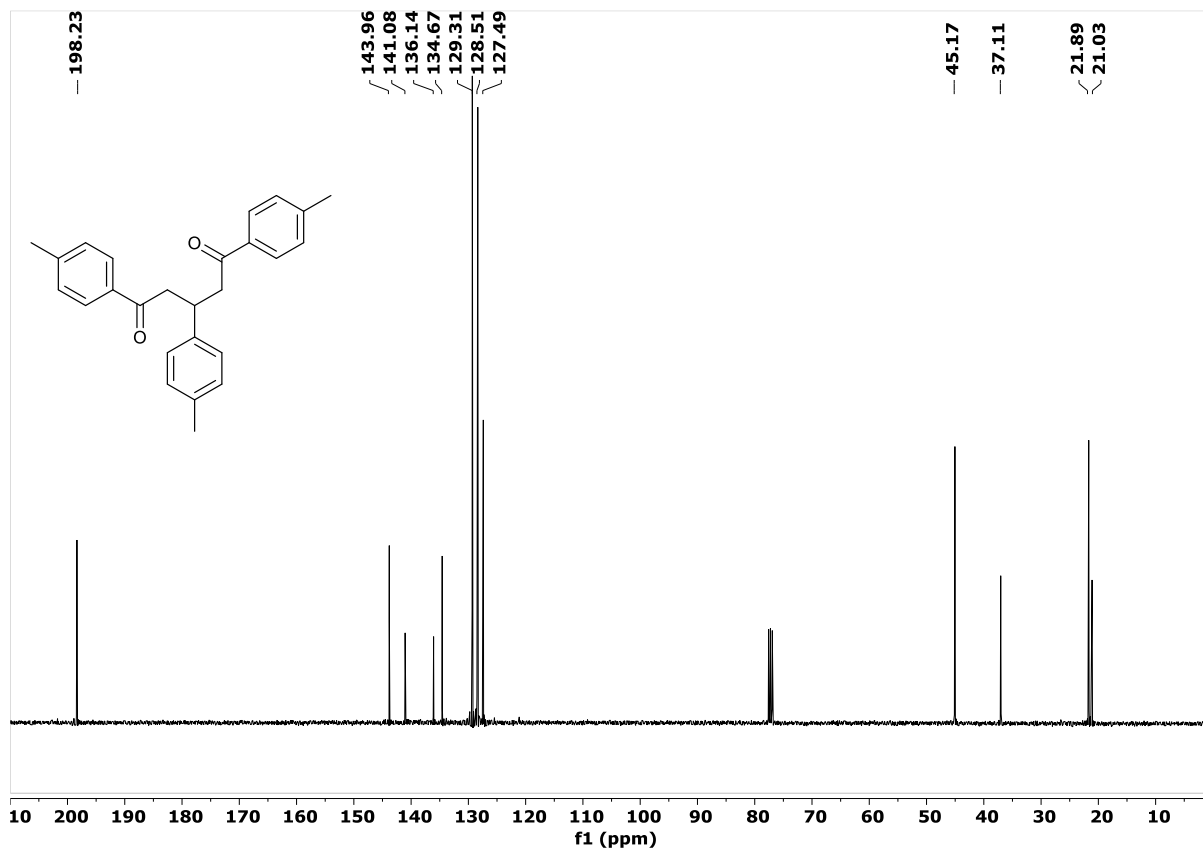


Figure S52. ¹³C NMR spectrum of compound **1b** in CDCl₃ at 298 K.

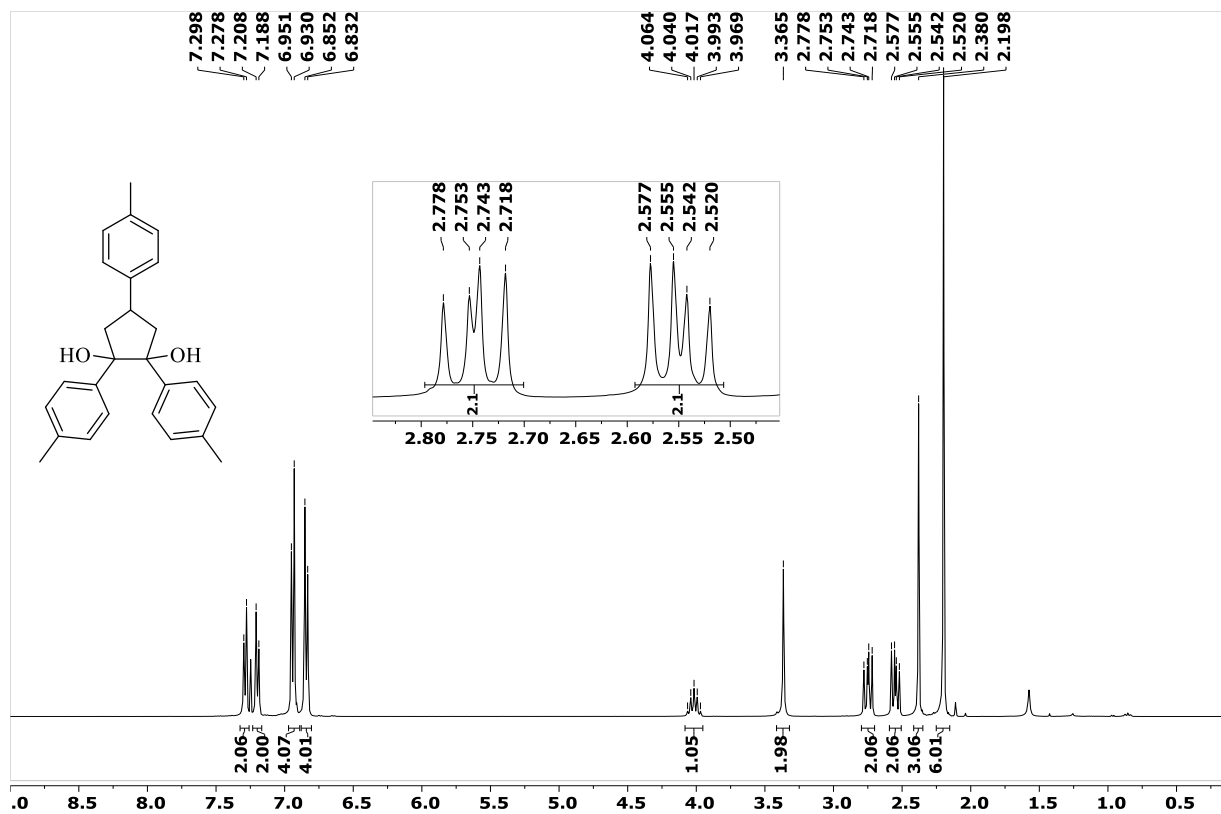


Figure S53. ¹H NMR spectrum of compound **2b** in CDCl₃ at 298 K.

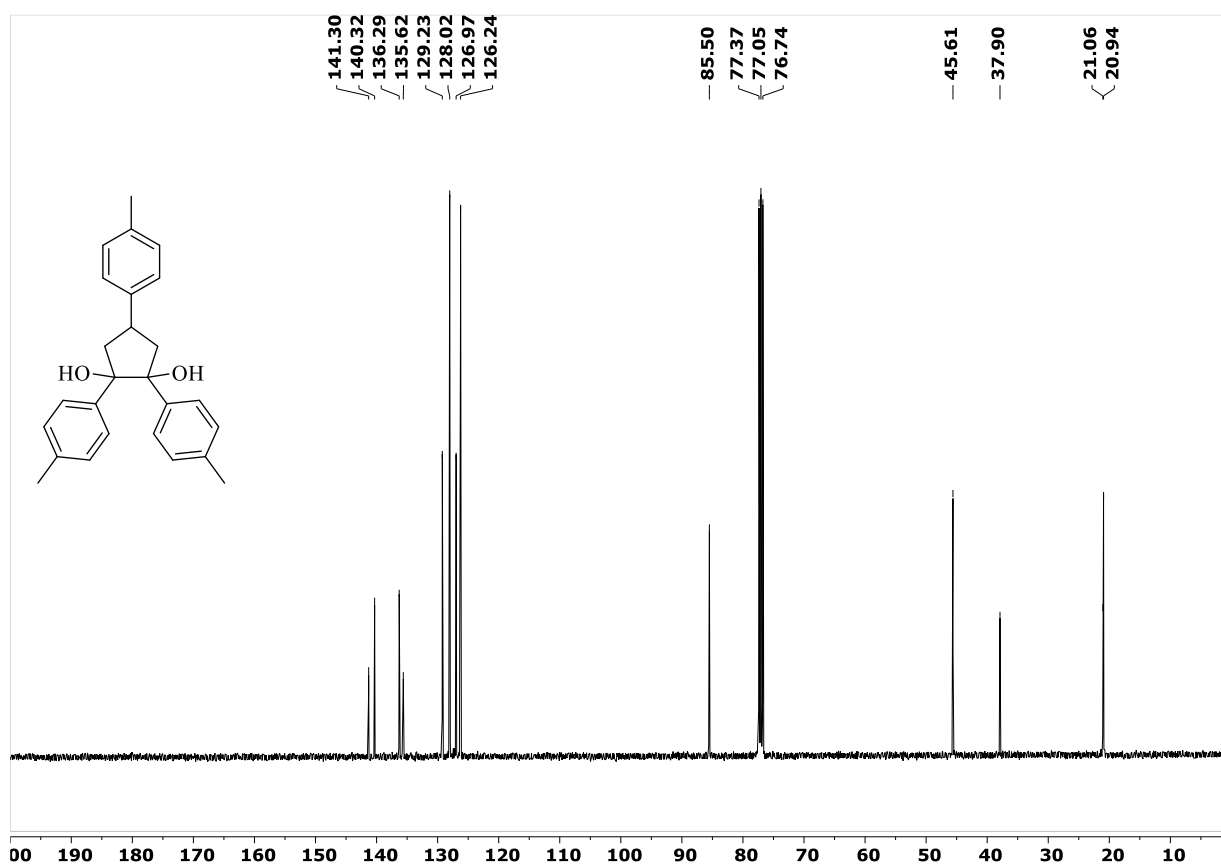
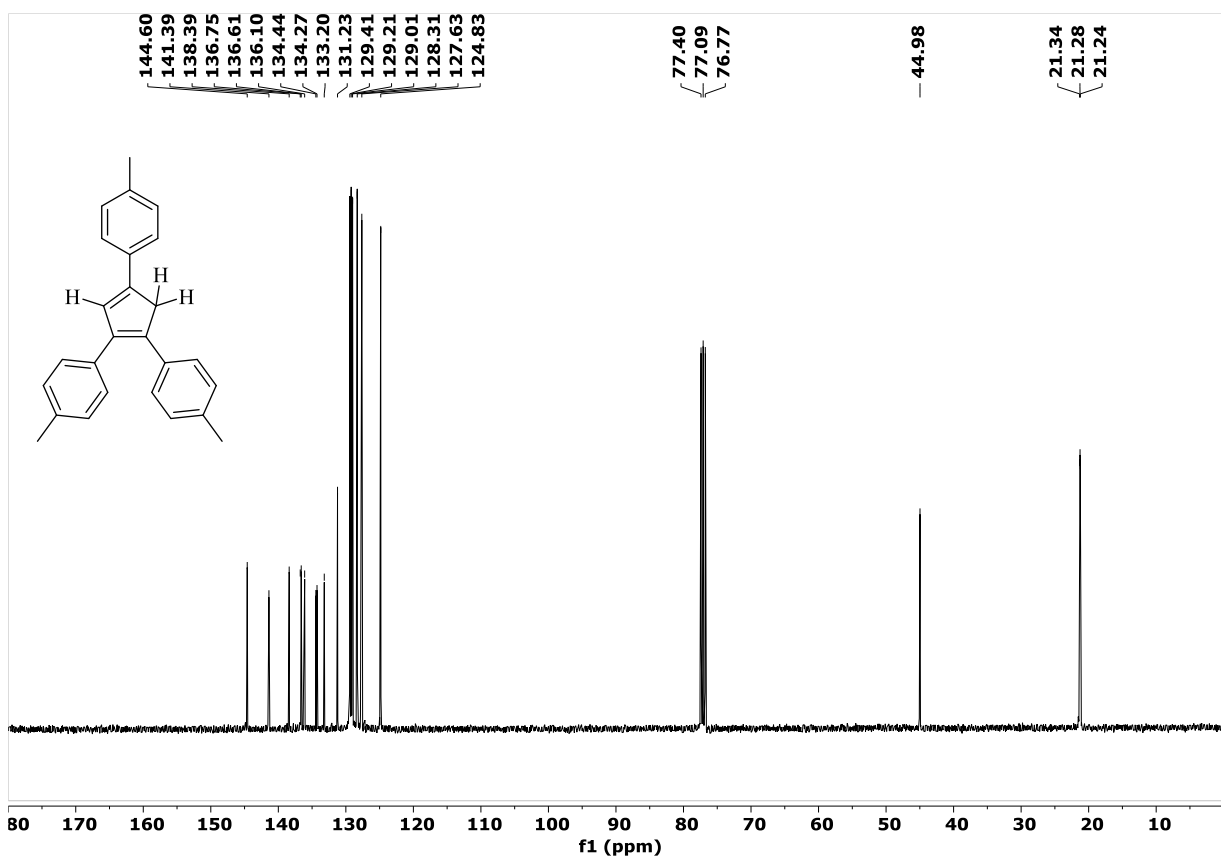
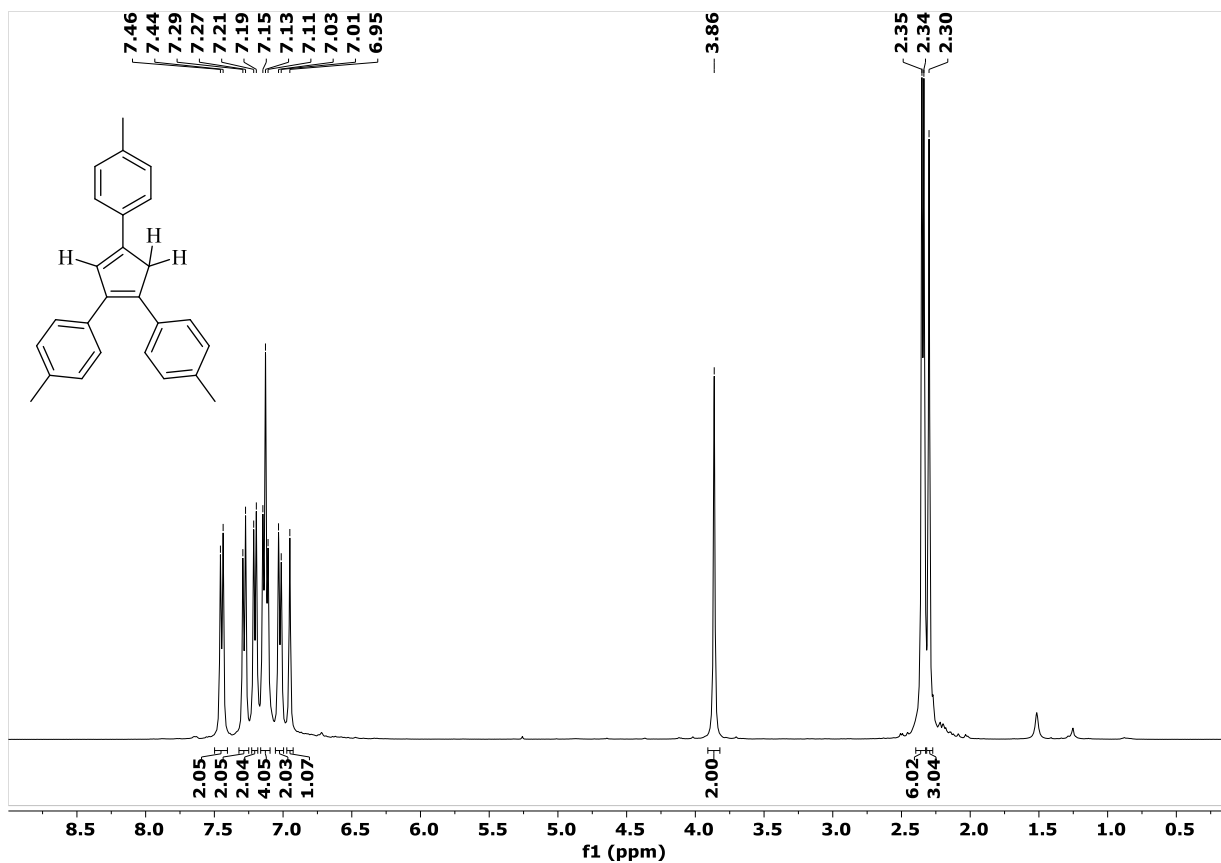


Figure S54. ¹³C NMR spectrum of compound **2b** in CDCl₃ at 298 K.



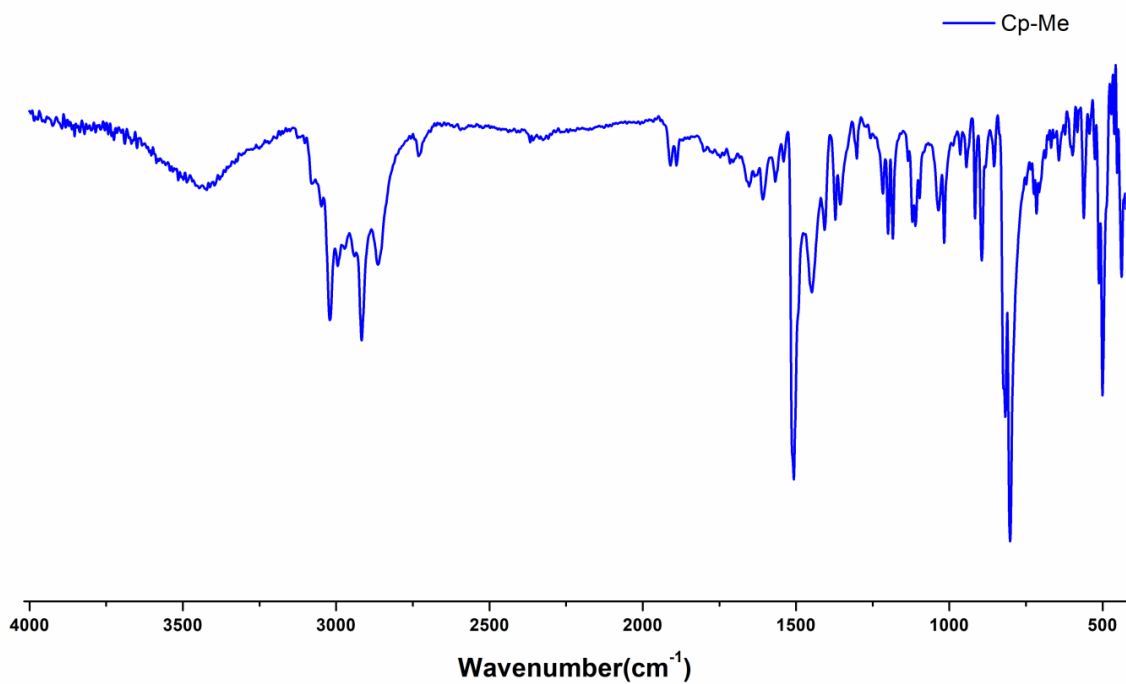
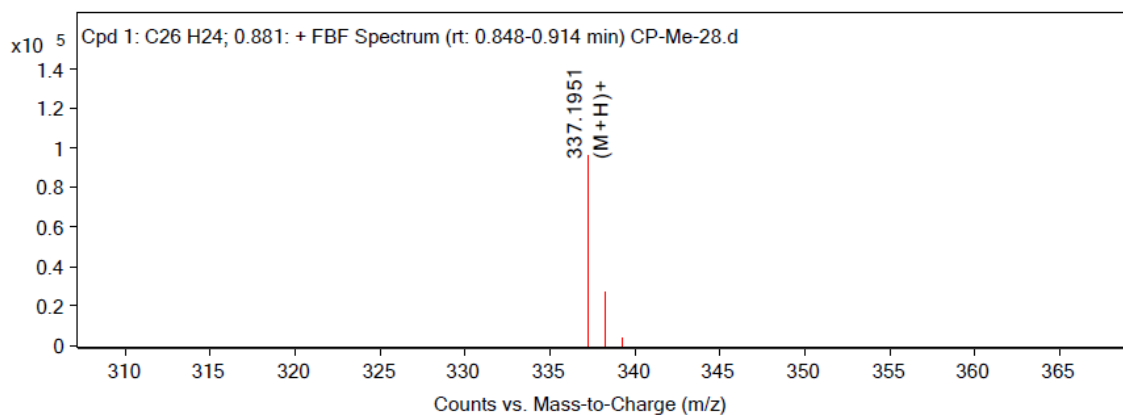


Figure S57. FT-IR spectrum of **2**.



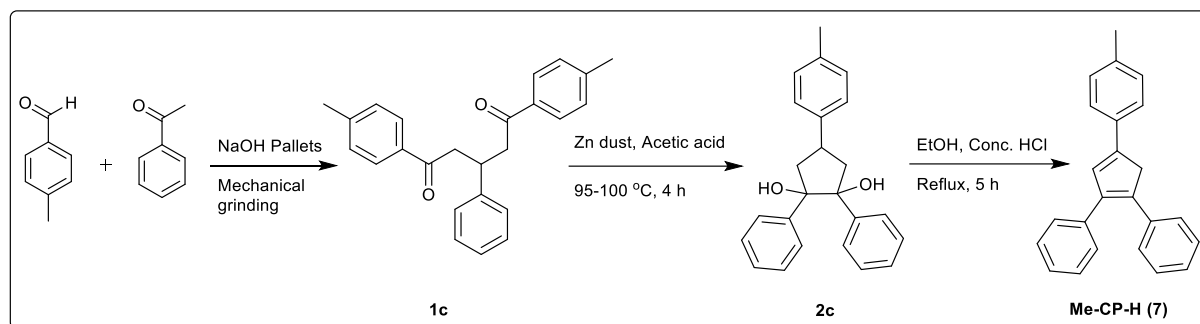
MS Spectrum Peak List

<i>m/z</i>	<i>z</i>	Abund	Ion
337.1951	1	95760.68	(M+H) ⁺
338.1986	1	17383.72	(M+H) ⁺
339.2027	1	2420.72	(M+H) ⁺

MS Spectrum

Figure S58. HRMS spectrum of compound **2**.

S9. Additional syntheses and spectral data



Scheme S3: Synthetic route for (4-(*para*-tolyl)cyclopenta-2,5-diene-1,2-diyl)dibenzene (**Me-CP-H**)

Synthesis of 1,5-diphenyl-3-(*para*-tolyl)pentane-1,5-dione (**1c**):

A mixture of 4-methyl benzaldehyde (7 g, 58.26 mmol), acetophenone (15.4 g, 128.18 mmol) and sodium hydroxide pellets (9.3 g, 233.04 mmol) were taken in a mortar and ground together with a pestle until to conversion of the liquid reactants into red solid. Further, the solid reaction mixture was dissolved in ethyl acetate: water (1:2 v/v) mixture and transferred into a 500 mL separating funnel. Ethyl acetate layer was extracted and dried under rotary reduced pressure. The resulting red sticky solid was dissolved in 100 mL hot ethanol. After 30 minutes, white solid of compound **1c** was precipitated out from EtOH. This was filtered through a Buchner funnel and washed several times with distilled water in order to remove un-reacted acetophenone and excess sodium hydroxide. The resultant pure white solid was dried under vacuum for 3 h. The weight of the isolated compound is 15.77 g (79% Yield).

Synthesis of 1,2-diphenyl-4-(*para*-tolyl)cyclopentane-1,2-diol (**2c**):³⁻⁴

The compound **1c** (15 g, 43.80 mmol) and Zn-dust (14.32 g, 219.02 mmol) were taken in a 500 mL round bottom flask, to this 200 mL glacial acetic acid was added. The reaction mixture was stirred and refluxed at 95-100 °C for 4 h. After completion of the reaction, as monitored by TLC, the un-reacted Zn was removed through filtration. The clear yellow filtration of acetic acid was poured into an excess crushed

ice with vigorous stirring which gave a light-yellow solid. The resultant yellow solid was filtered and washed several times with distilled water. In this point, the solid compound contains excess of water that can be removed by dissolving the solid compound in ethyl acetate and separated the water using separating funnel. Further, the ethyl acetate layer was separated and dried by passing over the anhydrous sodium sulphate. After evaporation of ethyl acetate under rotary reduce pressure, the pure white solid of compound **2c** was achieved by washing the crude yellow solid several times with distilled n-hexane (50 x 3 mL). The white solid of compound **2c** was dried under vacuum for 3 h. The weight of the isolated compound is the 10.45 g (69% Yield).

Synthesis of (4-(*para*-tolyl)cyclopenta-2,5-diene-1,2-diyl)dibenzene (MeCp-H) (7)

Compound **2c** (2.97 g, 8.62 mmol) was dissolved in 35 mL ethanol, to this 6 mL concentrated hydrochloric acid was added with vigorous stirring. The complete reaction mixture was stirred and refluxed until to conversion of di-alcohol reactant into corresponding yellow solid product. After completion of the reaction, as monitored by TLC, the resultant yellow solid product obtained during the reaction was filtered and dried in a temperature controlled hot air oven at 65 °C for 24 h. The compound **MeCp-H** was purified by column chromatography using EtOAc/hexane (5%) as eluent. The weight of the isolated compound is 2.12 g (80% Yield). **¹H NMR** (400 MHz, CDCl₃, 298 K): δ ppm: 7.48 (d, *J* = 8 Hz, 2H, ArH), 7.40-7.39 (m, 2H, ArH), 7.35-7.28 (m, 5H), 7.24-7.21 (m, 2H), 7.17 (d, *J* = 8 Hz, 2H, ArH), 6.99 (s, 1H, CpH), 3.93 (s, 2H, -CH₂-), 2.36 (s, 3H, Ph-CH₃). **¹³C NMR** (101 MHz, CDCl₃, 298 K): δ ppm: 145.06, 142.07, 138.72, 137.21, 136.90, 136.75, 132.99, 130.98, 129.38, 128.45, 128.38, 128.23, 127.72, 127.10, 126.40, 124.81, 44.92, 21.22.

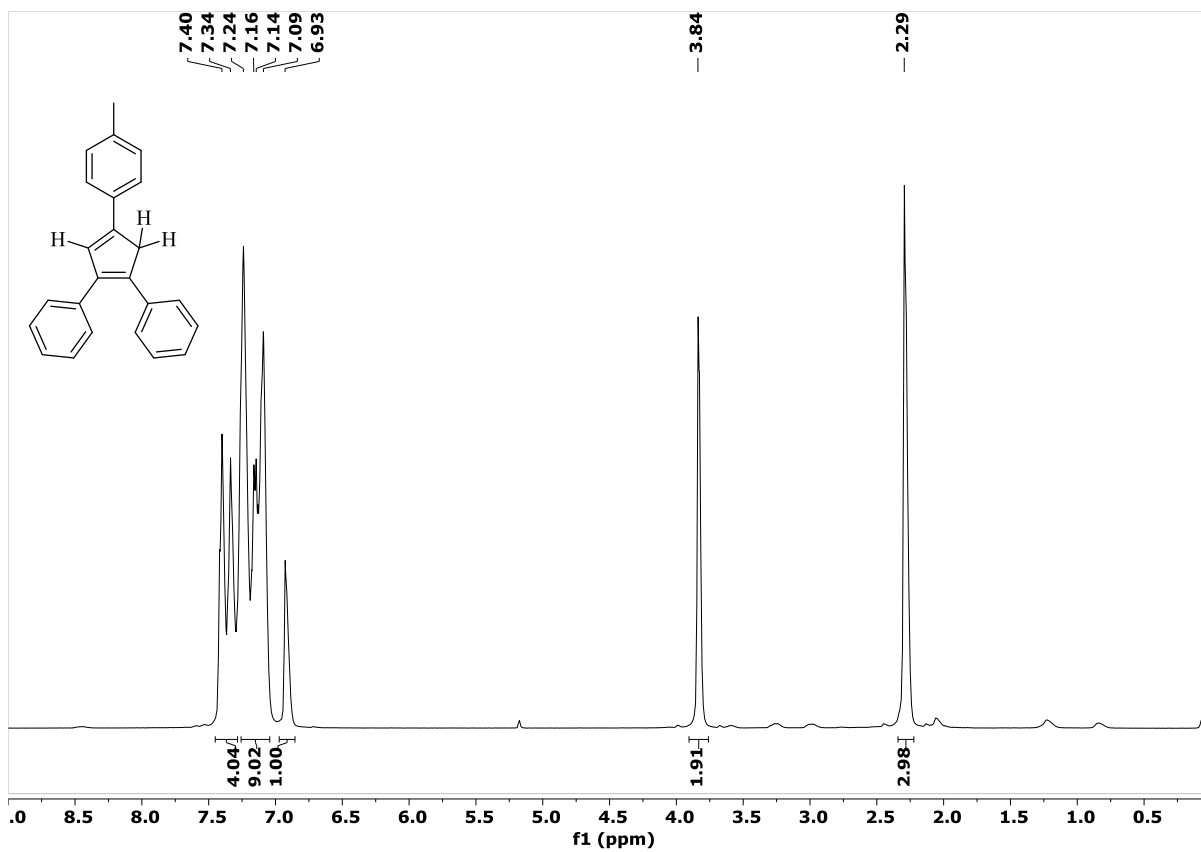


Figure S59: ^1H NMR spectrum of Me-Cp-H (7) in CDCl_3 at 298 K.

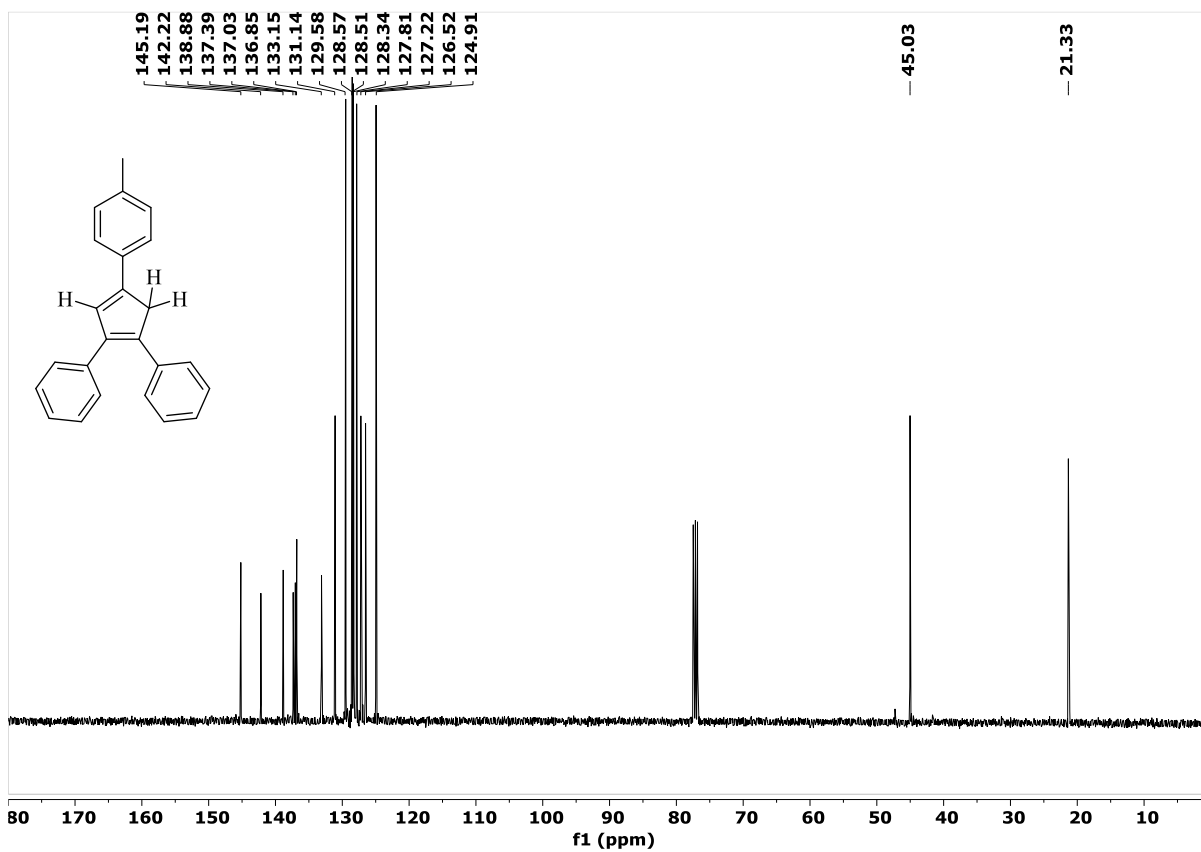
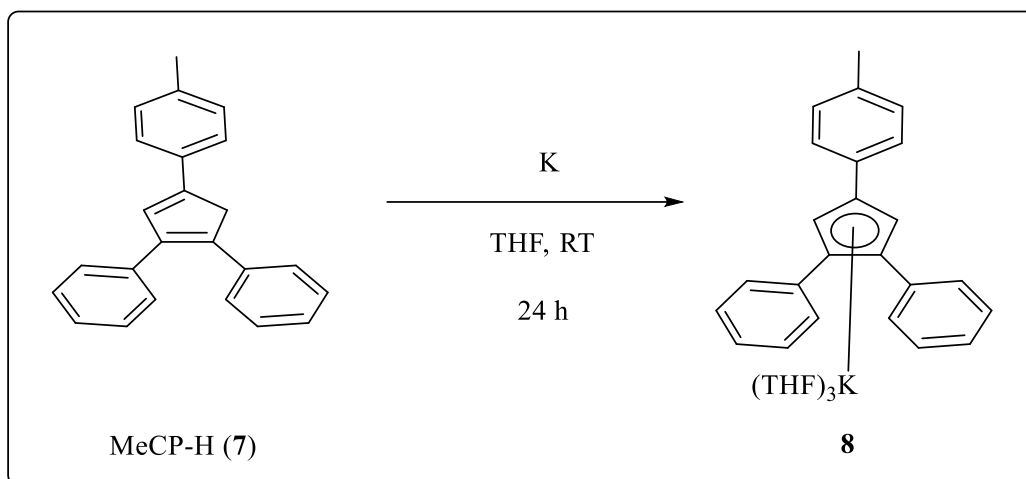


Figure S60: ^{13}C NMR spectrum of Me-Cp-H (7) in CDCl_3 at 298 K.



Scheme S4: Synthesis of Me-Cp-K(THF)₃ (**8**)

(4-(*para*-tolyl)cyclopenta-1,3-diene-1,2-diyl)dibenzene (**7**) (1 g, 3.24 mmol) was stirred in 10 mL of dry THF. Potassium (0.126 g, 3.24 mmol) was added in small pieces. Stirring was continued for 24 hours. A yellow color precipitate was formed was filtered out. Further, the precipitate filtered was given wash with dry *n*-hexane twice. Then the precipitate was dried under vacuum for 3 hours with occasional purging of argon. The weight of isolated compound was 1.2 g (87%). The ¹H NMR spectrum shows that there is one THF molecule coordinated. ¹H NMR (400 MHz, DMSO-*d*₆, 298 K) δ ppm: 7.23 (d, $J = 8$ Hz, 2H, ArH), 7.16 (d, $J = 8$ Hz, 2H, ArH), 7.00 (t, $J = 8$ Hz, 4H, ArH), 6.86 (d, $J = 8$ Hz, 2H, ArH), 6.73 (t, $J = 8$ Hz, 2H, ArH), 6.08 (s, 2H, CpH), 3.60 (m, 3H, THF), 2.18 (s, 3H, Ph—CH₃), 1.76 (m, 3H, THF). ¹³C NMR (101 MHz, DMSO-*d*₆, 298 K) δ ppm: 143.51, 139.41, 128.52, 127.63, 127.17, 126.57, 121.75, 121.21, 120.91, 120.35, 107.83, 67.01 (THF), 25.12 (THF), 20.60.

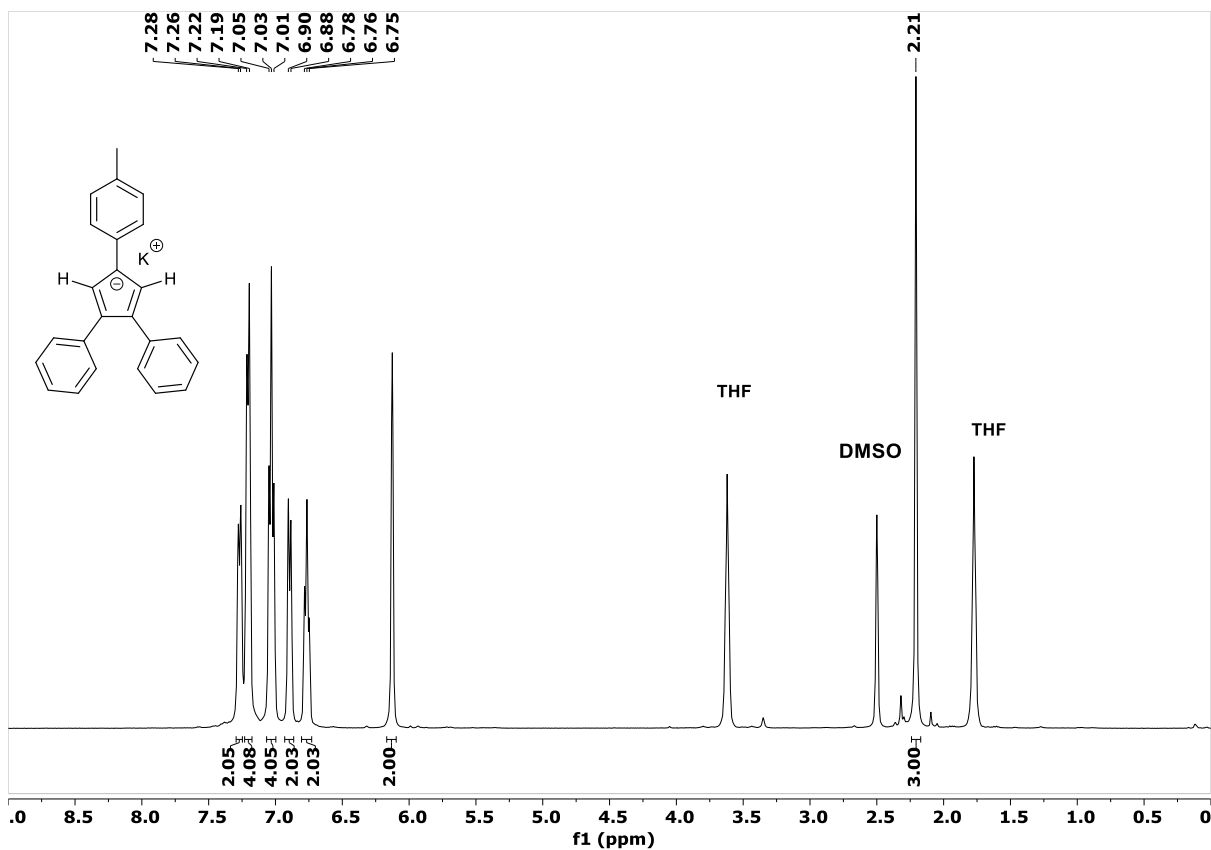


Figure S61: ¹H NMR spectrum of compound **8** in DMSO-D₆ at 298 K.

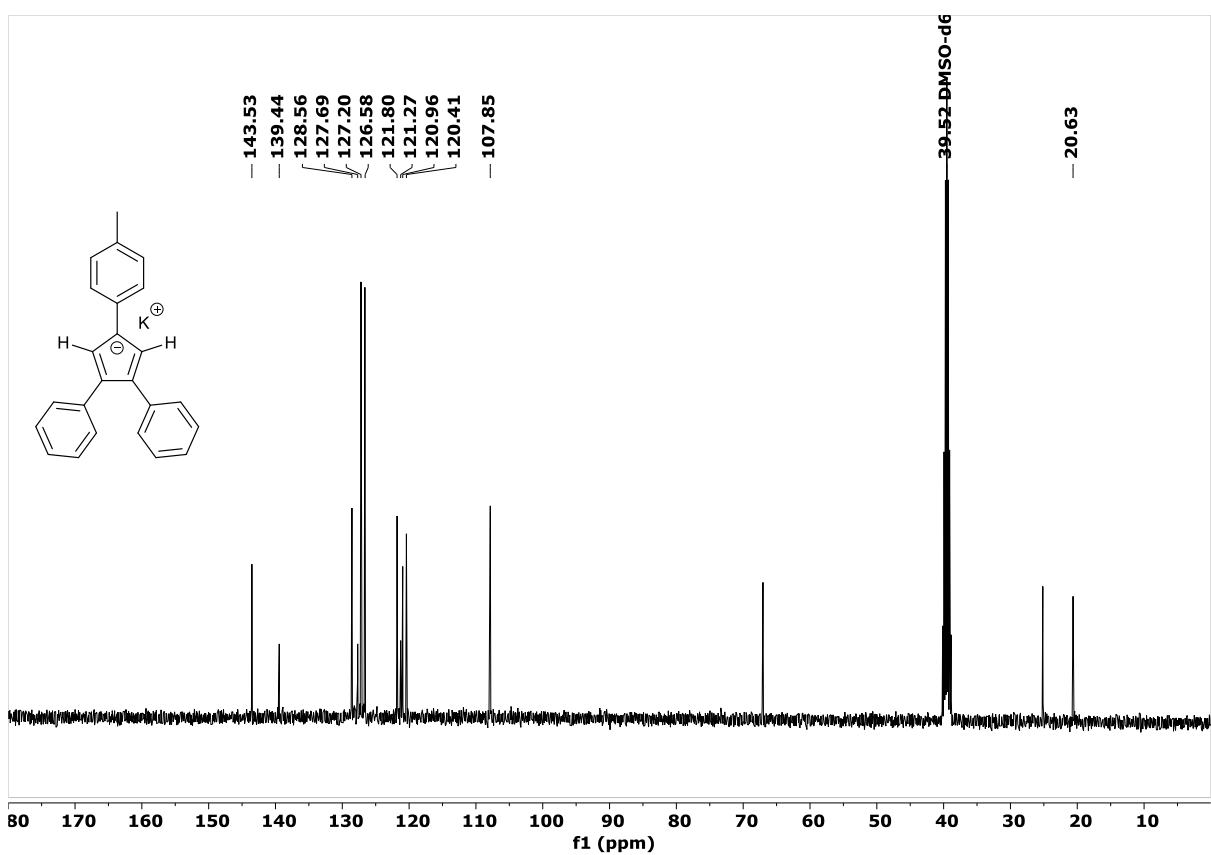


Figure S62: ¹³C NMR spectrum of compound **8** in DMSO-D₆ at 298 K.

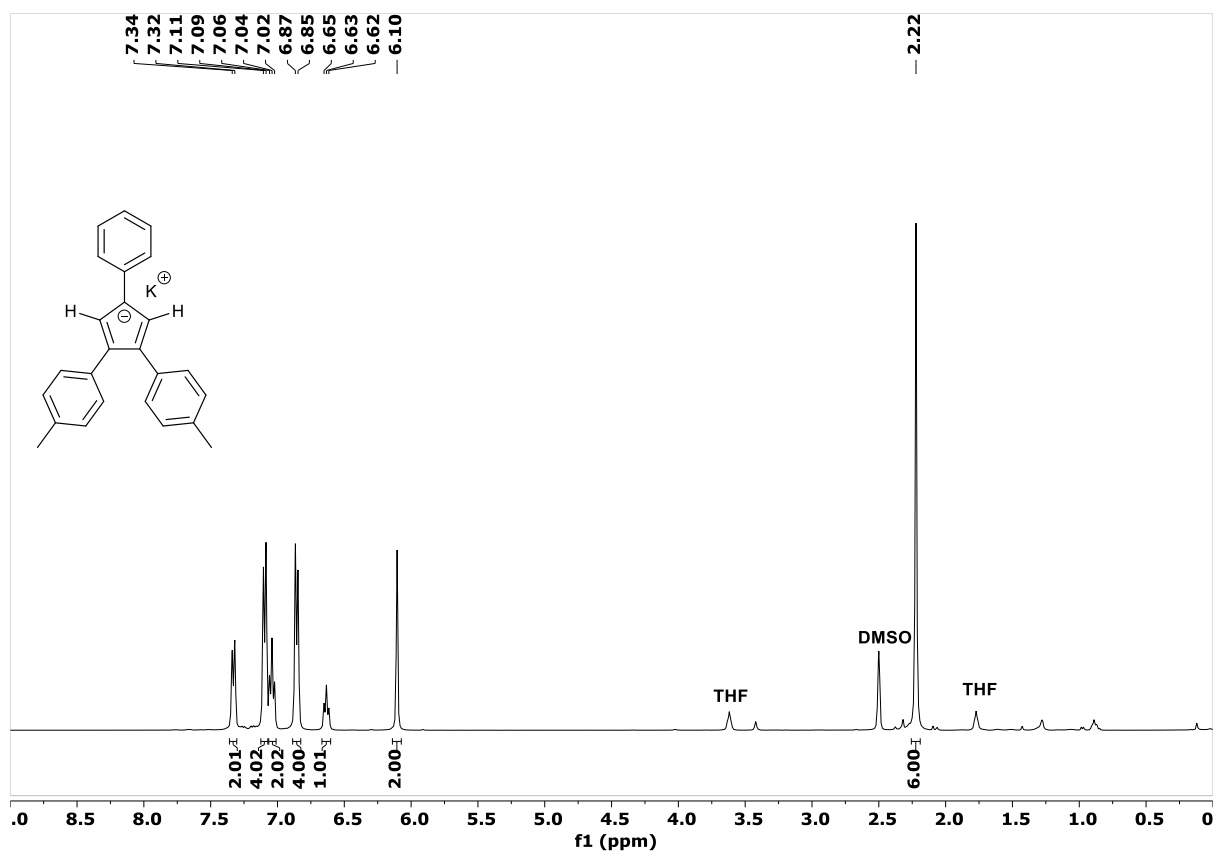


Figure S63: ¹H NMR spectrum of compound 3 in DMSO-D₆ at 298 K.

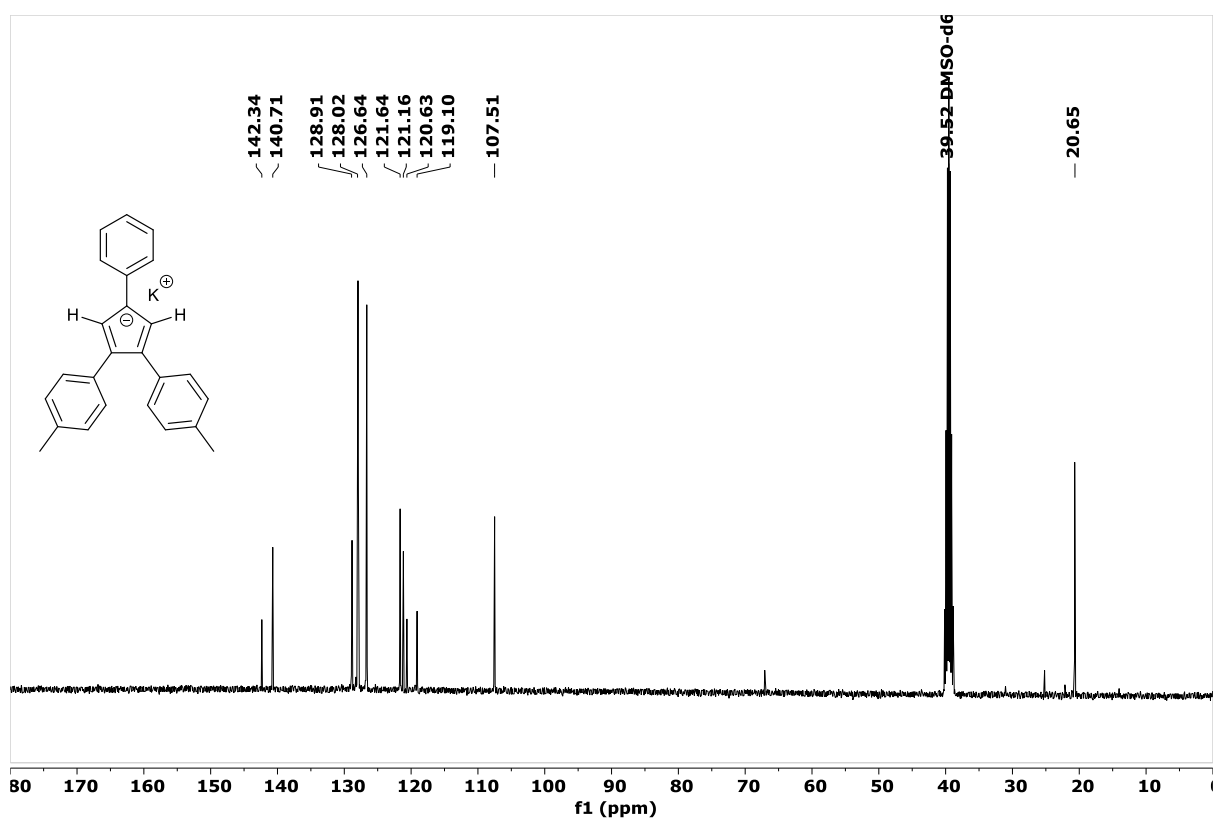


Figure S64: ¹³C NMR spectrum of compound 3 in DMSO-D₆ at 298 K.

S10. References

- 1) Bruker (2008). APEX2 (Version 2008.1-0). Bruker AXS Inc., Madison, Wisconsin, USA.
- 2) Bruker (2001b). SAINT-V6.28A. Data Reduction Software.
- 3) G. M. Sheldrick, (1996). SADABS. Program for Empirical Absorption Correction. University of Göttingen, Germany.
- 4) L. J. Farrugia, *J. Appl. Cryst.*, 1999, **32**, 837.
- 5) G.M. Sheldrick, (1997) SHELXL-97. Program for the Refinement of Crystal.
- 6) G.M. Sheldrick, *Acta Cryst.*, 1990, **A46**, 467.
- 7) (a) J. Ye, X. Huang, Y. Li, T. Zheng, G. Ning, J. Liang, Y. Liu and Y. Wang, *Dyes Pigments*, 2017, **147**, 465; (b) X. Zhang, J. Ye, L. Xu, L. Yang, D. Deng and G. Ning, *J. Lumin.*, 2013, **139**, 28; (c) J. Ye, D. Deng, Y. Gao, X. Wang, L. Yang, Y. Lin and G. Ning, *Spectrochim Acta A*, 2015, **134**, 22; (d) L. Yang, J. Ye, L. Xu, X. Yang, W. Gong, Y. Lin and G. Ning, *RSC Adv.*, 2012, **2**, 11529.
- 8) Q. Li, S. Yu, Z. Li and J. Qin, *J. Phys. Org. Chem.*, 2009, **22**, 241.
- 9) (a) M. J. Frisch, Gaussian 09, Revision E.01; (b) G. W. Trucks, H. B. Schlegel, G. E. Scuseria, M. A. Robb, J. R. Cheeseman, G. Scalmani, V. Barone, B. Mennucci, G. A. Petersson, H. Nakatsuji, M. Caricato, X. Li, H. P. Hratchian, A. F. Izmaylov, J. Bloino, G. Zheng, J. L. Sonnenberg, M. Hada, M. Ehara, K. Toyota, R. Fukuda, J. Hasegawa, M. Ishida, T. Nakajima, Y. Honda, O. Kitao, H. Nakai, T. Vreven, J. A. Montgomery, J. E. Peralta, F. Ogliaro, M. Bearpark, J. J. Heyd, E. Brothers, K. N. Kudin, V. N. Staroverov, R. Kobayashi, J. Normand, K. Raghavachari, A. Rendell, J. C. Burant, S. S. Iyengar, J. Tomasi, M. Cossi, N. Rega, J. M. Millam, M. Klene, J. E. Knox, J. B. Cross, V. Bakken, C. Adamo, J. Jaramillo, R. Gomperts, R. E. Stratmann, O. Yazyev, A. J. Austin, R. Cammi, C. Pomelli, J. W. Ochterski, R. L. Martin, K. Morokuma, V. G. Zakrzewski, G. A. Voth, P. Salvador, J. J. Dannenberg, S. Dapprich, A. D. Daniels, Ö. Farkas, J. B. Foresman, J. V. Ortiz, J. Cioslowski and D. J. Fox, Gaussian, Inc. Wallingford CT, 2010.
- 10) a) J. P. Perdew, *Phys. Rev. B.*, 1986, **33**(12), 8822; b) A. D. Becke, *Phys. Rev. A* 1986, **38**(6), 3098.
- 11) F. Weigend and R. Ahlrichs, *Phys. Chem. Chem. Phys.*, 2005, **7**(18), 3297.
- 12) S. Grimme, J. Antony, S. Ehrlich and H. A. Krieg, *J. Chem. Phys.*, 2010, **132** (154104), 1.
- 13) a) E. D. Glendening, A. E. Reed, J. E. Carpenter and F. Weinhold, *NBO Version 3.1* 2001; (b) A. E. Reed, L. A. Curtiss and F. Weinhold, *Chem. Rev.*, 1998, **88**, 899.
- 14) Y. Zhao, N. E. Schultz and D. G. Truhlar, *J. Chem. Theory and Comput.*, 2006, **2**, 364.